REPUBLIC OF TÜRKİYE

ALTINBAŞ UNIVERSITY

Institute of Graduate Studies

Mechanical Engineering Department

DYNAMIC ANALYSIS OF A SHOP CRANE AND DESIGN CUSTOMIZATION

Özgür HAMSİCİ

Master's Thesis

Supervisor

Assoc. Prof. Dr. Süleyman BAŞTÜRK

İstanbul, 2025

DYNAMIC ANALYSIS OF A SHOP CRANE AND DESIGN CUSTOMIZATION

Özgür HAMSİCİ

Department of Mechanical Engineering

Master's Thesis

ALTINBAŞ UNIVERSITY

2025

The thesis titled DYNAMIC ANALYSIS OF A SHOP CRANE AND DESIGN CUSTOMIZATION prepared by ÖZGÜR HAMSİCİ and submitted on 20/06/2025 has been **accepted unanimously** for the degree of Master of Science in Mechanical Engineering.

Assoc. Prof. Dr. Süleyman BAŞTÜRK
Supervisor

Thesis Defense Committee Members:

Prof. Dr. Sami Aydın ŞALCI	Department of Mechanical Engineering, Nişantaşı University	
Assoc. Prof. Dr. Süleyman BAŞTÜRK	Department of Mechanical Engineering, Altınbaş University	
Asst. Prof. Dr. Onur AĞMA	Department of Mechanical Engineering, Altınbaş University	

I hereby declare that this thesis meets all format and submission requirements for a Master's thesis.

I hereby declare that all information/data presented in this graduation project has been obtained in full accordance with academic rules and ethical conduct. I also declare all unoriginal materials and conclusions have been cited in the text and all references mentioned in the Reference List have been cited in the text, and vice versa as required by the abovementioned rules and conduct.

Özgür HAMSİCİ

Signature

DEDICATION

I would like to present my gratitude to my supervisor Assoc.Prof.Dr. Süleyman BAŞTÜRK for his support throughout the preparation of this thesis.

I would like to appreciate all my lecturers for their great contribution to my scientific knowledge in the era of Mechanical Engineering and for their great enthusiasm of passing along their scientific knowledge to Altınbaş University students.

I am grateful to my family for the patience during my studying hours absence.

ABSTRACT

DYNAMIC ANALYSIS OF A SHOP CRANE AND DESIGN CUSTOMIZATION

HAMSİCİ, Özgür

M.Sc., Mechanical Engineering, Altınbaş University,

Supervisor: Assoc. Prof. Dr. Süleyman BAŞTÜRK

Date: June/2025

Pages: 114

Lifting and carrying equipment have a considerable place among the construction equipment. There are several lifting equipment on a construction site. Tower cranes, mobile cranes, crawler cranes, construction telehandlers, electric hoists, back hoe loaders and even excavators are examples of lifting and carrying machines. Scissor lifts, cherry pickers are also other machines. All these machines have variable power sources, variable lifting capacities, and different work spaces. Some use chords and others do not. Some has hydraulic drives while the others have electric or diesel engines. On the other hand, floor or shop cranes are a type of Mobile Crane which are used mainly in industrial working environments, generally in factories, workshops, open logistic stores etc. Floor cranes are also used in the construction sites and this is for the applications of glass facade placements and such specific installation tasks. Floor cranes might have little lifting capacities from 200 kg and can reach up to a capacity of 1500 kg. The capacity depends on the required working load. The target of this study is to investigate the possibility of using a mini floor crane of 250 kg lifting capacity on a multistorey building construction, specifically for carrying and lifting operations on reinforced concrete slabs or newly poured fresh reinforced concrete slabs in order to carry, load and unload rebar frames, formwork pieces and falsework pieces.

A dynamic and a structural analysis are performed based on static and dynamic loads for customization in order to obtain a light crane assembly.

Keywords: Crane, Floor Crane, Shop Crane, Engine Crane, Crane Dynamic Analysis.

TABLE OF CONTENTS

Pages

LIST OF TABLES

Pages

LIST OF FIGURES

Pages

ABBREVIATIONS

AC	:	Alternative Electric Current
AI	:	Artificial Intelligence
ASME	:	American Society of Mechanical Engineers
ASTM	:	American Society for Testing and Materials
BIM	:	Building Information Model
BMW	:	Best and Worst Method
CE	:	Carbon Equivalent of a Steel Alloy
DC	:	Direct Electric Current
DOF	:	Degree of Freedom
FAT	:	Fatigue Strength Class based on $2x10^6$ Cycles
FEM	:	Federation Europeenne de la Manutention
HF	:	High Frequency – A welding Type
HFMI	:	High Frequency Mechanical Impact Treatment
HIC	:	Hydrogen Induced Cracking
HSLA	:	High Strength Low Alloy Steel
IIW	:	International Institute of Welding
IoT	:	Internet of Things
Imu	:	Inertia Measurement Unit
IR	:	Infrared
ISO	:	International Organization for Standardization
LIDAR	:	Light Direction and Ranging
M20	:	MAG Welding Gas

Max.	:	Maximum
MAG	:	Metal Active Gas Welding
MARCOS	:	Measurement of Alternatives and Ranking According to a Compromise solution
MIG	:	Metal Inert Gas Welding
M.O.R.	:	Modulus of Rupture
NiMoCr	:	Low Alloyed Solid Wire Electrode for High Strength Steels
PID	:	Proportional Integral Derivative Control
RFID	:	Radio Frequency Identification
RGB	:	Red Green Blue
RGB-D	:	Red Green Blue - Distance
S690	:	High Strength Low Alloy Steel with 690 MPa Yield Strength
S960	:	High Strength Low Alloy Steel with 960 MPa Yield Strength
OSHA	:	Occupational Safety and Health Administration
US	:	United States

LIST OF SYMBOLS

α	:	Angular Acceleration
a	:	Translational Acceleration
A	:	Area
Ah	:	Ampere-Hour
Ar	:	Argon
β	:	Angle of Contact in Pulley Friction
β	:	Natural Period Ratios of Pendulum for Horizontal Load Calculation
C	:	Carbon
C	:	Compressive Strength Class of Concrete
cm	:	Centimetre
CO_2	:	Carbondioxide
F	:	Force
f	:	Rolling Resistance
f_{ck}	:	Characteristic Compressive Strength of Concrete
Fe	:	Iron
g	:	Earth Gravity 9,81 m/s^2
γ_c	:	General Load Amplifying Coefficient for Case 1 and Case 2
η	:	Efficiency Value in Motors, Transmissions etc.
J	:	Joule
ψ	:	Vertical Hoist Inertia Force Amplification Factor
K_f	:	Fatigue Strength Factor
kg	:	Kilogram

k_{xi}	:	Support Spring Coefficient – x Direction
k_{yi}		Support Spring Coefficient – y Direction
k_{zi}		Support Spring Coefficient – z Direction
km/h	:	Kilometer per Hour
kW	:	Kilowatt
l	:	Rope Length of a Pendulum
lbs	:	Pound
m	:	Meter
m	:	Mass
m^2	:	Square-meter
mm	:	Millimeter
μ	:	Mass Ratio of Crane and Pendulum for Horizontal Load Calculation
MPa	:	Mega Pascal
Mn	:	Manganese
n	:	Gearbox Ratio
N	:	Rotational Speed - rev/min
N	:	Newton
Nb	:	Niobium
P	:	Power
P	:	Phosphorus
psi	:	Pound per Square Inch
q	:	Wind Pressure
r	:	Radius
ρ_1	:	Payload Amplification Factor for Case 3

ρ_2 : Payload Amplification Factor for Case 3

s : Second

S : Sulphur

S : Stress Representation in a Fatigue S-N Curve

$S_{Counterweight}$: Counterweight Load

S_G : Self-Weight of Crane

S_H : Horizontal Inertia Load

Si : Silicium

S_L : Design Payload of Crane

S_T : Buffer Load

S_{UT} : Ultimate Tensile Strength

S_W : Wind Load

S_{WMAX} : Maximum Wind Load out of Service

S_Y : Yield Strength

T : Torque

T : Natural Period of a Pendulum

T_L : Natural Period of Load Pendulum in S_H Calculation

T_m : Mean Duration of Acceleration in S_H Calculation

t : Ton

t : Time in Second

Ti : Titanium

V : Vanadium

V : Velocity

V_L : Vertical Hoist Linear Velocity

V_S : Wind Speed

ω	:	Angular Velocity
w_0	:	Total Travel Resistance at 0 m/s Wind Speed
w_8	:	Total Travel Resistance at 80 N/m^2 Wind Pressure
w_{25}	:	Total Travel Resistance at 250 N/m^2 Wind Pressure
ξ	:	Coefficient of Jib Crane for Vertical Hoist Inertia Force Amplification

1. INTRODUCTION & PURPOSE

Cranes and derricks lift and lower loads, by means of ropes and pulleys, and move the loads horizontally. The height of the load, the weight of the load, and the speed of the operation are the vital criteria that determines what kind of a crane shall be used in the operation. The crane's degree-of-freedom depends on its mechanism design. A mobile crane with a telescopic swivel (i.e. slewing) and luffing boom is a 3 degree-of-freedom mechanism. One degree of freedom from the slider-joint of the boom plus one degree of freedom from the slewing rotation plus one degree of freedom from luffing rotation, that is to say two rotation and one translation. A tower crane, for instance, that has no luffing property and only swiveling has two degrees-of-freedom. One DOF by swivel rotation plus one DOF by hoisting rope. When a jib raises or lowers its jib and changes the radius of its working space, this operation is called luffing. When a crane mast rotates around its own vertical axis, this operation is called slewing or swivel. One another criterion for the suitable crane selection is the safety issue. Because rigging, which is the compound action of moving, securing, lifting, carrying and putting down a load is a dangerous action prone to falling, tipping, overturning, tilting, breaking, tearing, entangling and rupture etc. However, lift planning and not to be hasty are regarded as the best safety precautions for rigging operations. The cranes are equipment that are used in the operations as loading, unloading, installation and transportation of heavy loads that human cannot perform or cannot perform as fast as a crane. Therefore, they are one of the most favoured machines of industrial applications such as manufacturing, storage or construction applications. Assembling a crane connects the disciplines of principally Mechanical Engineering and Structural Analysis. Besides, the electronic devices, appliances and gadgets are inevitable pieces of a secure crane design. So, many of engineering branches need to collaborate in order to bring out a safe, endurable, practicable, and efficient crane.

1.1 MOTIVATION OF THE THESIS

In the sector of the construction industry, recently, demand for mobile cranes shows a significant ascent. This tendency is also expected to grow up to and beyond 2027. Instead of other types of cranes, nowadays, mobile cranes are the first option for the construction companies and managers. Moreover, these companies began to prefer mobile cranes even instead of tower cranes and derricks. The motive of this selection is that mobile cranes are more cost-effective, more rapid and more flexible at the operations. Recently, there is a worldwide reconstruction of old and longstanding cities where the population, city's daily activities, existing buildings, city centers, urban transportation, public transportation, large avenues, street's physical conditions produce restrictions and obstacles for a construction site. On the other hand, mobile cranes are the riskiest heavy equipment among all crane types. Hence, mobile crane selection is both a matter of safety planning and machine management. Selecting the correct type of mobile cranes minimizes the risk of accidents. Amid the mobile crane operations on a site, rigging light loads (100 kg – 300 kg) that arises from lifting formworks, falseworks, reinforcements, timbers etc. holds an important place. And even this kind of light loads are handled with large capacity mobile cranes. More attractively, these loads are carried by labourers in a number of repetitive performing. In this study, it is considered whether a floor crane with less payload capacity has validity, efficacy and applicability to be operated on a newly poured fresh floor of a multi-story building construction, it is aimed to clear out the ambiguity of utilizing a lightweight, detachable floor crane on a freshly poured concrete without giving rise to concrete microcracks or concrete large cracks or a decrease in the ultimate strength of the floor concrete. A minimized vehicular mass with reduced vehicle dimensions is also going to be a leading object of the analysis.

Construction equipment is frequently placed on the reinforced concrete slab but mainly after assuring that the concrete slab is adequately hardened, cured, and gained 70% of its compressive and flexural strength. Especially the concentrated point loads stemming from the rubber tyres makes the situation complicated. In addition, the braking and acceleration forces of the tyres bring about a wearing force on the floor, and in the case of a fresh concrete, this can make significant abrasion damage.

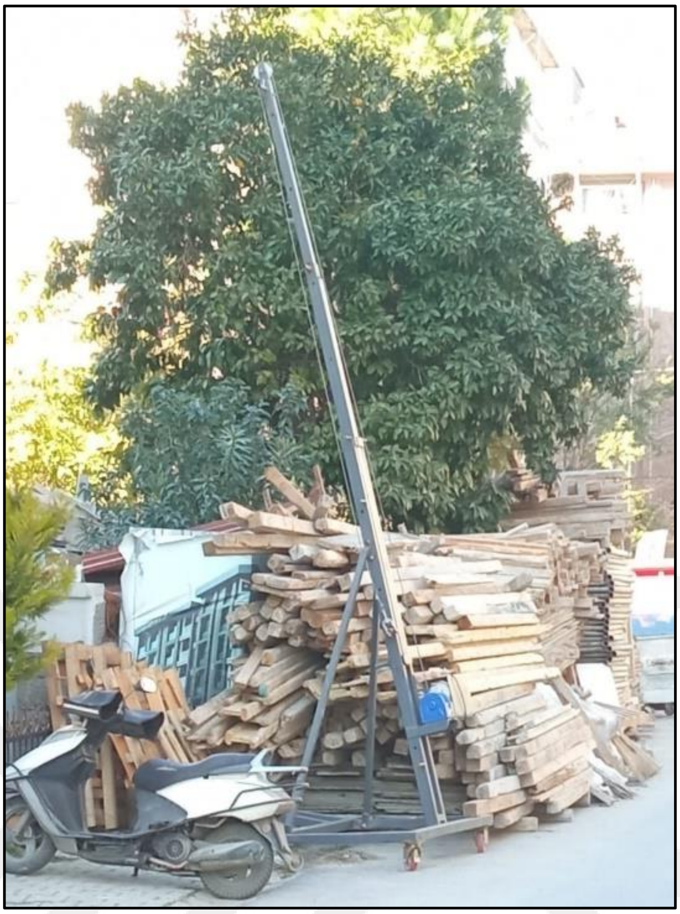

Figure 1.1: A Mobile Construction Hoist.

As illustrated in above figure, it might be easily derived that construction people need this kind of equipment heavily in their job site but they are not able to find the optimum customization and obliged to create their own solutions. However, the figure also proves that such innovative solutions without a scientific touch may result in hazards in the apparatus as bending, buckling, torsional buckling etc. The mobile hoist shown is heavily bended on the base structure frames due to overloading.

The below figure is another example of the necessity to optimize the right mobile crane for the present hoisting task. In the figure, a 30 Tons capacity mobile crane is assembled to hoist the column reinforcement frames which weigh about 200 kg each. One can easily realize that the crane is totally clogging one lane of a two-lane road.

Figure 1.2: A Mobile Crane Hoisting a Load Much Below Its Capacity.

1.2 GENERAL INFORMATION ABOUT CRANES AND DERRICKS

According to US' Occupational Safety and Health Administration Specification OSHA-1910.179 [1], a crane is a machine that has a hoisting mechanism as a fixed attachment to the machine and a crane is able to lift a load, lower a load or move a load horizontally. According to OSHA-1910.181 [1], a derrick is an apparatus assembled from a mast held at the head by guys or braces, with or without a boom.

Unlike a crane, a derrick has a stationary mast, i.e. a vertical post that is attached to a movable boom. The boom structure and the mast structure are connected to each other by braces or wires and are braced together. On the other hand, a crane has generally a boom and a mast connected together as one member and moves also horizontally. Derricks are generally preferred and found helpful for jobs that require high-rise rigging, that lasts for long durations and when the jobs impact into the street and pedestrian traffic is a matter of handling. Figures 1.3 and 1.4 illustrate the subtle distinction between a derrick and a crane, as described by Maritime Safety Innovation Lab LLC [2].

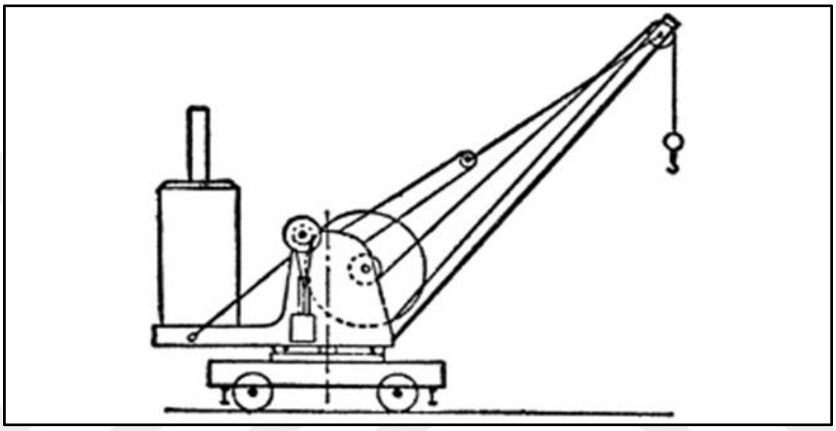

Figure 1.3: A Crane [2].

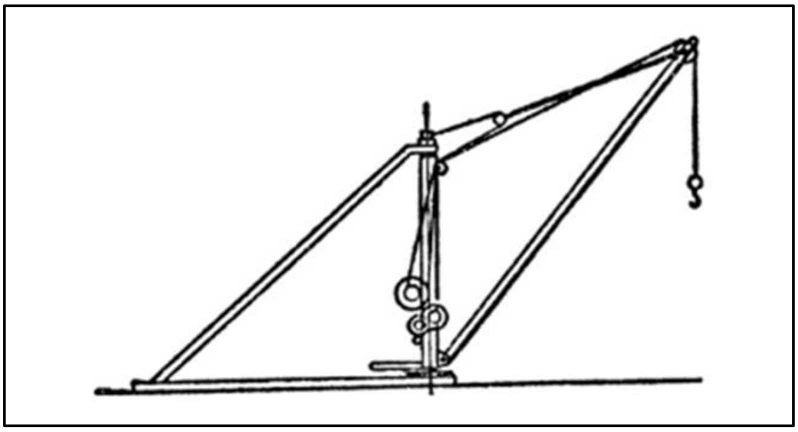

Figure 1.4: A Derrick [2].

The derricks in general might be classified as A-Frame, Basket, Breast, Chicago Boom, Gin Pole, Guy, Shear-leg, Stiff-leg and Oil derrick. In the maritime industry especially two types of derricks are common. These are Velle Derrick and the Hallen Derrick.

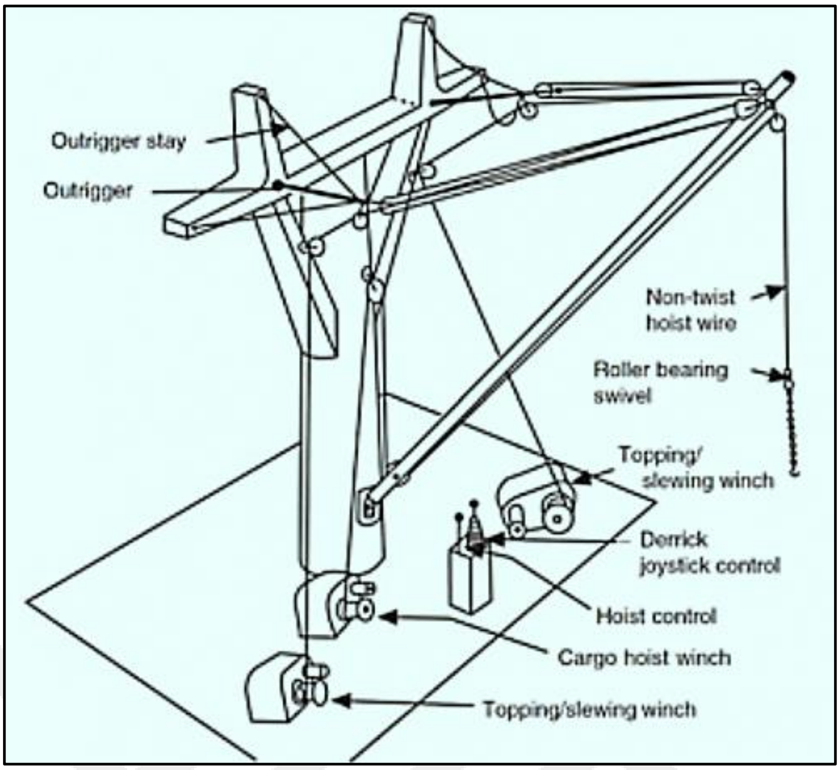

Figure 1.5: A Hallen Derrick [2].

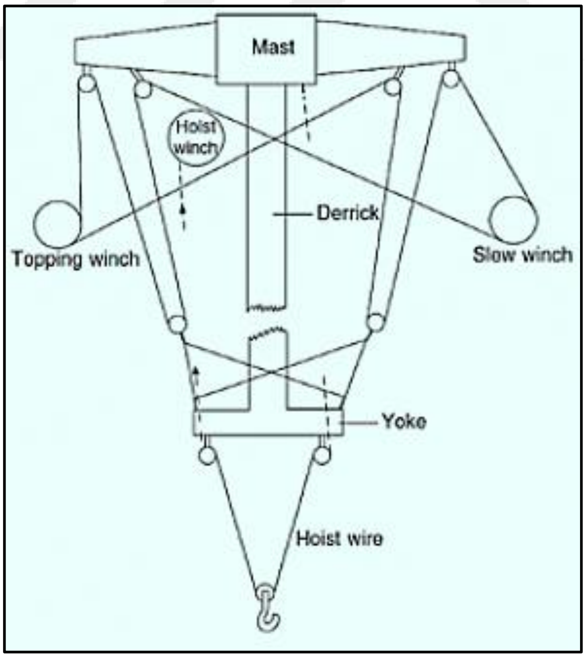

Figure 1.6: A Velle Derrick [2].

The cranes can be categorised in two main groups as static cranes and mobile cranes. Some examples of static cranes are over-head cranes with its sub classes bridge, gantry, jib, monorail and workstation cranes, tower cranes, hammer head tower cranes, self-erecting tower cranes and luffing tower cranes. Mobile cranes vary from truck cranes, crawler cranes, rough terrain cranes, all-terrain cranes, floating cranes, carry-deck cranes, stacker cranes and telescopic cranes and telehandlers. The figure below illustrates some of the most used ones in the industry.

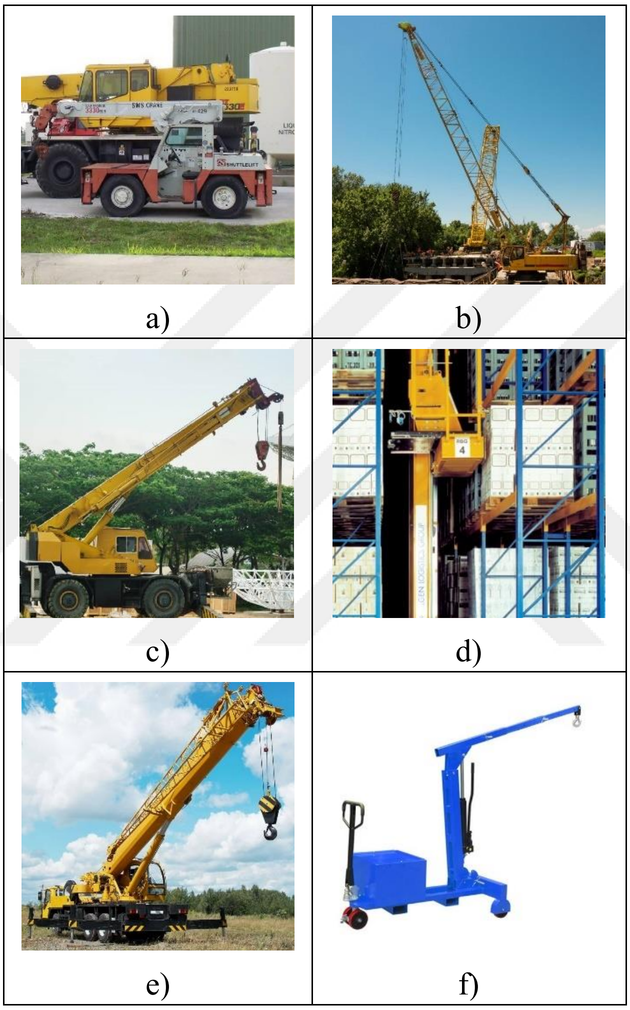

Figure 1.7: a) Carry-Deck Crane. b) Crawler Crane. c) Rough Terrain Crane. d) Stacker Crane e) Small Size Shop Crane [3].

Concerning the structural design of the cranes and most load lifting construction equipment, an exceptional calculation is necessary compared to other vehicles which is the tipping moment calculation as shown in Formula 1.1 in its basic form. This topic covers an important role in the overall design of such assemblies. To prevent the tipping moment about any corner point of the crane, there are many methods. Installing outriggers as extending outward supports to enable the weight of the crane to create a counter-moment against the overturning moment, locking mechanism between the guide rails and the bogies or implementing additional counterweights to the assembly are some of these methods. The point or support on which a lever force rotates is named as the fulcrum point. The crane fulcrum points are either the edge point of the outriggers, the edge line of crawlers or the rear or front axles depending on the load direction.

$$tipping\ moment = force\ x\ lever\ arm\ to\ the\ tipping\ edge \qquad (1.1)$$

1.3 AVAILABLE FLOOR CRANE MACHINERY ON THE MARKET

There are several types of the machinery. The machinery might be categorized as motor-driven and hand driven as well as luffing and non-luffing or slewing and non-slewing. The load capacity is in the range of 500 kg to 2 Tons. These categorizations depend on the designated duty of the equipment such as operating in a workshop, installation of facade members of a building etc. The figures below give a rough description of the equipment on the market.

Figure 1.8: ULINE Hydraulic Floor Crane BL-2853. Capacity 2 Tons Max. Retracted [4].

Figure 1.9: VESTIL Electric Powered Shop Crane. Capacity 2500 lbs. Max. Retracted [5].

Figure 1.10: BRANDON 6 Mini Glass Lifter. 24 V Battery Powered [6].

1.4 ADVANTAGES AND DISADVANTAGES OF PREFERRING FLOOR CRANES

Floor cranes are used in the construction sites at only restricted conditions due to health and safety issues. Table 1.1 illustrates a comparison of advantages and disadvantages of utilizing such an equipment on a multi-storey building construction.

Table 1.1: Advantages and Disadvantages of a Floor Crane.

Advantages	Disadvantages
More ergonomic than a mobile crane, could be placed in any corner or side of a floor compared to a mobile crane which requires a location of assembly.	Mobile cranes might reach more points once they are placed and located safely.
Possible to operate for fine finishing works inside a story when boom length of the floor crane is modified and shortened.	It is also impossible to operate floor cranes on narrow aisles or through narrow walls and door gaps.
Easy to operate with any lectured labor, doesn't need an operator as a mobile crane.	In case of a distraction of the operator, the machine might hit anything or a person in the vicinity.
More cost-effective than a mobile crane as can be used in any time of the work hours, daily or weekly.	The load capacity is lower, when it is necessary to lift heavy weights, the floor crane cannot do it, for example steel bundles, steel hot rolled or cold rolled profiles etc.
No need of path preparation as a mobile crane, the floor crane operates right on the concrete slab.	There is the danger of the machine to fall down from the floor.

Table 1.1: Advantages and Disadvantages of a Floor Crane "Table Continued".

Doesn't make a traffic obstruction as a mobile crane to the residential units, roads, nearby traffic flow.	The floor crane cannot be sufficient and efficient as a mobile crane when a loaded truck of construction material is going to be unloaded on site.
The floor crane on a slab might reduce the risk of workers to get injured by lifting heavy loads.	It cannot reach every point on the slab, especially the edges of the slab where there is a risk of falling, the columns and shear walls outside facades, nearby the spacings like staircases, shaft gaps of the floors etc.
In the absence of another crane on site, the floor crane is an identical spare equipment for handling the duties of the primary crane that is absent or out of order.	It cannot be operated in rough terrain and needs smooth surfaces for the rubber tyres.

2. LITERATURE REVIEW

2.1 GENERAL REVIEW

There are various mobile crane variants which are already described in the previous chapter and floor cranes are not the first options to be manipulated in a construction site. According to Yogesh & Krishan [7], the hydraulic floor crane was invented in New Castle-United Kingdom in order to hoist coal into barges by William Armstrong. Given that multistorey building constructions necessitate high mobile crane booms, higher crane load capacities arising from the boom extension and more precise security appliances by the crane, construction management staff generally make a crane selection decision over mobile cranes or stable fixed tower cranes. On the other hand, this study aims to bring about a floor crane that has the possibility and practicality to be a substitute of a mobile crane and that will be lifted easily and placed on the latest slab of a multistorey building construction, it is still a requirement to assign the investigation to the mobile cranes. After all, a floor crane is statically and dynamically a sort of mobile crane and has exactly the same task with the mobile crane. According to Duragkar et al. [8] for carrying loads within a short distance, floor cranes seem to be one of the most effective ways. A floor crane might be designed with different properties and members such as counterbalances, outriggers, the ability to slew or to luff in order to extend the booms working space, stiffened and braced chassis, locking mechanisms, safety instruments etc. A locking device for example is an additional assembly to prevent static failure when hydraulic cylinder for luffing mission is out of order and it was released by Chukwulozie et al. [9]. Mini cranes are efficient in tight space environments. In this sense, top of a concrete floor slab being a crowded area full of columns, timbers, falsework and formwork pieces, steel profiles etc. is a perfect example of this type of working environments. The mini cranes are also efficient as a low-cost alternative to other types of mobile cranes according to Jadhav et al. [10]. The work clarified a good design example of a mini workshop crane with a mast height of 117.5 cm [10]. A self-propelled crane was designed by Safarzadeh et al. [11]. The target of the self-propelling in this study was again the accident-prone state of mobile crane lifting operations.

The literature review also shows that the surveys about cranes might be classified in five different sub-divisions. These are dynamic motion and static tipping-overturning analysis', structural design of the mechanism by Finite Element Method, health and safety-based path planning and lift planning surveys, investigations and design of appliances that are used in the mobile cranes and technological safety appliances that are attached to the overall system.

Safety based modeling for example; recommends models as Building Information Plan by Peng and Chua [12]. Here it is stated that in year 2014, 60 fatal accidents in Singapore were involving mobile crane lifting operations. Path planning studies cover spatial constraints and interactions within the environment to specify a safe route for the crane as defined by Sangmin et al. [13].

Mini cranes are dynamic machines that are on translational motion while travelling and on rotational motion while luffing, slewing or changing its translational direction. These studies delicately deal with finite element method analysis during the design process. Dynamic motion and overturning stability analyses are other subdivisions of the crane studies. Urbas et al. [14] focused on dynamic effects that originates from different load shape geometries and different rope sling systems by presenting a dynamic model of Lagrange equations. Dawid and Pawel [15] concentrated on the effect of rope system and its interaction of wind pressure. There are also multiple available dynamic analysis and inertia loads that mobile cranes are exposed to. Fujioka [16] defined inertia loads for different dynamic states about angles and motions and composed a detailed overturning stability analysis based on these inertia affects. Finally, a full thorough review of technologies in crane-lift automation in construction industry is available by Zhu et al. [17].

2.2 REVIEW FOR DYNAMIC AND DESIGN ANALYSIS OF CRANES

Urbas et al. [14] presented a thorough dynamic analysis of crane loading and unloading motion by taking into consideration different geometrical types of loads instead of using a lumped mass, boom and drive flexibility and different rope sling systems. Loads were classified as cylinder, log shaped and block shaped. Variants of rope sling systems of interest were one, two, three and four rope attachments to the crane's hook. The open-loop kinematic chain with auxiliary sub-chains dynamic system model was inspected under varying rope length and load shapes. Validation of the mathematical model was tested with software programs of MATLAB, MSC.Adams and ANSYS-MSC.Adams interface. The influence of flexibilities of boom, drive and rope sling system via their spring-damping properties were added to the general second order Lagrange equations. Likewise, spring-damping properties of outriggers and two back twin wheels were also evaluated together with overall crane system. It was summarized that compared to simplified dynamic systems, the kinetic energy of the load after crane's motion cycle and its completion causes free oscillations of the load and that these afterward oscillations have significant influence on the dynamic forces on the crane. The loads when considered as lump mass and when considered as complete geometries of several mass moment of inertias definitely vary. Moreover, the open-loop kinematic chain is heavily refined by adding hydraulic pistons as sub-chains.

Fujioka [16] investigated the tip-over stability analysis of a mobile crane under different conditions. First a static analysis was performed assuming that the crane is under stable position where the payload and the rope do not have any swing, in other words there is no pendulum motion of the payload. It has been observed that a full static analysis gives a basic understanding of the relationship between tip-over stability and the moment contribution of the payload mass to the crane overall structural frame. Then, a pseudo-dynamic analysis was held assuming that the maximum payload swing angle is a constant value rather than a time dependent value. Here, it was observed that the maximum possible payload is related to acceleration and velocity inputs of the boom. Also, it is proved to be a good method to foresee the tip-over risk of the crane. Next, the analysis was extended to a pseudo-dynamic analysis with a double pendulum effect. The double-pendulum effect is more realistic due to the hook's contribution to the swinging motion of the payload. And finally, a real-time full dynamic tip-over analysis was implemented by adding software programs MATLAB and AUTOLEV to the investigation where the luffing motion of the boom and the slewing motion of the boom exerts elaborate inertial forces to the overall structure. Naturally, the full dynamic analysis is composed of various initial acceleration, velocity and position (luffing and slewing angles) inputs. It has been evaluated that different dynamic motion inputs results in different inertial forces, yet pseudo-dynamic analysis is a valid means to predict tip-overs.

Chukwulozie et al. [9] presented design and fabrication of a mini floor crane of 1000 kg. maximum payload is realized. The boom, the mast, the base are made of mild steel and a load locking facility is added in between the boom and mast which is produced from High Carbon Steel. A counterbalance load of 260 kg. served to balance the tip-over balance. The overturning moment factor of safety has been calculated as 3,034. A hydraulic piston is attached to the overall system to enable the crane to make the luffing motion. The boom height is 2 m, the mast height is 1.5 m and the length of the crane is 1.3 m. The assembly has been mainly completed by welding pieces together and a test load has checked the system that it is capable as it is designed.

Towarek [18] inspected the dynamic stability of a crane placed on a flexible soil during the rotation motion of the boom. The basic scientific method of adding the soil effects might be described as the three-dimensional semi-infinite soil medium is reduced to separated elastic structures with various degrees of freedom under each outrigger of the crane. Each four outrigger stands on six degrees of freedom massless springs. Therefore, the main crane mass m is also modeled as six degrees of freedom rigid solid suspended on 12 springs, three of them under each outrigger. Via Second order Lagrange equations and Duhamel integral and the dissipation functions of the plastic soil type, it has been concluded that the kinematic parameters, especially the rotation (slewing) is a significant parameter on the deflection of the rope with the weight hoisted.

Dawid and Pawel [15] focused on a deformable rope system of Kevin-Voigt is presented and analysed. The load is accepted as a rigid body, the chassis and body of the crane are assumed as non-deformable parts resting on the ground and the boom is taken as infinitely stiff member with variable telescoping motion. Second order Lagrange equations were established for cranes rotational motion, booms telescopic sliding joint motion and presented second degree Kevin-Voigt model of hanging load is also attached to the overall dynamic system. The system was observed and evaluated by software under wind pressure that is defined by ISO Guidelines. The effect of wind on load trajectory was desolately analysed and later combined with the overall reaction of the dynamic system. It has been concluded that wind pressure has a significant impact on load trajectory and is capable of changing the trajectory of load during hoisting, rotation and luffing and special attention should be given to sudden gusts during hoisting motion of the load.

Jadhav et al. [10] presented an optimization of a rotating hydraulic crane is performed and the equipment was manufactured and tested for several conditions as strength, cost efficiency and load range. The hydraulic system is composed of mild steel S_{ut}=250 MPa, and the hand powered gearbox system of Plain Carbon Steel S_{ut}=750 MPa. The maximum payload capacity of the crane is 2 tons, even when the boom is rotated 90^0 to the left or right. The gearbox provides the slewing motion of the crane and the 150 MPa internal pressure, 60 cm stroke luffing piston is hand-powered. The crane stability factor is almost 1.00 when the piston stroke is at maximum position.

Safarzadeh et al. [11] realized the design and manufacture of a self-propelled crane. The object of self-propelled crane is to attach the whole assembly to a remote-control system and provide the operator a safer working environment and make the person capable of all operations of crane remotely. The study claimed the remote control of a mini-crane is a safer option since the operator will be able to see, to observe or to realize anything that is on the path of the crane from a safe distance. The study states that according to OSHA regulations, 15.2% of crane events took place in manufacturing environments and these are places deemed as messy, crowdy, disorganized, untidy and most importantly frequently in a rush. The total mass of crane is 850 kg as a lot of driving unit and hydraulic units are added in the configuration. A hydraulic unit for boom rotation and luffing with a tank and a drive, a speed reduction gearbox, two pieces of 12V x 200 Ah batteries, another 4 kW electromotor for driving the crane, three wireless cameras are assembled together. The main motivation of the machinery is to overcome the visibility problems of the crane operator which is stated to be the reason for 80% of the truck-forklift accident that has occurred. In particular, the design velocity of the crane is planned to be 2 km/h and a maximum speed of 2.8 km/h which are also designated especially to prevent hit-stop and crash accidents. The dynamic stability analysis is established according to ISO 4305 Specification.

Romanello [19] developed a MATLAB code as a mathematical model for determination of outriggers of a mobile crane. The analysis was performed on the basis of Static Theory of Rigid Body. Ground is characterized by a linear elastic constitutive law and the crane as a rigid body. The wind force is neglected. The hypothesis of linear elastic ground makes it convenient to eliminate the statically indeterminate system's unknowns and solves the system equation matrix for outrigger reaction.

Posiadala [20] is the first to integrate the behavior of the crane support system to the equations of dynamic motion matrix. The paper presented four points of crane support with 3 translational degrees of freedom. The spring constants k_{xi}, k_{yi} and k_{zi} represents the elastic suspension of the point support. Further, the equations of motion are computed by an algorithm to extract the forced motion lifted load motion's trajectory by time. From the extracted position values, the three reaction components of the crane support point F_X, F_Y and F_Z are calculated with respect to time. The load kinematic behavior is described with the addition of taking into account the crane support system.

Umut and Mete [21] dealed the same subject of the crane mathematical modeling of dynamic equations and implement a PID Control to the mathematical model. The PID control minimizes the effect of pendulum motion of the load on the crane solid system by manipulating the speed and actuation of the boom extraction, rotation, and luffing.

2.3 REVIEW FOR LIFTING OPERATIONS

Ömer & Gürkan [22] presented a mobile selection algorithm using Best and Worst Method (BWM) and fuzzy Measurement of Alternatives and Ranking according to compromise solution (MARCOS). The study emphasized that a mobile crane is the fundamental equipment for modular constructions that are going to be assembled on site such as wind turbines, autoclaves, power plants, and industrial unit installations. The fuzzy model that is a mix of MARCOS approaches consists of five stages that handles the weights and ranks of the criteria and prepares an initial fuzzy matrix. The hierarchical structure criteria of the fuzzy matrix consisting of a primary matrix of 3 elements that are aspects of technique, economy, and quality and a sub-matrix of 15 elements that are load capacity, hoist height, drive engine power, crane engine power, driving speed, the total weight of the crane, fuel reservoir, energy consumption, costs of consumables, costs of maintenance, availability in second-hand market, purchasing price, emission class of crane, brand awareness and safety. After typical best values, worst values, comparisons, optimization, ideal non-ideal cases processes of the methods, the sensitivity analysis finalizes with comparing results of MCDM approaches such as MABAC, F-TOPSIS, MOORA, and MAIRCA.

Le Peng et al. [12] presented a decision support system for mobile crane lifting plan with Building Information Modeling (BIM). The motivation of the research comes from the insufficiency of single engineering experience for planning mobile crane lift operations which is claimed to be error-prone. The research combines a Building Information Modeling software such as Autodesk Revit with the mobile crane information model and the lifting task. The building information modeling provides the input of the working environment and space that is consisting of the existing structures, the construction site borders, geometric information of other construction equipment, and the boundaries of the site. The mobile crane information supplies the information about the mobile crane structure, the outriggers, jib lengths, boom lengths, rope lengths, the clearance space for safe operation, load chart of the crane for different luffing-slewing, positional parameters of the crane such as loading point on site and unloading on site, parametric lifting task and extendable dimensions of the crane. Gathering these data, the decision support system automates a lifting capacity check and an obstruction check and determines the lifting constraints and the lifting plan with an algorithm.

2.4 REVIEW FOR MOBILE CRANE AUTOMATION

Zhu et al. [17] in their review made an efficient summarization of the safety technologies as attached appliances to several types of tower and mobile cranes. The main smart sensing technologies are Lidar (acronym for light direction and ranging), IoT (acronym for internet of things), Imu (acronym for inertia measurement unites), RFID (acronym for radio frequency identification), IR cameras (Infrared cameras), RGB cameras (red green blue cameras), RGB-D cameras (red green blue distance imaging camera), environmental sensors, encoder sensors and force sensors. Translational velocity of the crane is measured by encoder sensors. Acceleration of the crane might be measured by the encoder and also by the Imu sensor. RGB and Lidar are utilized for detection of obstacles and collision. Environmental sensors measure wind speed. RFID can detect the surrounding workers, machines and materials. Force sensors and contact sensors can foresee the overturning and tipping of the crane while computing the crane's shifting centre. Force sensor is capable of determining the payload that the crane is lifting.

2.5 REVIEW FOR CRANE TRAFFIC LOADING OF 1 DAY AGE CONCRETE SLAB

Reinforced concrete is not a prefabricated material. It comes to site as a plastic viscous fluid and it is casted in the formwork. When it starts solidifying, this chemical reaction is called setting of concrete. This chemical reaction is a type of hydration reaction and it starts just in the following few hours after placement and the concrete begins losing its plasticity. Concrete gains its ultimate strength by this water-cement hydration within almost 28 days. At the end of 28 days, 99% of the designed concrete strength is reached. However, concrete can reach 65% to 70% of its ultimate compressive strength in 7 days. Below Table 2.1 is from Midtech website where time-strength variation of fresh concrete can be seen [23];

Table 2.1: Compressive Strength of Fresh Concrete During its Setting Duration.

Age of Concrete	Gained Compressive Strength
1 Day	16%
3 Days	40%
7 Days	65%
14 Days	90%
28 Days	99%

The characteristic compressive strength of the concrete f_{ck} is of the utmost importance owing to the fact that concrete structures bear to compressive stresses through the medium of concrete compressive strength. Despite, it is contradictorily rather weak in tensile capacity. Especially in the early stages of the setting process, the bonding between the reinforcement steel and concrete is low. Chapman and Shah [24] called this phenomenon as the bond-slip behavior of early age concrete. Cooper stated that early ages loading of concrete may result in excessive deflection and cracking [25]. Taking into consideration the bond-slip and the cracking behaviour in the early stages, it is merely the flexural strength of concrete but not the contribution rebars that will bear the bending and the tensile forces exerted on a slab. The conducted tests by Song et al. [26] identifies that early loading might result in severe deflection and concrete cracking on the concrete slabs and beams. For slabs of early concrete ages and unbonded concrete overlays, by the nature of a loaded beam laying on an elastic surface, wheel loads cause critical flexural tensile stresses at the bottom of the slab below the neutral axis and flexural compressive stresses above the neutral axis. As mentioned above, this critical condition is a consequence of yet unbonded concrete overlays and lack of bonding between rebars and fresh concrete. According to Cole and Okamoto [27], for typical concrete slabs in new construction and unbonded concrete overlays, it is commonly accepted that traffic loads bring in critical flexural tensile stresses at the bottom of the slab and flexural compressive stresses at the top.

As a result, minimizing the fatigue damage by repetitive flexural cracking to the concrete slab during the construction period at early stages is of primary importance. Loading a freshly poured reinforced slab is not a construction operation that can be realized without hesitation. However, concrete pavement construction industry tells us a lot about opening a road to wheel loads at early stages. This idea is summarized as Fast-Track Paving. There is a generous amount of conducted researches, specs and collected data about the Fast-Track Paving application. According to Cavalline et al. [28], the compressive strength required for pavement openings typically ranges from 2,200 to 3,500 psi (15.2–24.1 MPa) when intended for construction vehicle traffic, and increases to between 3,000 and 4,500 psi (20.7–31.0 MPa) for standard traffic loads. Similarly, flexural strength values generally fall between 500 and 650 psi (3.4–4.5 MPa) for both construction and regular traffic conditions. Cavalline et al. [28] also states that Minnesota State Highway guidelines specify a required flexural strength between 350 and 500 psi (2.4–3.4 MPa), with the exact value contingent on the thickness of the concrete slab.

The formula for converting Concrete Compressive Strength to Concrete Flexural Strength (Modulus of Rupture) or also Concrete Tensile Strength in Flexure is;

$$M.O.R = 0{,}7.\sqrt{f_{ck}} \tag{2.1}$$

Below is a table where time-strength variation of fresh concrete C30 (28 Compressive Strength f_{ck} 30 MPA) is seen;

Table 2.2: Flexural Strength of C35 Concrete in the Course of its Setting Process.

Age of Concrete	Gained Compressive Strength	Gained Flexural Strength
1 Day	16% = 5.6 MPa	1.66 MPa
3 Days	40% = 14 MPa	2.62 MPa
7 Days	65% = 22.75 MPa	3.34 MPa
14 Days	90% = 31.5 MPa	3.93 MPa
28 Days	99% = 34.65 MPa	4.12 MPa

Under these circumstances of collected and calculated data, it is impossible to utilize any heavy equipment on a concrete slab before 7 days such as a rather light shop crane. However, several concrete admixtures in order to obtain High-Early-Strength are available on the construction materials market. Below figure shows the compressive strength of fresh concrete with different early-strength admixture proportions by Tezel et al. [29].

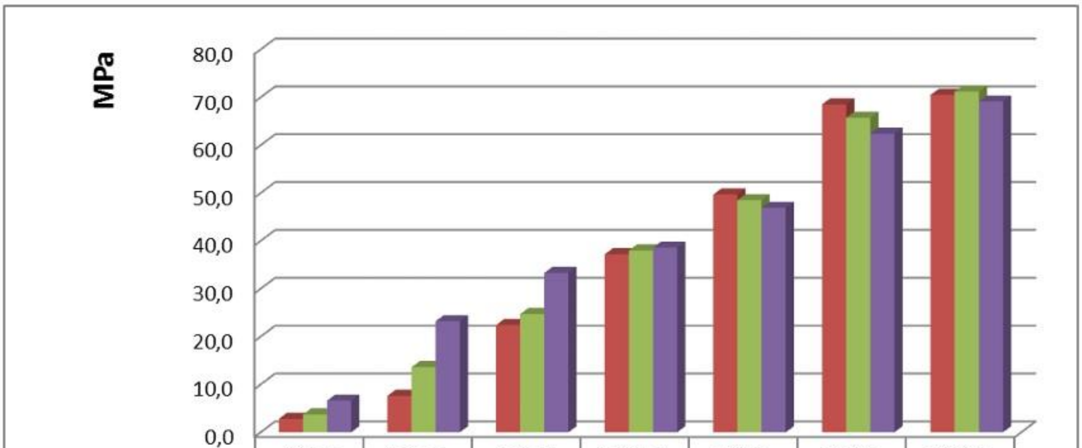

	4 Saat	6 Saat	8 Saat	12 Saat	1 Gün	7 Gün	28 Gün
CEM A-%0YNPH	2,8	7,6	22,4	37,2	49,7	68,5	70,5
CEM A-%2,5YNPH	3,7	13,6	24,7	38,0	48,5	65,7	71,2
CEM A-%4YNPH	6,6	23,2	33,3	38,6	46,9	62,4	69,1

Figure 2.1: Concrete Compressive Strength-Time Diagram for Different Proportions of Early-Strength Admixture [29].

It can be stated from Figure 2.1. that when a new-age early-strength admixture is added to the concrete mix design with different proportions, it is possible to attain half the compressive strength of concrete within 12 hours. For a typical structural concrete C30, this corresponds to a value of 15 MPa. According to [28], for a typical C30 MPa concrete, this is a sufficient strength value to utilize a light traffic equipment on the concrete, in this case a crane. In conclusion, in order to operate the crane after 12 hours on a fresh slab concrete, there is a necessity of high early strength admixture in the concrete mix design.

3. METHODOLOGY

3.1 OBJECTIVE AND SCOPE

Initially, a preliminary static-structural design is conducted since there is a definite known payload, and there are definite target crane dimensions. The payload for design is taken as 250 kg and factored to 350 kg for the initial design. An approximated 100 kg horizontal load is also assigned to the analysis that is representing any lateral load. Under these loading conditions, the crane structural sections are determined as 100x100x5 mm box sections.

Using this information, a main design is accomplished by using the load multiplication factors for several loads from FEM 1.001 [30]. The standard is only used as an auxiliary source for defining design load conditions and for assessment of dynamic loads from MATLAB environment. There are numerous standards for floor crane and mobile crane manufacturers. Even in USA, more than one standard is available as being the most favourable ASME B30. However, FEM 1.001 [30] is a standard that covers the designation for Erection and Dismantling Cranes for power Stations, shop cranes etc. in its appliance group A2-A4 and the designation of Workshop Cranes in its appliance group A3-A5 [Table T2.1.2.5 FEM 1.001]. As a result, especially the design load multiplication factors are taken from this standard. The crane width and length are taken as 1.5 m to 1.5 m, allowing it to wander around construction obstacles, columns walls, timber pile or steel pile easily while reaching any narrow corners in order to install a column reinforcement or a shear wall reinforcement or concrete forms for these members. The length of the jib is selected as 1.6 m and the spacing between the two side frames of the chassis 1.5 m provides a 1.5 m x 1.3 m projected area for the load that will be stuffed into this gap, hoisted and carried to final position.

An AC Motor Drive wheel, an AC Hoist Motor and Lithium-Ion batteries that can be customized for length and weight are selected from the market. All members of the structure such as jib, boom, chassis are to be manufactured from High Strength Low Alloy Steel. The market brand of the HSLA Material is StrenX1100. The steel is provided to the customer in the quenched or quenched and tempered form. Square Box sections can be directly purchased from the supplier.

Next, having clarified the detailed masses such as crane body, counterweight and appliances, a dynamic analysis is performed with the software MATLAB_Simscape_Multibody and inertial dynamic effects of acceleration, deceleration and impact collision are calculated.

The Figure 3.1 and Figure 3.2 show the design dimensions of the shop crane.

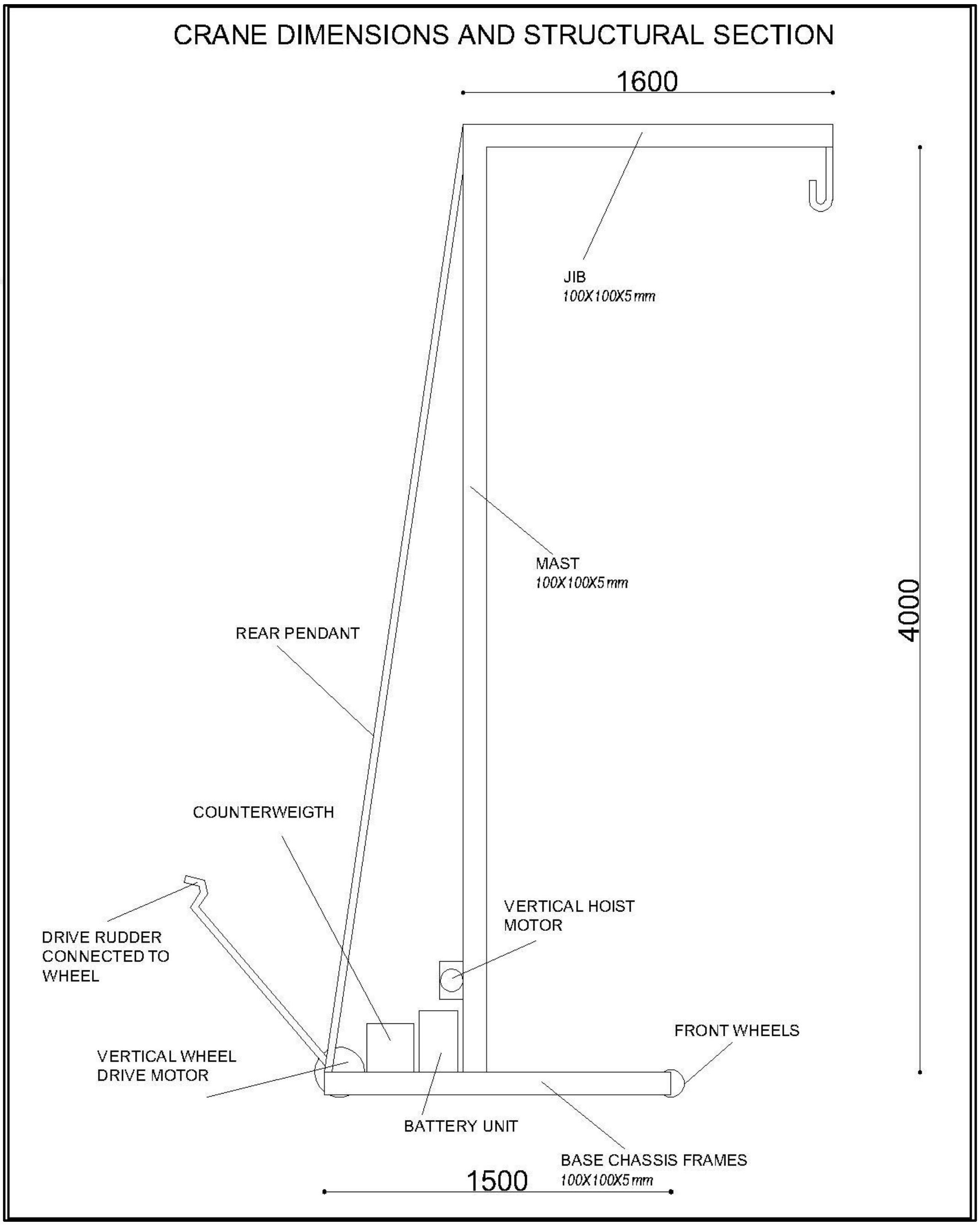

Figure 3.1: Shop Crane Dimensions and Structural Sections.

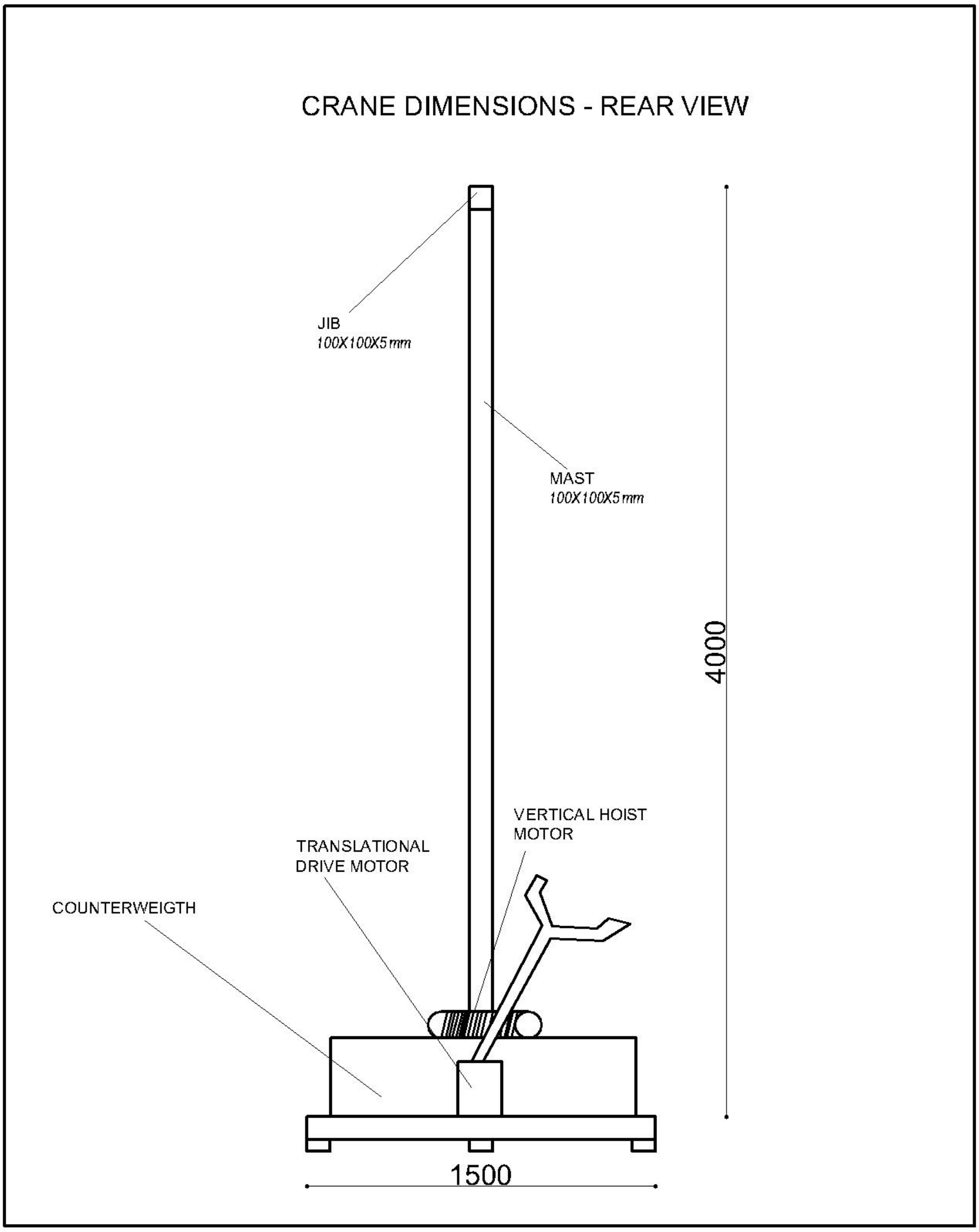

Figure 3.2: Shop Crane Dimensions and Structural Sections.

3.1.1 High Strength Low Alloy Steel and its Mechanical Properties

High Strength Low Alloy Steel (HSLA) is a steel type which has better mechanical properties and better corrosion resistance. It has a higher strength-weight ratio that makes automobile, agriculture equipment, transport equipment, and lifting equipment industries to prefer this material. The high strength to weight ratio advantage of this steel provides the products to be manufactured lighter in the range of 20 to 30%. The steel is provided by supplier in the Quenched or Quenched and Tempered form [31]. By these thermomechanical treatment techniques, the fine grain structure and impact toughness of HSLA are obtained. According to Dhua and Sen [32], accelerated cooling is for the purpose of fine grain structure and quenching is for the purpose of obtaining a good weldability and good toughness. For a typical automobile industry HSLA Steel, one can notice the following chemical composition below.

Table 3.1: Typical Chemical Composition for a Market Product HSLA-STRENX960MC [31].

C-Carbon (Max %)	**SI-Silicium (Max %)**	**Mn (Max %)**	**P (Max %)**	**S (Max %)**	**Nb-Niobium (Max %)**	**V (Max %)**	**Ti (Max %)**
0.12	0.25	1.30	0.020	0.010	0.05	0.05	0.07

Fine ferrite-grain size is the main property of HSLA Steels. In order to manufacture HSLA, refining the grain size is the main task to increase the yield strength of a steel alloy and for every halving of the mean grain diameter, there is a 50% yield strength increase. The more the ferrite increase and perlite form decrease, the more increase in strength is attained. In the case of carbon steel, the structure is coarse, it is composed of alpha ferrite and cementite and has a low yield strength. On the contrary, HSLA matrix is finer, it is composed of ferrite, perlite and sometimes bainite and martensite and copper, titanium, vanadium are mixed to the composition for this strengthening purpose, to modify the microstructure. Metals as Vanadium, Titanium and Niobium have an affinity to free carbon in the composition. They attach to free carbon, form the carbides and more carbide in the matrix means more grain refinement. These are called grain refiners. Carbides are stable structures against thermal processes and do not dissolve and decompose during thermal processes. Therefore, in general, HSLA is regarded to have a higher weldability property compared to plain carbon steel Fe + C. A carbon content in the range of 0.05 to 0.25% is added to continue formability and weldability as the primary hardening element, on the contrary it creates a low ductility. Manganese (Mn) is added for increasing strength, toughness, hardenability and hot working properties of the steel. Molybdenum also increases the machinability, resistance to corrosion, enhances the alloying with other elements as well as also contributing to the fine grain structure. Phosphorus is also used for the same purposes but to a maximum 0,05%. Besides, copper, silicon, nickel, chromium, and phosphorus create a corrosion resistance on the steel alloy. Borum is another hardener admixture of the alloy and its content is in the range of 0,0005%-0,005%. Nickel has the contribution of increasing the yield strength and toughness of the alloy.

Below is a typical market product material table of HSLA producer. The product is preferred widely in lifting industry in the manufacture of aerial work platforms, loader cranes, mobile cranes, forestry cranes, concrete pumps, lattice-boom cranes, tower cranes and telehandlers with reduced weight in the static structure of the equipment. All equipment manufactured of this type of steel has the advantage of more load capacity and further reaching range. Especially in the lifting equipment industry, structural hollow sections made of hot-rolled high-strength steels are available for example with a yield strength of 960 MPa, 40 J Impact energy, min. 6% elongation and section wall thickness range 4.0-6.0 mm. The prefabrication process of such ready to use steel hollow sections is completed by cold-forming and HF-weld, high frequency welding of bended profiles.

Table 3.2: Mechanical Properties of Different HSLA Products [31].

HSLA Yield Strength (MPa)	**Thickness (mm)**	**Elongation (%)**	**Impact Energy CHARPY V (10x10 Specimen -40^0)**
700	4.0-53.0	14	27 J
900	4.0-120	12	27 J
960	4.0-53.0	12	27 J
1100	5.0-40.0	8	27 J
1300	4.0-15.0	8	27 J

Weldability of HSLA is quite high compared to plain carbon steel owing to its high CE-Carbon Equivalent content. However, this process depends on four main aspects. These are preheating process, weld process, kind of filler material and post-weld-heat treatment. HSLA has a good compatibility with most welding processes such as gas metal arc welding (MIG Welding, MAG Welding), gas tungsten arc welding, plasma arc welding etc. However, extra care should be given for electro slag welding, electro gas welding and submerged arc welding. As mentioned earlier, HSLA has a high carbon equivalent due to presence of alloys that form carbides and this property necessitates a preheat process and a low Hydrogen practice. On this purpose, welding consumables with a low hydrogen content is an obligation. Whenever there is preheating in the required zone which is maximum of plate thickness or approx. 75 mm, the heat transfer from the weld area to the vicinity by conduction or convection decreases, to put it another way, the cooling rate of the base and filler is reduced in the weld area. As a result, excessive hardening and cracking tendency risk diminish. Also, with reduction in the cooling rate, martensitic formation in the welding area matrix reduces, the residual stress development in the heat affected zone reduces and hardness in the area reduces. An increase in the cooling rate means rapid heat expansion and contraction which will increase the cracking tendency too. Besides, hydrogen cracking should be avoided by reducing the hydrogen content in the process. Preheating temperatures are available in ASTM for type of HSLA or one can supply it from the provider's data sheet. Post-welding-heat-treatment aims to relieve the residual stresses and prevent the formation of a brittle structure. Post heating also decreases the potential of HIC, hydrogen-induced-cracking. Evacuating the weld region free from hydrogen immediately after the weld process, a post heating is necessary.

The product suppliers of HSLA steels [31] prove that HSLA Steels with yields strengths such as 700 MPa, 960 MPa, 1100 MPa etc. has good compatibility with MAG Welding. In the research conducted by Gür [33], the compatible welding gas is defined as M20 (8%CO_2, 92%Ar) and the compatible filler material is defined as ER110SG (NiMoCr). This filler material has same strength characteristics as a 700 MPa HSLA steel. Consumable filler material selection is significant in the aspects of strength, mechanical preparation, low Hydrogen content and response to the heat treatment. In the work, the test specimens of the welded sections give similar mechanical results with the product supplier of the HSLA Steel especially in terms of Yield Strength and Ultimate Yield Strength. It is also clarified in the paper that this kind of steel has a high utility in manufacturing of lifting equipment even in the military sector. According to the supplier SSAB [31], unalloyed, low alloyed and stainless-steel consumables should be preferred while welding a Strenx steel.

Leitner et al. [34] conduct the fatigue analysis of the welded area subjected to High-Frequency-Mechanical-Impact-Treatment (HFMI) combined with Post-Heat-Treatment (PHT) is researched. HFMI is a mechanical post-weld-treatment that reduces the geometrical notch, emerges a compressive residual stress and increases the local hardness. The research covers the two HSLA Steels S690 and S960. The search is conducted under the strong recommendation of International Institute of Welding (IIW) that the fatigue strength of welded structures is independent of the base metal which is an HSLA Steel for the case. Therefore, enhancement in the weld area is an obligation before the welding as preheat and inter-pass or post HFMI-treatment. Figure 3.3 shows the results of weld test for 960 MPa steel.

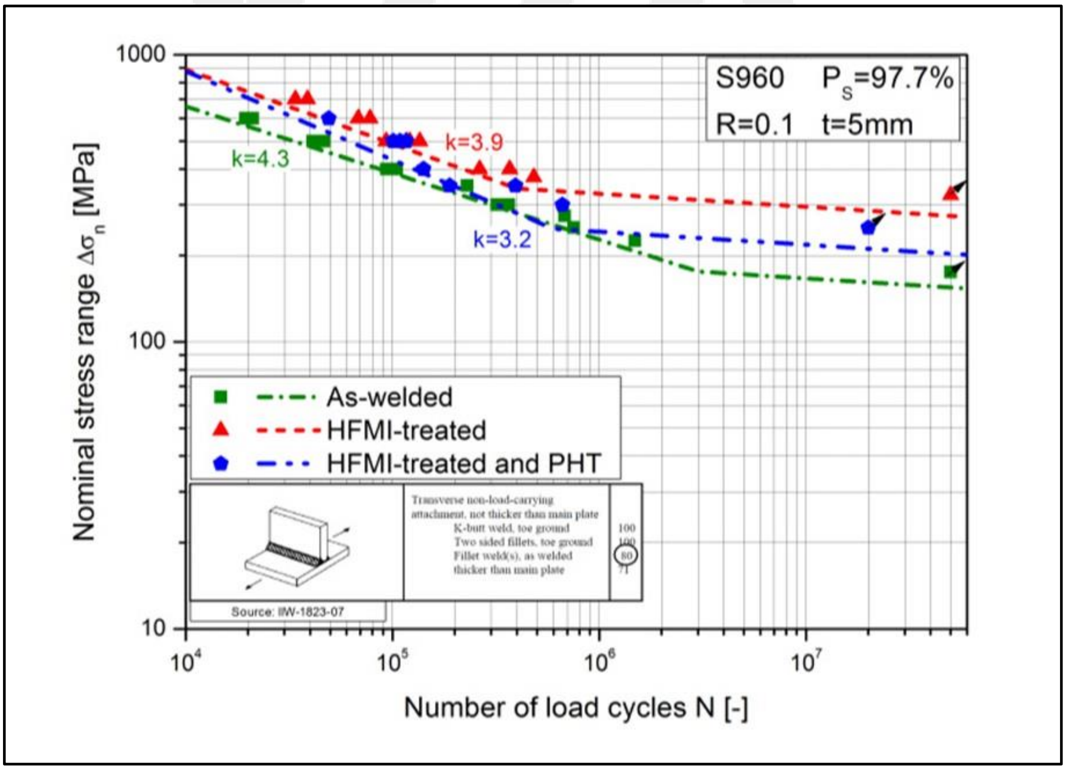

Figure 3.3: S-N Curve by Leitner et al. [34].

Table 3.3 shows the results that Leitner et al. [34] obtained for HFMI-treated S960 Steel fatigue stress S-N logarithmic curve. The values are taken from the above test data by the deriving a general logarithmic-curve formula for the given values of Leitner et al. [34].

$$A.(x)^n = y \tag{3.1}$$

$$5582{,}89.(Number\ of\ Cycles)^{-0{,}1982} = Nominal\ Stress \tag{3.2}$$

Table 3.3. below gives some of the values for the above equation.

Table 3.3: S-N Curve Values for S960 HSLA Derived from Logarithmic Curve Formula.

Stress [MPa]	N (Cycles)
314,99	2.10^6
361,38	1.10^6
387,84	7.10^5
458,74	3.10^5
570,30	1.10^5
900,00	1.10^4
960,00	0

A similar weld fatigue behavior test is conducted by Jonsson et al. [35] for 1100 MPa yield strength HSLA steel. The results of them are also similar to that of Leitner et al. [34] for HFMI-treated welded steel.

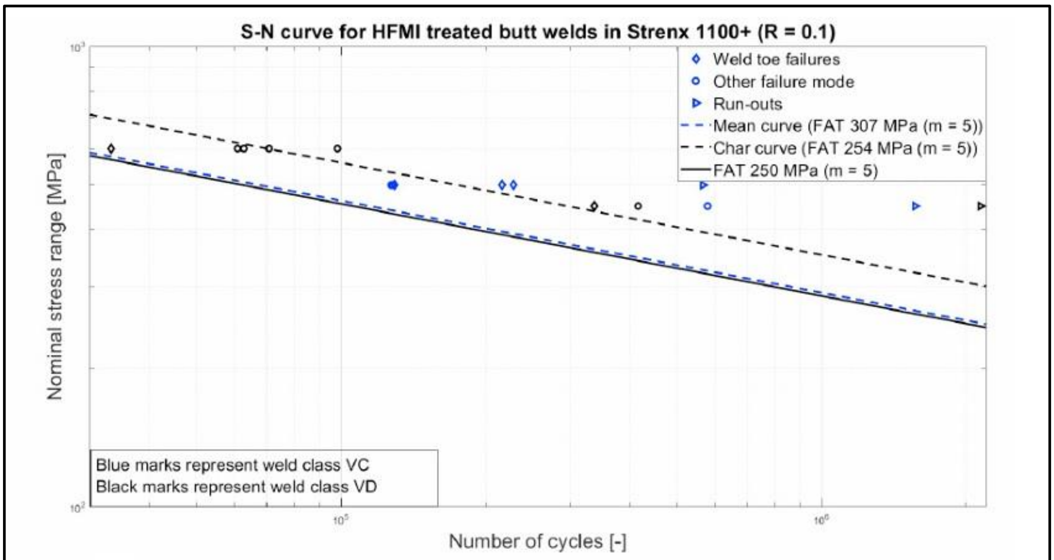

Fatigue evaluation of HFMI treated Strenx® 1100Plus butt welds.

Figure 3.4: S-N Curve by Jonsson et al. for STRENX-1100 [35].

Same formula derivation is executed like the above test data for the table values of Jonsson et al. [35].

The general logarithmic curve, given by Eq. (3.1), is used again to model the data.

$$4551{,}40.(Number\ of\ Cycles)^{-0{,}20} = Nominal\ Stress \qquad (3.3)$$

Table 3.4. below gives some of the values for the above equation.

Table 3.4: S-N Curve Values for STRENX1100 HSLA Derived from Logarithmic Curve Formula.

Stress [MPa]	N (Cycles)
250,00	2.10^6
287,17	1.10^6
300,28	8.10^5
378,93	$2{,}5.10^5$
455,14	1.10^5
721,34	1.10^4
1100	0

Both successive S-N Curve data for 960 MPa and 1100 MPa HSLA steels prove that for the fatigue case of welded HSLA steel members, the base metal strength is not an exact parameter and the weld fatigue strengths mainly depend on other factors such as preheating temperature, inter-pass times, consumable metal, base metal composition etc. Therefore, a 1100 MPa Steel strength can be selected with a fatigue data inserted from Table 3.4. It can be noticed that for 250.000 cycles, the maximum allowable stress is 378,93 MPa.

3.2 DESIGN LOADS AND LOADING COMBINATIONS ACCORDING TO "FEM 1.001-RULES FOR THE DESIGN OF HOISTING APPLIANCES"

In the chapter 2 of Specification FEM 1.001 [30], loads subjected to the structure and mechanism of the hoisting appliances are clarified separately. The floor crane loads are determined via this standard [30]. Primarily, the following abbreviations should be presented:

Table 3.5: Forces and Force Multiplication Factors that are Considered in the Structural Design.

Force	Description
S_G	All Dead Weights in the Crane including Self Weight, Counterweight etc.
S_L	Design Payload of the Crane
S_H	Horizontal Inertial Effect Contribution of the Payload
S_W	Wind Force on Payload and Crane
S_{WMA}	Maximum Wind Force for the Case of Gust-Sudden Wind
S_T	Buffer Load, i.e., Collision Impact Load
q	Wind Pressure
γ_C	Load Amplifying Coefficient from Table T.2.3.4. FEM 1.001 [30]
ρ_1	Dynamic Test Coefficient for Hoisting Motion Acceleration from Clause 8.1.1. FEM 1.001 [30]
$\rho 2$	Dynamic Test Coefficient for Hoisting Motion Acceleration from Clause 8.1.2. FEM 1.001 [30]
ψ	Dynamic Coefficient of Vertical Payload for Hoisting Motion Acceleration
ξ	Flexible Jib Crane Experimentally Determined Coefficient from Section 2.2.2. FEM 1.001 [30]

S_G is the *Dead Load* on the crane. S_L is the *Crane Working Load*, that is payload of the crane. S_H is the *Horizontal Inertia Load* on the crane. S_W is the *Wind Load* on the crane and the load material. S_{WMAX} is the *Maximum Wind Load* on the crane for the designated working environment elevation when the crane is out of service. S_T is the impact load due to collision. The working load or payload is designated previously as S_L=*250 kg*.

The loads are combined in four separate cases according to the specification Section 2.3. [30]. All cases have a different force content or different amplification factors. Table 3.6 summarizes the force content of each combination;

Table 3.6: Loading Combinations.

Combination No.	Combination Content
CASE 1	All Self Weights, Payload, Driving Acceleration Force
CASE 2	All Self Weights, Payload, Driving Acceleration Force, Wind Force
CASE 3	All Self Weight, Payload, Max. Wind Load, Collision Impact Load
FATIGUE CASE	All Self Weights, Payload, Driving Acceleration Force with γ_C=1

CASE 1 includes all the dead loads, the design payload and the driving acceleration horizontal effect.

CASE 2 adds the contribution of wind load to CASE 1.

CASE 1 and CASE 2 load amplification factors are the same except the wind load.

FATIGUE CASE is only slightly different from CASE 1. The load amplifying coefficient γ_c of CASE 1 is omitted and taken as 1. It can be commented that the FEM 1.001 [30] doesn't take wind loads, gust loads and collision impact loads as influential repetitive loads for fatigue design.

CASE 3 looks into extraordinary conditions such as maximum wind load in a gust event, impact load that a collision generates and last one the sudden changes in vertical hoisting motion acceleration.

The load combinations and with the corresponding coefficients for each are as follows;

$$CASE\ 1 = \gamma_C(S_G + \psi S_L + S_H) \tag{3.4}$$

$$CASE\ 2 = \gamma_C(S_G + \psi S_L + S_H) + S_W \tag{3.5}$$

$$CASE\ 3 = Max\ (S_G + S_{WMAX}\ ; S_G + S_L + S_T\ ; S_G + \psi\rho_1 S_L\ ; S_G + \rho_2 S_L) \qquad (3.6)$$

$$CASE\ Fatigue = (S_G + \psi S_L + S_H) \qquad (3.7)$$

ρ_1=1.2 and ρ_2=1.4 according to Item 8.1.1. and 8.1.2. [30].

According to International Organization for Standardization standard ISO 12482-1:1995 [36], cranes are designed for a finite lifetime duty and this lifetime is typically 10 to 20 years for industrial cranes. FEM 1.001 [30] also arranges the crane design based on a specific design lifetime. Table T.2.1.2.5. [30] identifies the shop crane classification as A3 class, A4 class and A5 class. The class quality increases with the numbers. For the lifetime of an A4 class workshop crane, the standard then directs the user to Table T.2.1.4. [30] where the maximum allowable load cycle class for a moderate loading regime is U4 and for a moderate to heavy loading regime is U3. When one refers to table T.2.1.1. [30] once again, U4 class defines a life cycle of maximum 250.000 cycles. Over a rough exaggerated estimation of using the crane 40 times a day, 310 days a year and for a lifetime of 20 years, this makes 40x310x20=248.000 cycles. This life time in the yearly base is very close to that suggested by ISO [36]. Moreover, regarding a construction environment, an average per day hoist loading cycle might be considered 20 cycles as well which then corresponds to class U3 in the specification [30]. General load coefficient γ_C is then determined from Table 2.3.4. [30] based on the class. For the selected A4 class γ_C is found as 1.11 from Table 2.3.4.

γ_C=1.08 according to Item 2.3.4. [30].

ψ is the Dynamic Coefficient Factor for the vertically hoisted working load. These loads result from the acceleration or deceleration of the hoisting motion and the inertia shock that the mass creates under the vertical acceleration. The coefficient is calculated according to Item 2.2.2.1.1 of the spec [30]. The item clearly identifies a factor for jib cranes as ξ=0.3 because the jibs are none-rigid members of a structure and the flexibility of this member makes a decrease in the dynamic coefficient compared to more rigid overhead travelling cranes and bridge cranes. As a safe assumption, a hoist motor of V_L=1 m/s vertical motion is selected.

$$\psi = 1 + \xi V_L \qquad (3.8)$$

$$\xi = 0.3 \; for \; Jib \; Crane$$

By substituting the values of ξ and V_L into Eq. (3.8), we obtain ψ=1.3.

By using the vertical hoisting acceleration dynamic coefficient factor, ψ, there is no need for further vertical hoisting dynamic analysis in MATLAB. This factor accounts for an inertial acceleration of 3 m/s², which corresponds to an additional inertial load of 750 N (i.e., 75 kg for a 250 kg payload). This value is significantly higher than the expected motor acceleration, which corresponds to an operating speed of 1 m/s.

In conclusion, the combinations with amplification factors applied are the following;

By substituting the factors into Eq. (3.4), *Case 1* yields 1.08 × (S_G + 1.3S_L + S_H),

Into Eq. (3.5), *Case 2* yields 1.08 × (S_G + 1.3S_L + S_H) + S_W,

Into Eq. (3.6), *Case 3* yields *max* |S_G + S_{WMAX} ; S_G + S_L + S_T ; S_G + 1.3×1.2 × S_L ; S_G + 1.4S_L|,

Into Eq. (3.7), *Case Fatigue* yields (S_G + 1.3S_L + S_H).

3.2.1 Determination of Wind Load S_W and Maximum Wind Load S_{WMAX}

The standard FEM 1.001 table T2.2.4.1.2.1.[30] defines 3 types of wind condition. These 3 types and the related wind speed values are given in Table 3.7;

Table 3.7: Wind Speeds.

Type of Appliance	Wind Speed in Service (m/s)
Lifting appliance in light wind and erection operations	14
All normal types of cranes installed in the open	20
Appliance which must continue to work in high winds	28

The floor crane is designated to carry formwork loads or steel rebar loads in erection operations. As it will be operated on a fresh concrete slab, heavier design assemblies should be avoided as much as possible. Therefore, it is not designated for heavy storms or gusts. Selecting the minimum design wind speed option will reduce the overall dimensions and counterweight of the crane. Furthermore, it is an erection crane as specification states [30].

A conventional prefabricated reinforced column form has an approximate area of *3m x 1 m = 3 m^2*. The FEM Standard defines [30] the dynamic wind pressure correlated with wind speed by the formula where wind speed V_s is in m/s and wind pressure q is in N/m^2. V_s=14 m/s and the related wind pressure q as 125 N/m^2.

$$q = 0.613\, V_s^2 \tag{3.9}$$

By substituting the value of V_S into Eq. (3.9), q yields 125 N/m^2.

The action of the wind on the hook is related with projected wind area of the load;

$$F = S_W = 2{,}5.\, A.\, q \tag{3.10}$$

By substituting the values of A and q into Eq. (3.10), S_W yields 937.5 N.

Table T.2.2.4.1.2.2 [30] clarifies the out of service maximum wind pressure q_{max} as 800 N/m^2 up to heights of 20 m. elevation. ANSYS has an option to assign the wind pressure directly. However, the projected area of steel box section profiles of the floor crane is calculated as;

$$A_{crane} = 0{,}10 * (4 + 1{,}5 + 1{,}5 + 1{,}5 + 1{,}5) = 1\, m^2 \tag{3.11}$$

By substituting the values of A_{crane} and q_{max} into Eq. (3.10), S_{WMAX} yields 2000 N.

3.2.2 Determination of Horizontal Load S_H

Driving acceleration and deceleration inertial loads of the crane are derived from the dynamic analysis performed by MATLAB_Simscape_Multibody software. The dynamic moving pendulum effect is in general related to these specified parameters; *the rope length, mass of the suspended load, the total mass of the crane, the ratio of these subsequent masses, mean duration of acceleration or deceleration, period of free oscillation and finally the value of acceleration or deceleration*. Keeping this information in mind, the MATLAB analysis is performed with modeling a crane-pendulum system that has similar mass distribution with real case. That is to say, the counterweight of the crane which is installed far from the fulcrum point is exactly modeled as in the real case because this mass and its position has significant effect on overall mass distribution and inertia matrix of the system. MATLAB results from Dynamic Analysis show that for a mean 0.*33 m/s^2* acceleration or deceleration to stop or to pace the crane to *1 m/s* velocity in 3 seconds, the maximum acceleration of the total crane and 250 kg suspended load system is computed as;

a_{max}=0,47 m/s^2

$$F_{inertia} = m.a \tag{3.12}$$

By substituting the values of a_{max} and *250 kg mass* into Eq. (3.12), S_H yields 117.5 N.

3.2.3 Comparison of Force S_H of MATLAB and Recommended Value of FEM 1.001

"Section A2.2.3.-Calculation of Loads Due to Acceleration of Horizontal Motions" [30] in standard describes an identical method to find out the inertia effect of payload during a horizontal motion with the above variables computed one by one.

T_m: Mean Duration of Deceleration = 3 seconds

L: Length of the Suspended Load= 2 m

T_L: Period of Oscillation of the Suspended Load

$$T_l = 2.\pi.\left(\frac{l}{g}\right)^{0,5} \tag{3.13}$$

T_l=2,84 seconds

m: Total Mass of the Crane System Other Than the Load = 667 kg (rotational inertias negligible)

m_1: Mass of Payload = 250 kg

F_{cm}: Mean Inertia Load

J_m: Mean Acceleration or Deceleration = 0,33 m/s^2

$$\mu = \frac{m_1}{m} \tag{3.14}$$

By substituting the values of m_1 and m into Eq. (3.14), μ yields 0.375.

$$\beta = \frac{T_m}{T_1} \quad (3.15)$$

By substituting the values of T_m and T_1 into Eq. (3.15), β yields 1.056.

ψ_h: Load Amplification Factor for Inertia Load

$$\psi_h = 2 \; for \; \mu < 1 \quad (3.16)$$

Equation (3.12) is again applied using the variables F_{cm}, m_1 and J_m.

By substituting the values of m_1 and J_m into Eq. (3.12), F_{cm} yields 82.5 kg.m/s^2.

$$F_{cmax} = \psi_h . F_{cm} \quad (3.17)$$

By substituting the values of ψ_h and F_{cm} into Eq. (3.17), F_{cmax} (i.e., S_H) yields 165 N.

S_H found from the MATLAB Simscape Multibody Analysis is 117,7 N and S_H derived from FEM 1.001 Standard [30] is 165 N. The value of S_H for static-structural analysis is taken as 117,7 N for ANSYS calculations.

3.2.4 Description of Buffer Load S_T

As the English Language meaning of “to hit the buffer” means “to come to an unwanted end”, the buffer effect on the suspended load is the impact load of accidental collisions with the surrounding obstacles and according to the FEM 1.001 [30] Standard Item 2.2.3.4, “*it can be computed by considering that the horizontal force applied at the lever of the load which is capable of causing two of the crab wheels to lift”.* This load is calculated from moment arm equilibrium in Section 3.2.7 with taking again into consideration the total counterweight load as $S_{counterweight}=450$.

$$S_T \cong 131.00\,kg = 1310\,N$$

$$S_T = \frac{S_{COUNTERWEIGTH} * MomentArm_{S_{CW}} + S_G * MomentArm_{S_G} - S_L * MomentArm_{S_L}}{MomentArm_{S_T}} \quad (3.18)$$

3.2.5 Overturning Moment Calculations and Specifying the Counterweight

The design working load or in other words payload of the crane is 250 kg.

$$S_L = 250\ kg \cong 2500\ N$$

The total counterweight of the crane consists of an additional ballast that will be mounted separately, a lithium-ion battery, an AC type driving electric motor and a hoist motor. Despite lead-acid batteries have several other advantages, the lithium-ion battery is the most suitable option for this model because it will be hoisted up or down in a construction site and lead-acid batteries cannot be tilted or turned upside down that will cause leakage.

The counterweight is determined from the most inconvenient loading combination. Remembering CASE 1 doesn't cover wind load which has a significant overturning moment arm and CASE 3 is about extreme cases after all the masses, forces and loads are clarified, CASE 2 is the most unfavourable one for overturning of the crane. In the above overturning moment check table, after a couple of trial and errors, a minimum counterweight is calculated as 450 kg.

It should be emphasized that increasing the counterweight is anytime possible for a higher overturning safety as it will be proved later by additional MATLAB investigation. Finite element analysis by ANSYS and motor calculations are also held for 800 kg counterweight. However, the crane is intended to be used on fresh concrete and the lighter it is, the more practical it will be to operate on slabs and high floors. The counterweight is derived from Case 2 as it is the most inconvenient loading case.

From Eq. (3.5), we recall that *Case 2* is given by $1.08 \times (S_G + 1.3S_L + S_H) + S_W$.

S_W, S_H, S_L induces an overturning moment about fulcrum with a (-) sign and S_G and $S_{COUNTERWEIGHT}$ creates a resistive moment against overturning with a (+) sign. Fulcrum Point is the front wheel axle of the crane. To prevent the overturning of the crane subjected to above loads, additional counterweight is necessary which will be installed adjacent to battery and hoist motor units.

Table 3.8: The Moment Equilibrium About Fulcrum for Loading CASE 2.

CASE 2 LOADING	Force (N)	x (m)	y (m)	a (m/s^2)	Inertia Force (N)	CASE 2 Moment (N.m)
1,08*$S_{CRANESELFWEIGHT}$	1,08*217*9,81	0,82	_	_	_	+1885,24
Inertia Effect of 1,08*$S_{CRANESELFWEIGHT}$	_	_	1,61	0,47	1,08*217*0,47	-177,34
1,08*$S_{COUNTERWEIGHT}$	1,08*450*9,81	1,16	_	_	_	+5530,49
Inertia Effect of 1,08*$S_{COUNTERWEIGHT}$	_	_	0,20	0,47	1,08*450*0,47	-45,68
1,40*S_L	1,4*250*9,81	0,70	_	_	_	-2403,45
1,08*S_H	1,08*117,5	_	4	_	_	-507,60
S_{WIND}	937,5	_	4	_	_	-3750
Total Moment About the Fulcrum						+531,66 N.m

The overturning stability factor of the crane is defined as the ratio of $M_{Resisting}$ to $M_{OverTurning}$. In the static lifting case without wind, the factor of safety against overturning is 3.14, including dynamic effects. Under wind conditions, the overturning stability factor can reach to values which complies with relevant standards such as ISO [36] by increasing the counterweight up to 800 kg as mentioned previously.

3.2.6 Specifying the Buffer Load S_T

As mentioned earlier in Section 3.2.4, buffer load is the minimum overturning load applied to the loading point which is able to destabilize the moment equilibrium about fulcrum.

From Eq. (3.6), we recall that *Case 3* is given by *max* $|S_G + S_{WMAX}$; $S_G + S_L + S_T$; S_G + 1.3×1.2 × S_L ; $S_G + 1.4S_L|$.

S_T and S_L induces an overturning moment about fulcrum with a (-) sign and S_G and $S_{COUNTERWEIGHT}$ creates a resistive moment against overturning with a (+) sign.

Table 3.9: The Moment Equilibrium About Fulcrum for Loading CASE 3 and Determining S_T Buffer Load.

CASE 3 Loads	N	x (m)	y (m)	a (m/s^2)	Inertia Force in	CASE 3 Moment N.m
$S_{G\_CRANE\ SELF\ WEIGHT}$	217*9,81	0,82	_	_	_	+1745,59
$S_{G\_COUNTER\ WEIGHT}$	450*9,81	1,16	_	_	_	+5120,82
S_L	250*9,81	0,70	_	_	_	-1716,75
S_T	1310	_	4	_	_	-5240
Total Moment About the Fulcrum						$<\approx$ 0,00

Buffer load is calculated as S_T=*1310 Newton*.

3.3 DIAGRAM OF ALL DESIGN LOADS

Figure 3.5 and Figure 3.6 show a brief description of the unfactored loads and their corresponding moment arms;

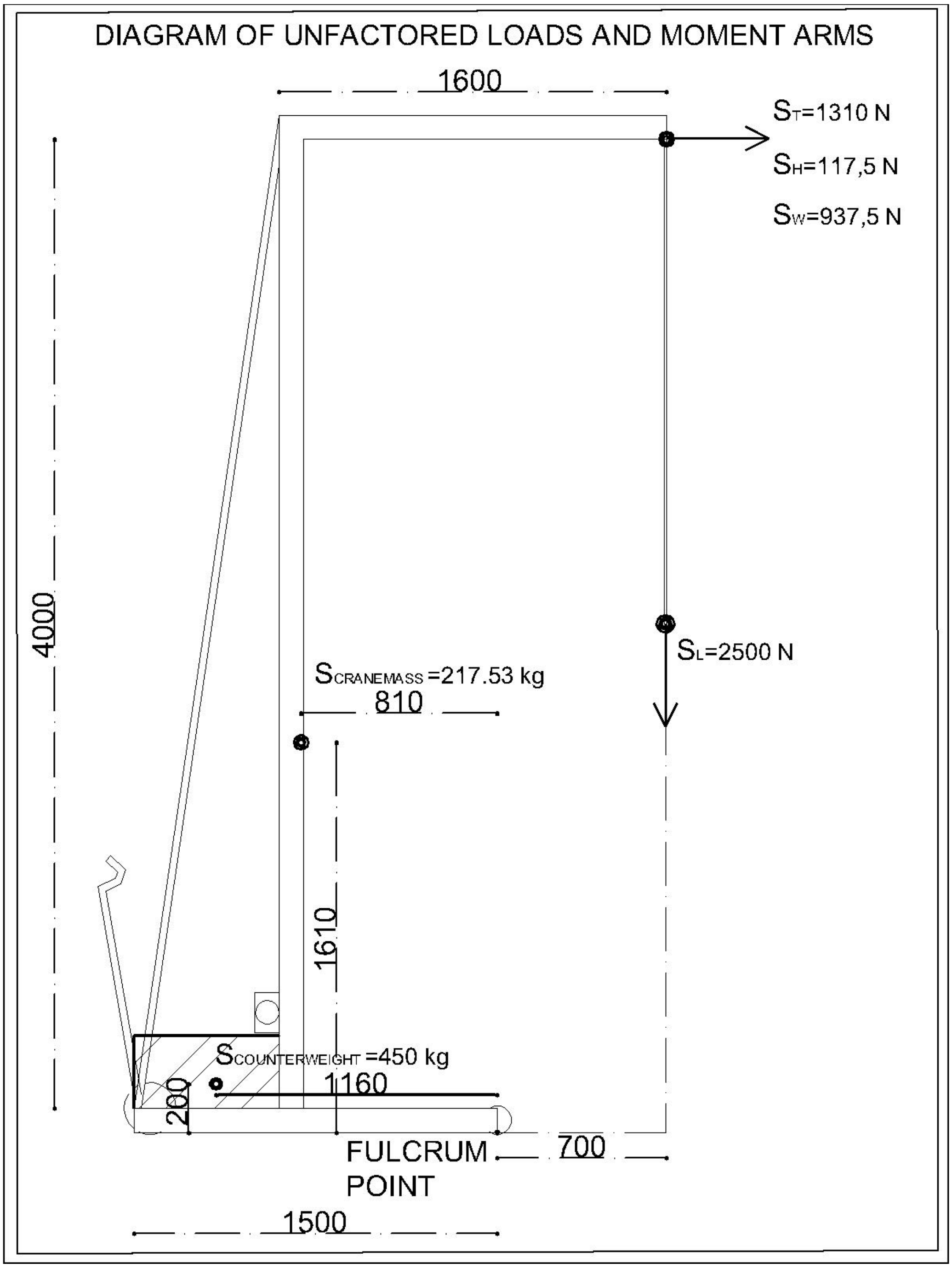

Figure 3.5: Unfactored Design Loads and Corresponding Moment Arms About Fulcrum.

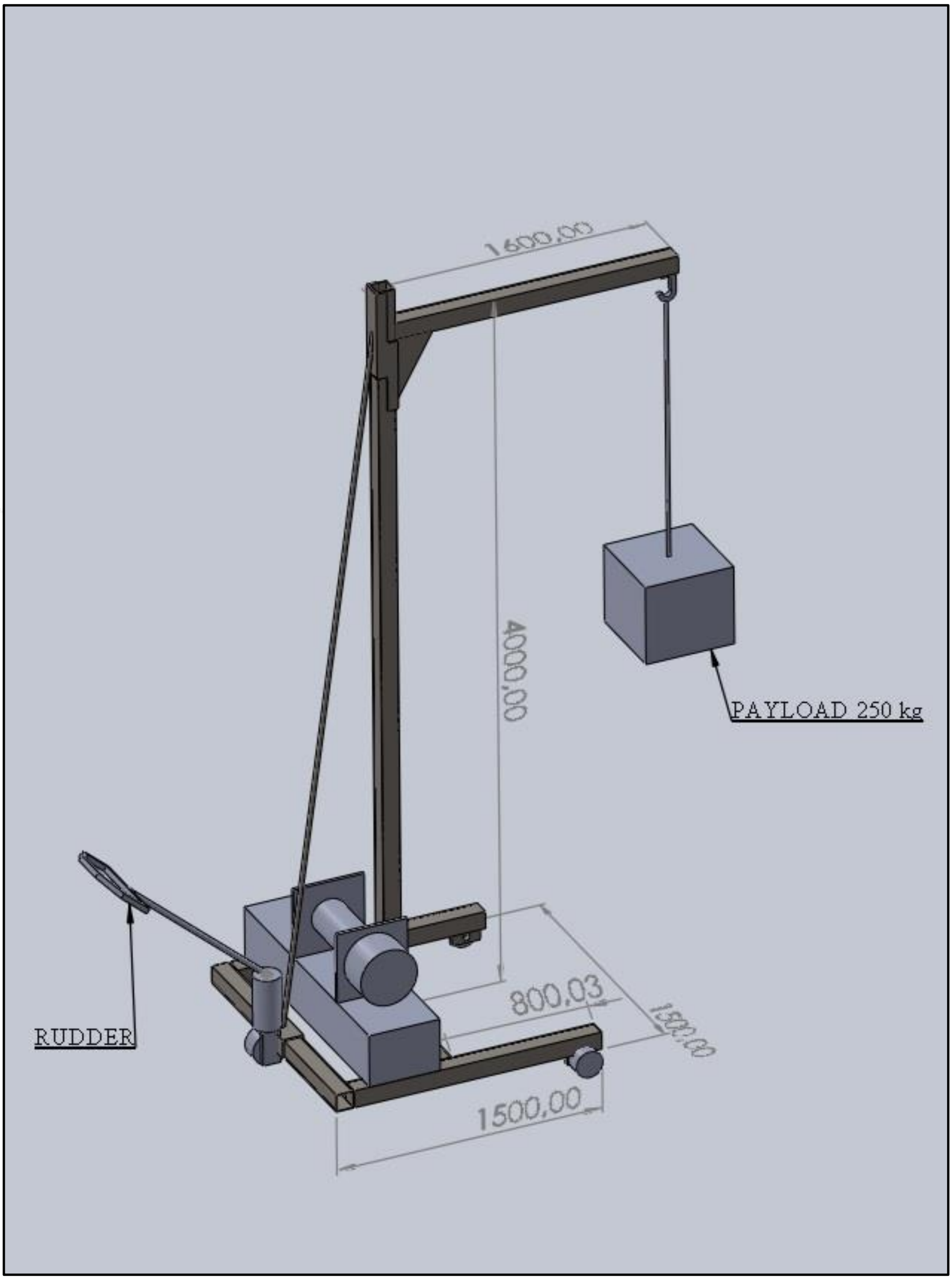

Figure 3.6: Dimensions of the Crane.

3.4 MOTOR CALCULATIONS

In the succeeding subsections, the contribution of masses of these appliances to the counterweight will be inspected. Afterwards, this information will be used to determine whether an additional ballast is necessary or not for counterweight.

The floor crane is a 2 degree-of-freedom machine. It needs a hoisting motor for the vertical axis and another motor for driving the crane horizontally on the floor. The vertical hoisting motion is delivered with a hoist motor which generates a rotational motion by electric energy and transfers it to translational motion directly from the pulley. The horizontal driving motion of the floor crane is also converted from the rotational motion of the second motor and converted to linear motion via a gear system.

Fundamental criteria for choosing the right electric motor according to Groschopp Electric Motor Company [37] are speed, start or stall torque, duty cycle, size, weight, motor life expectancy, maintenance, noise, surrounding temperature, available input power source such as voltage-frequency-current-control, running periodically or running continually, price, quality, and delivery.

There are a variety of electric motors in the market. Common examples are universal AC, universal DC, DC, AC, brushless DC or asynchronous AC. But mainly AC type motors use alternating current and DC type motors use direct current.

For an outdoor construction floor crane, asynchronous AC motors seem to be a good option as the below following reason

a. Asynchronous motors are cheaper than brushless dc motors

b. Good speed regulation with a control

c. High starting torque where for a crane, the load is available before the start of the motor

d. Long life with long maintenance which is limited only by bearings

e. No common wearing parts that must be renewed regularly

f. Maintaining speed over a wide range of torque

g. Gearbox compatibility

In spite of the fact that AC motors have a low efficiency between 40% - 70%, poor speed regulation, higher cost per horsepower and low power levels comparative to size, its durability makes it a better choice for outdoor heavy construction conditions. Moreover, it is recently more preferable in the electric car industry at the same time.

3.4.1 Translational Drive Motor Selection from Conventional Motion Resisting Forces

To attain the required motor size and power, there are 3 factors. These are constant torque, load inertia on acceleration, and desired speed of the total mass. Constant torque is the load torque when the mass is at constant speed with a balancing counter force that creates the opposite torque. It stems from frictional forces and gravitational forces. Meanwhile, the acceleration torque is the amount of force to compel the total mass of the system to reach the required velocity within the required time by overcoming the inertial resistance of all masses against changing their velocity. This is merely Newton's Second Law of motion that states that *'the acceleration of an object is directly related to the net force and inversely related to its mass'* [38].

The following relationship, first introduced in Eq. (3.12), is used again: $F=m.a$

The acceleration torque of the motor might be calculated by usual way or from the FEM 1.001 Standard [30]. Previously, the usual way is used with general formulations via Vehicle Dynamics and next the required torque value of the FEM [30] standard is calculated and the most inconvenient of these two is selected. The relation of acceleration and angular acceleration and torque are;

$$a = r.\alpha \tag{3.19}$$

$$F = m.r.\alpha \tag{3.20}$$

$$T = F.r \tag{3.21}$$

$$T = m.r^2.\alpha \tag{3.22}$$

For dynamic susceptibilities of the freshly poured slab concrete which is resting on a falsework and the dynamic susceptibility of the crane impact loads due to collision with surrounding obstacles and or visible object, Linear acceleration and Linear velocity of the crane is kept as low as possible.

$$V = 1\,m/s \;\text{ and }\; a = 0.33\,m/s^2$$

According to table T2.2.3.1.1. [30], having an average acceleration rate $0.33\,m/s^2$ and gaining the speed to be reached $1\,m/s$ in acceleration time 3 seconds, the crane is regarded as a high speed-high acceleration device.

The crane frame structural mass is 217 kg, m_{crane}=217 kg. For counterweight;

$$m_{motor} + m_{battery} + m_{ballast} = 800\,kg \tag{3.23}$$

$m_{Payload} = 250\,kg$. Therefore, total load for motor design is;

$$m_{total} = m_{counterweight} + m_{cranefame} = 800 + 217 + 250 \tag{3.24}$$

$$m_{total} = 1267\,kg$$

Diameter of the drive motor wheel is $\phi = 30\,cm$ and radius $r = 0.15\,m$;

The angular velocity of the motor is;

$$V = \omega.r \tag{3.25}$$

Alternatively, Eq. (3.25) can be rearranged to express ω as $\frac{V}{r}$.

By substituting the values of V and r into Eq. (3.25), the angular velocity ω is calculated as 6.67 rad/s (i.e., rotational speed N=63.7 rpm).

The necessary time to gain the angular speed is again 3 seconds which makes

$$\alpha = \frac{d\omega}{dt} = \frac{6{,}67}{3} = 2{,}23\,rad/\sec^2 \tag{3.26}$$

The acceleration torque T_a (running up to speed) of linear mass system can also be obtained from Eq. (3.22).

By substituting the values of m_{total}, α and r into Eq. (3.22), the acceleration torque T_a is calculated as 63.57 N.m.

Additional inertial force comes from the rotational inertia of shaft and wheel but since these are small and negligible amounts, it is neglected and considered as perishing in the factor of safety multiplication of the Torque. However, one can easily add these values from the following formulas;

$$J = \frac{mxr^2}{8} \tag{3.27}$$

and the rotating pieces' additional torque

$$T_{Rot} = Jx\alpha \tag{3.28}$$

For calculating the total travel resistance torque, one needs the Rolling resistance f of the crane. Rolling resistance f of a body, i.e. rolling friction or rolling drag is the friction force that is resisting while a body is rolling on a surface. For floor crane on rubber tire, this value is $f = 0.015$. This value is taken from Decadura Solid Tires internet site showing the frictional resistance of rubber tyre electric stackers or rubber tyre electric forklifts [39]. It is stated that a solid tire rolling friction is 15% higher than that of a pneumatic rubber tire which has a coefficient value 0.013.

The total travel resistance force is calculated as;

$$F_s = f.m.g = 0{,}015x1267x9{,}81 = 186{,}44\ N \tag{3.29}$$

By substituting the values of F_S and r into Eq. (3.21), the travel resistance torque $T_{TravelResistance}$ is calculated as 27.96 N.m.

$$T_{Total} = T_a + T_{TravelResistance} \tag{3.30}$$

By substituting the values of T_a and $T_{TravelResistance}$ into Eq. (3.30), the total torque T_{Total} is calculated as 91.53 N.m.

General motor power formula is given by:

$$Power\ (kW) = \frac{f_s x T_{total} x N}{9548} \tag{3.31}$$

The load multiplication factor of safety is randomly taken as $f_s = 2$ to stay on the safe side. Thus, the required torque for driving electric motor is found by substituting the values of f_s, T_{Total} and rotational speed N into Eq. (3.31) as 1.22 kW.

$$Power_{DRIVINGMOTOR}=1.22\ kW$$

3.4.2 Translational Drive Motor Selection from FEM 1.001

So far, the necessary power selection of the driving motor according to a basic Vehicle Dynamics approach is attained. On the other hand, FEM 1.001[30] set forth also some other conditions based on same Vehicle Dynamics understanding. The following computation shows FEM 1.001 [30] approach for determining necessary torque of horizontal motion motor from section 5.8.3.

$$m = equivalent\ mass\ of\ loads, structure\ and\ rotating\ parts$$

$$m_L = Mass\ of\ lifted\ load, w_0 = Travel\ Resistance\ at\ Zero\ Wind,\ a = Acceleration$$

$$V = Travel\ Speed\ of\ the\ Crane\ ,\ n_m = Rotation\ Speed\ of\ Motor\ rev/min$$

$$\eta = Overall\ efficiency\ of\ the\ mechanism$$

$$w_8 = Total\ Travel\ Resistance\ at\ wind\ pressure\ q = 80\ N/m^2$$

$$w_{25} = Total\ Travel\ Resistance\ at\ wind\ pressure\ q = 250\ N/m^2$$

$$Case\ 1\ \ T = [a.(m + m_L) + w_0].V.\frac{60}{2.\pi.n_m.\eta} \tag{3.32}$$

$$Case\ 2 = Max\left|[a.(m + m_L) + w_8.Area].V.\frac{60}{2.\pi.n_m.\eta}; w_{25}.Area.V.\frac{60}{2.\pi.n_m.\eta}\right| \tag{3.33}$$

Remembering the general formula

$$V\left(\frac{m}{s}\right) = n_m\left(\frac{Rev}{Min}\right) * 2\pi\left(\frac{Rad}{Rev}\right) * 1\left(\frac{min}{sec}\right) * \frac{r}{60} \tag{3.34}$$

And if we extract r from the above general formula above

Alternatively, Eq. (3.34) can be rearranged to express *r as* $V.\frac{60}{2.\pi.n_m}$

It is apparent that the FEM Standard [30] uses the general formula $Torque = Force * radius$ identically with a slight difference of using an efficiency parameter. With an estimated efficiency $\eta = 0.80$

By substituting the values of w_8 (i.e., F_S), w a, m, m_L, V, n_m (i.e., N), η into Eq. (3.32), *Case 1 Torque T* yields 113.28 N.m.

$$Case\ 1\ Torque\ T \cong 113{,}28\ N.m$$

By substituting the values of w_0, w_8, w_{25}, *load area*, a, m, m_L, V, n_m (i.e., N), η into Eq. (3.33), *Case 2 Torque T* yields from Max|203.23; 316| as 316 N.m.

$$Case\ 2\ Torque\ T = 316\ N.m$$

One can notice that a travel resistance counting a wind load effect of a $2x3\ m^2$ load particle with a wind pressure of $q=250\ N/m^2$ generates a great difference in the final Torque that is necessary for the motor compared to $P=1.24\ kW$ from the general approach.

Equation (3.31) can be again applied using the variables maximum torque T_{FEM} from FEM 1.001 [30] and rotational speed N to calculate the required motor power $Power_{FEM}$ according to FEM 1.001 [30].

By substituting the values of N and *Case 2 Torque* T_{FEM} into Eq. (3.31), $Power_{FEM}$ yields 2.11 kW.

$$Power_{DRIVINGMOTOR\_FEM} = 2.11\ kW$$

$$P_{DRIVING\ MOTOR\ FEM} = 2.11\ kW > P_{DRIVING\ MOTOR\ VEHICLE\ DYNAMICS} = 1.24\ kW$$

The translational motor power required by FEM 1.001 [30] is significantly higher than that estimated by a general vehicle dynamics approach, as the standard [30] accounts for increased wind resistance acting on the load.

The closest market production for this requirement is a 2500 Watt – 1800 kg – Forklift driving Wheel Assembly Wheel Drive System with a mass m=56.4 kg.

$$m_{drivingmotor} = 56.4\ kg$$

3.4.3 Vertical Hoisting Motor Selection from FEM 1.001

FEM 1.001 Standard 5.8.2. section [30] also presents the below formulas for determination of the required power for Motors of Vertical Motion, in other words, for a hoisting motor;

$$P_{Nmax} = L * V_L * 10^{-3} * \eta \tag{3.35}$$

Where:

L=maximum nominal permissible lifting force [N] = 250kg x 9,81m/s^2

V_L=lifting speed [m/s] = 26 m/min = 0.43 m/s

η=efficiency of the machinery (0,82 for a standard market product construction hoist)

By substituting the values of L and V_L and η into Eq. (3.35), P_{Nmax} yields 0.86 kW.

$$T_{Nmax} = P_{Nmax} * \frac{9550}{N_m} \tag{3.36}$$

Given a drum radius r=0.075 m and and a linear velocity V_{linear} = 26 m/min (i.e., V_{Linear}=0.433 m/s), the angular velocity ω can be calculated from Eq. (3.25) as 5.77 rad/s.

$$N_m = 5{,}77\left(\frac{rad}{sec}\right) * 60 * \left(\frac{sec}{\min}\right) * \frac{1}{(2\pi)\left(\frac{rev}{rad}\right)} = 55{,}1\ rev/min \tag{3.37}$$

By substituting the values of N_m and P_{Nmax} into Eq. (3.36), T_{Nmax} yields 149.01 N.m.

The specification [30] requires that $T_{max} \geq 1{,}4 * T_{Nmax}$ for all types of motors supplied by voltage, where T_{max} is the maximum torque of the motor. In other words, this increases the required torque by applying a specific safety factor.

$$T_{max} = 1.4 * 0{,}86 * \frac{9550}{55{,}1} = 208{,}68\ N.m \tag{3.38}$$

Then the maximum required power of the hoisting motor, according to FEM 1.001 [30], is calculated from Eq. (3.31) by substituting T=T_{max} and N=N_m, yielding 1.20 kW.

$$P_{MAX\_FEM\,STANDARD} = 1.20\ kW$$

3.4.4 Vertical Hoisting Motor Selection Verification from a Real-time Site Hoist that is Mounted on a Derrick

The above value *1.20 kW* is the required torque according to the specification [30]. It is also possible to check the selected market electric hoist motor directly from the efficiency values of the product [40].

Hoist Motor Selection from Market Products:

Mass = 60 kg, Lift capacity = 250 kg

Drum Speed (V_{Linear}) = 24 m/min. = 0.4 m/sec

Power – 2 Hp = 1.5 kW

Gearbox Efficiency =0.80

25 m rope –AC – Low Noise & Weight – Pulley Radius r=7.5 cm – Speed up Time 1 second

By substituting the values of r and V_{Linear} into Eq. (3.25), the output angular speed of the motor ω_{out} is calculated as 5.333 rad/s.

Gearbox efficiency $\eta=0.80$

$$T_{OUT} = T_{acceleration} + T_{Gravitation} + T_{Pulleyfriction} \tag{3.39}$$

$$T_{out} = \left(F_{acceleration} + F_{Gravitation} + F_{Pulleyfriction}\right) * r \tag{3.40}$$

$$F_{Pulleyfriction} \approx T - T * e^{\mu\beta} \tag{3.41}$$

Coefficient of friction μ=0.1 for steel rope and cast-iron pulley.

Angle of contact for pulley $\beta = \pi/2$

Pulley tension force T=250 kg = 2500 N is on the maximum side of the pulley. By substituting the values of Pulley Tension T, β and μ into Eq. (3.41), the pulley friction force $F_{Pulleyfriction}$ is calculated as 425 N.

$$T_{Out} = \left(m.a + m.g + F_{Pulleyfriction}\right) * r \tag{3.42}$$

By substituting the values of Lift Capacity m, Linear Acceleration a, r and $F_{Pulleyfriction}$ into Eq. (3.42), the output torque T_{out} is calculated as 223.3 N.m.

$$T_{In(actual)} = \frac{\dfrac{T_{Out}}{n_{gearboxratio}}}{\eta} \tag{3.43}$$

$$T_{In(actual)} = \frac{\dfrac{223,3}{0,8}}{n_{gearboxratio}} = \frac{279,13}{n\ _{gearboxratio}} N.m \tag{3.44}$$

$$Power(W) = T_{in} * \ \omega_{in} = T_{in} * \omega_{out} * n_{gearboxratio} \tag{3.45}$$

$$Power(W) = \left(\frac{279,13}{n_{gearboxratio}}\right) * \left(5,333 * n_{gearboxratio}\right) = 1488\ W \approx 1500\ W \tag{3.46}$$

Mass of the electric hoist motor product of these power values on the market is 65kg [40].

Figure below displays an example of construction hoist in the same class;

Teknik Bilgiler	Model / Km - V250
Motor Gücü	2 Hp 380 V
Kaldırma Kapasitesi	380V 250KG
Hız	26-30 m/dk
Halat Boyu	25 /50 m
Halat Çapı	Ø8 mm
Ağırlığı	~65 Kg

Figure 3.7: Construction Hoist from the Market [40].

4. RESULTS

4.1 STRUCTURAL ANALYSIS RESULTS

The crane model is defined in ANSYS Finite Element Method Software with precision. Some of the significant parameters that are used in ANSYS are shown in Table 4.1.

Table 4.1: ANSYS Parameters.

ANSYS Parameters	
Average Skewness	0,25 (Vertex Sizing on stress concentration areas)
Wheel Supports	3 Cylindrical Supports in the location of rubber wheels
Equivalent Uniaxial Stress Value of Stress Tensor	Equivalent Von-Mises (since steel is a ductile material)
Overall Fatigue Strength Factor	K_f=0,60
Desired Fatigue Analysis life-time Cycles	250.000
Fatigue Analysis Theory	Goodman Theory
Fatigue Analysis Method	Stress-Life Method (over 100.000 cycles)

The fatigue analysis S-N curve is taken from Table 3.4 by Jonson et al. [35]. The computed fatigue analysis safety factor for 250.000 cycles is FS=1,47. Mesh damage is not observed as all damage results for 250.000 cycles in the fatigue analysis.

The closest loading combination to a real-time operation is Fatigue-Case loading and maximum payload loading of Case 3. The deformations of the jib in vertical direction are found as 29,99 mm and 34,62 mm respectively with the bending of the jib cantilever.

The maximum stress value appears in the Case 2 loading where wind direction is applied both in plane and toward the out of plane as 385,86 MPa in the jib-mast joint. This value corresponds to a Factor of Safety FS=2,85 for static loading cases for a 1100 MPa HSLA steel. The minimum stress value appears in the Gust Wind Loading Case while the crane is out of service. Minimum stress value is 116,86 MPa. This value corresponds to a Factor of Safety FS=9,41.

4.1.1 Case 1 Loading Combination Results

For this case, the maximum Equivalent Von Mises' Stress is calculated as 283,93 MPa. The following figures are the ANSYS Structural Analysis results for Case 1 Loading;

Figure 4.1: Equivalent Von Mises' Stress. Case 1 Loading.

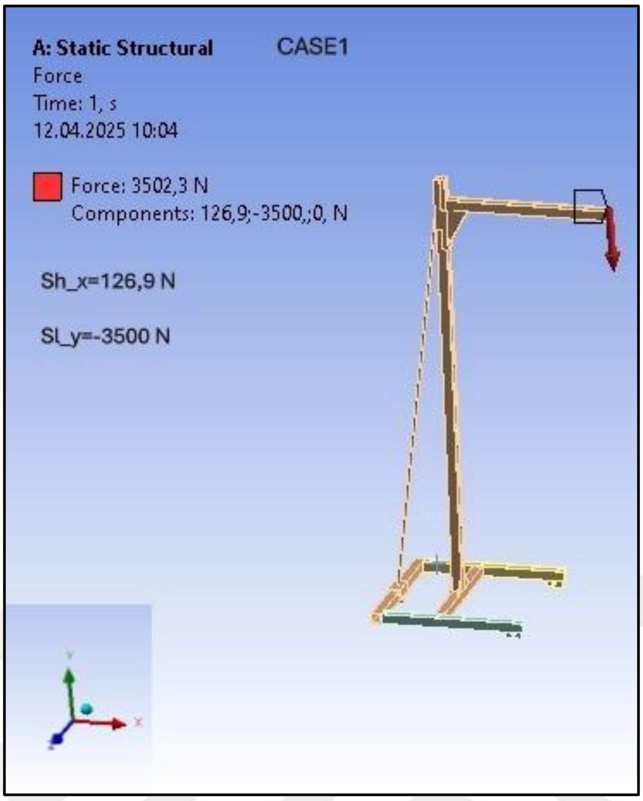

Figure 4.2: Forces. Case 1 Loading.

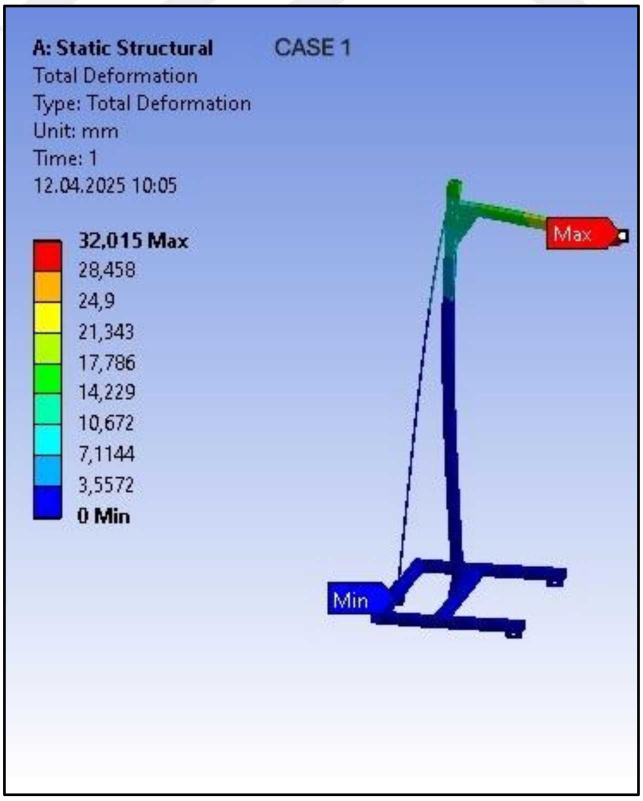

Figure 4.3: Jib Deformation. Case 1 Loading.

4.1.2 Case 2-Wind in X Direction Loading Combination Results

For this case, the maximum Equivalent Von Mises' Stress is calculated as 356,64 MPa. The following figures are the ANSYS Structural Analysis results for Case 2-Wind X Loading;

Figure 4.4: Equivalent Von Mises' Stress. Case 2-Wind X Loading.

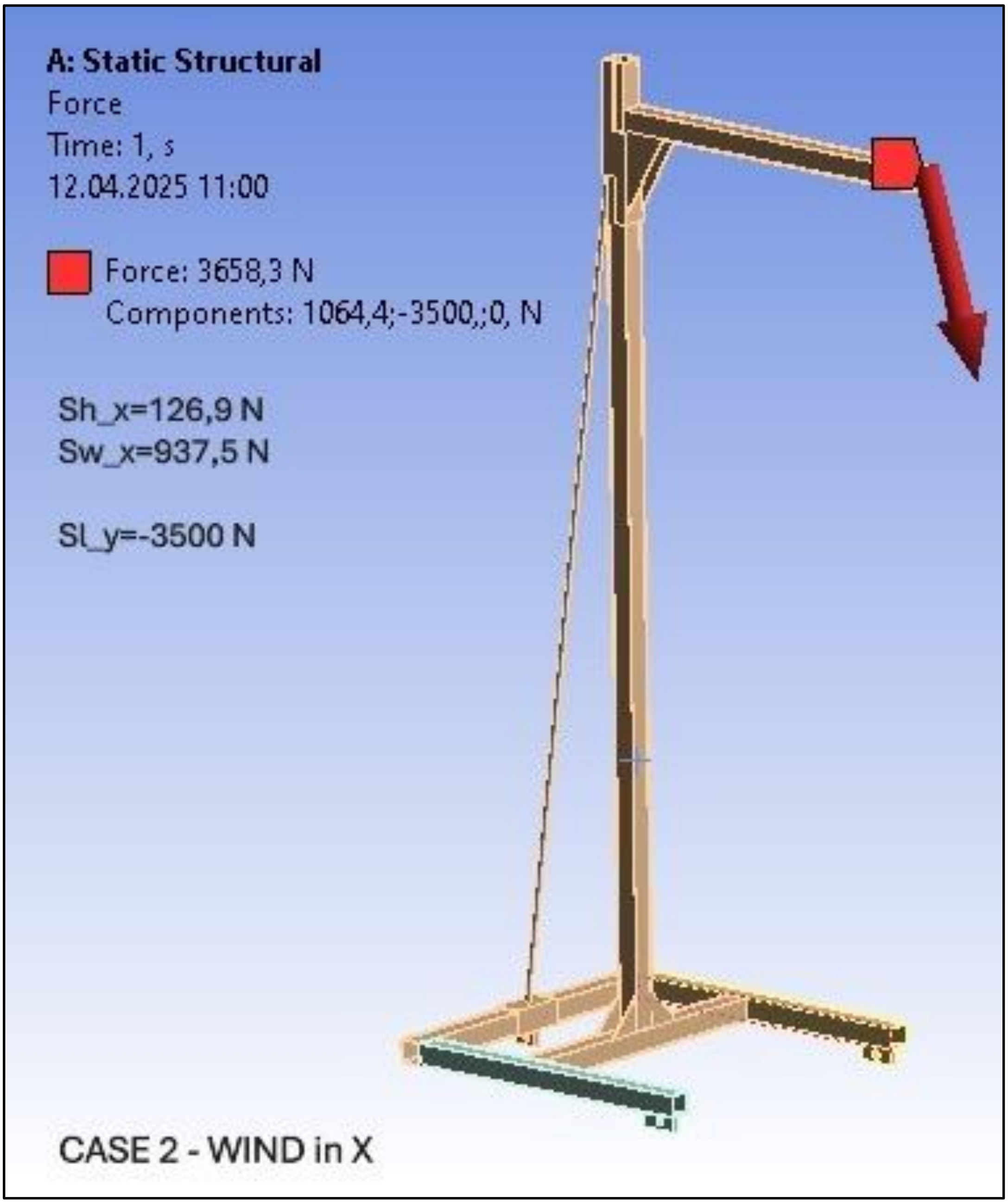

Figure 4.5: Forces. Case 2-Wind X Loading.

4.1.3 Case 2-Cross Wind Loading Combination Results

For this case, the maximum Equivalent Von Mises' Stress is calculated as 385,86 MPa. The following figures are the ANSYS Structural Analysis results for Case 2-Cross Wind Loading;

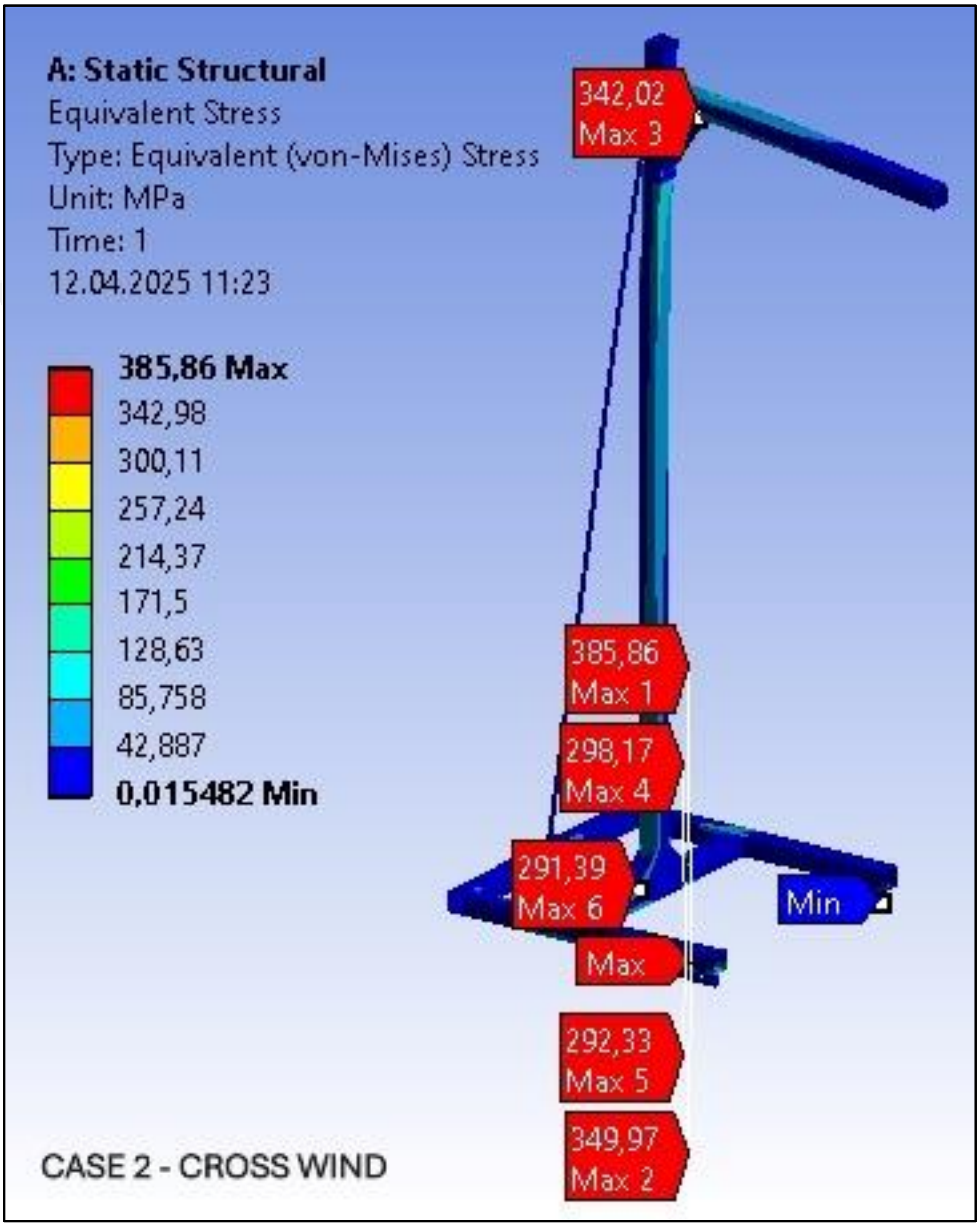

Figure 4.6: Equivalent Von Mises' Stress. Case2-Cross Wind Loading.

Figure 4.7: Forces. Case 2-Cross Wind Loading.

4.1.4 Case 2-Wind in Z Direction Loading Combination Results

For this case, the maximum Equivalent Von Mises' Stress is calculated as 366,83 MPa. The following figures are the ANSYS Structural Analysis results for Case 2-Wind Z Loading;

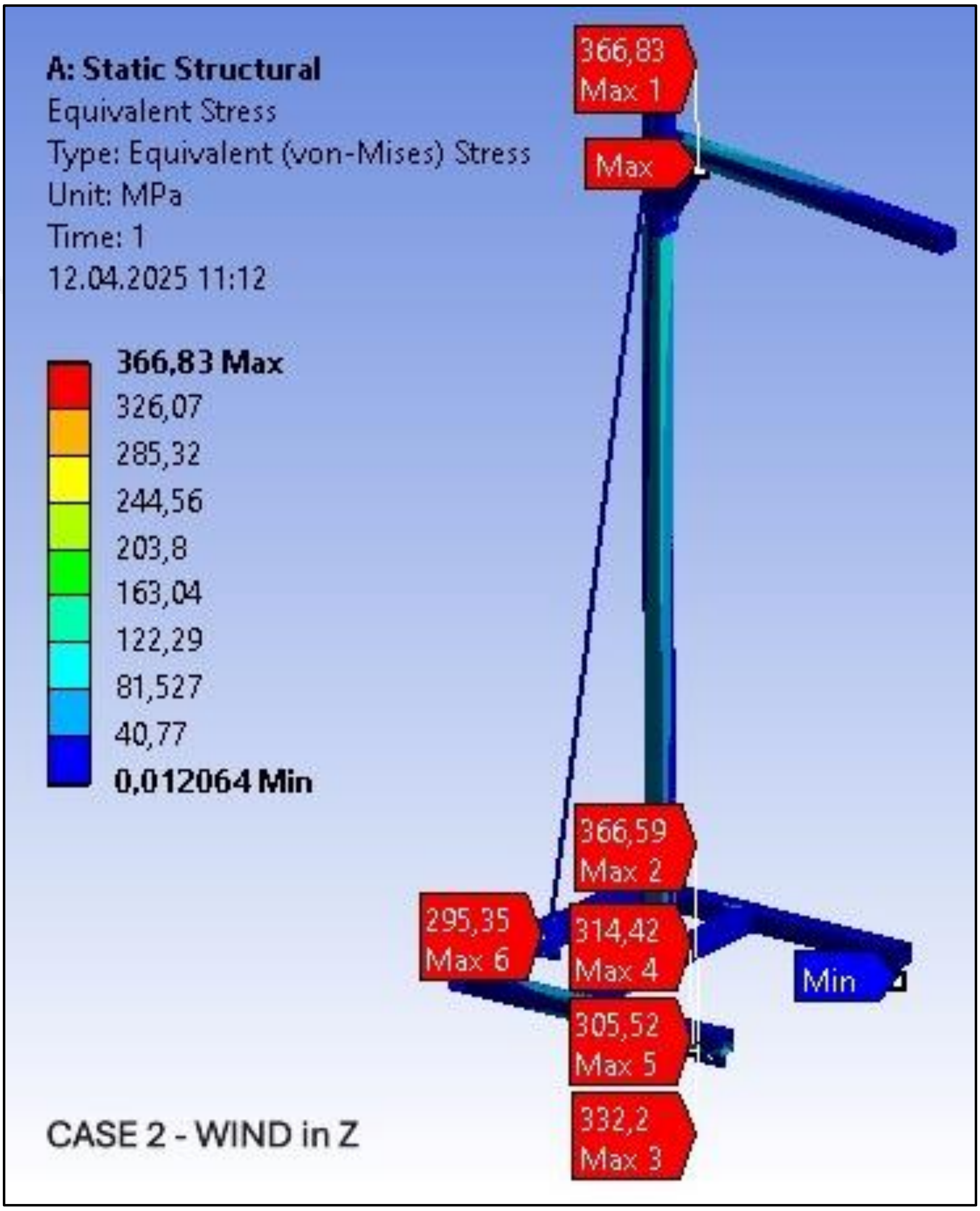

Figure 4.8: Equivalent Von Mises' Stress. Case 2-Wind Z Loading.

Figure 4.9: Forces. Case 2-Wind Z Loading.

4.1.5 Case 3-Collision Loading Combination Results

For this case, the maximum Equivalent Von Mises' Stress is calculated as 320,37 MPa. The following figures are the ANSYS Structural Analysis results for Case 3-Collision Loading;

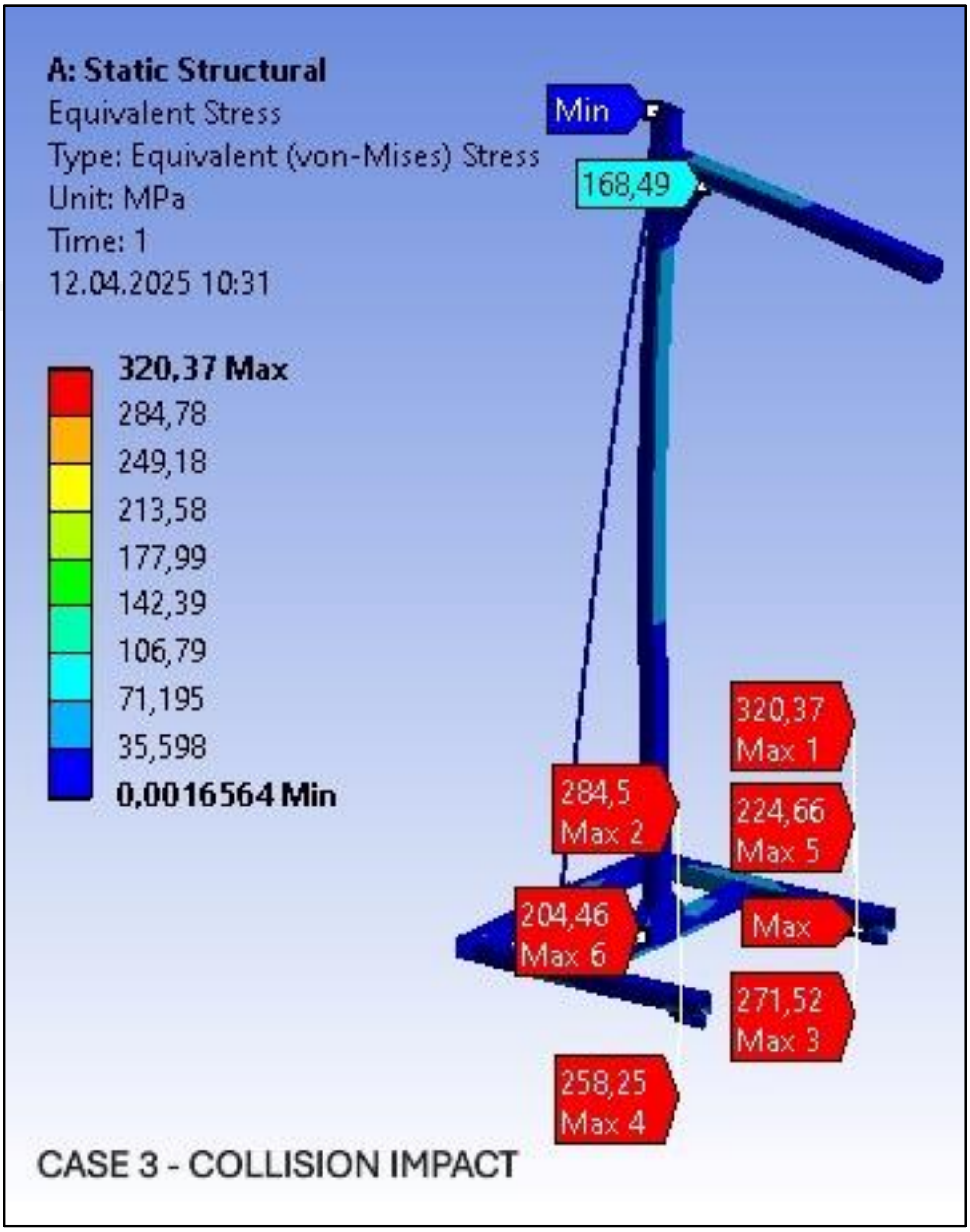

Figure 4.10: Equivalent Von Mises' Stress. Case 3-Collision Loading.

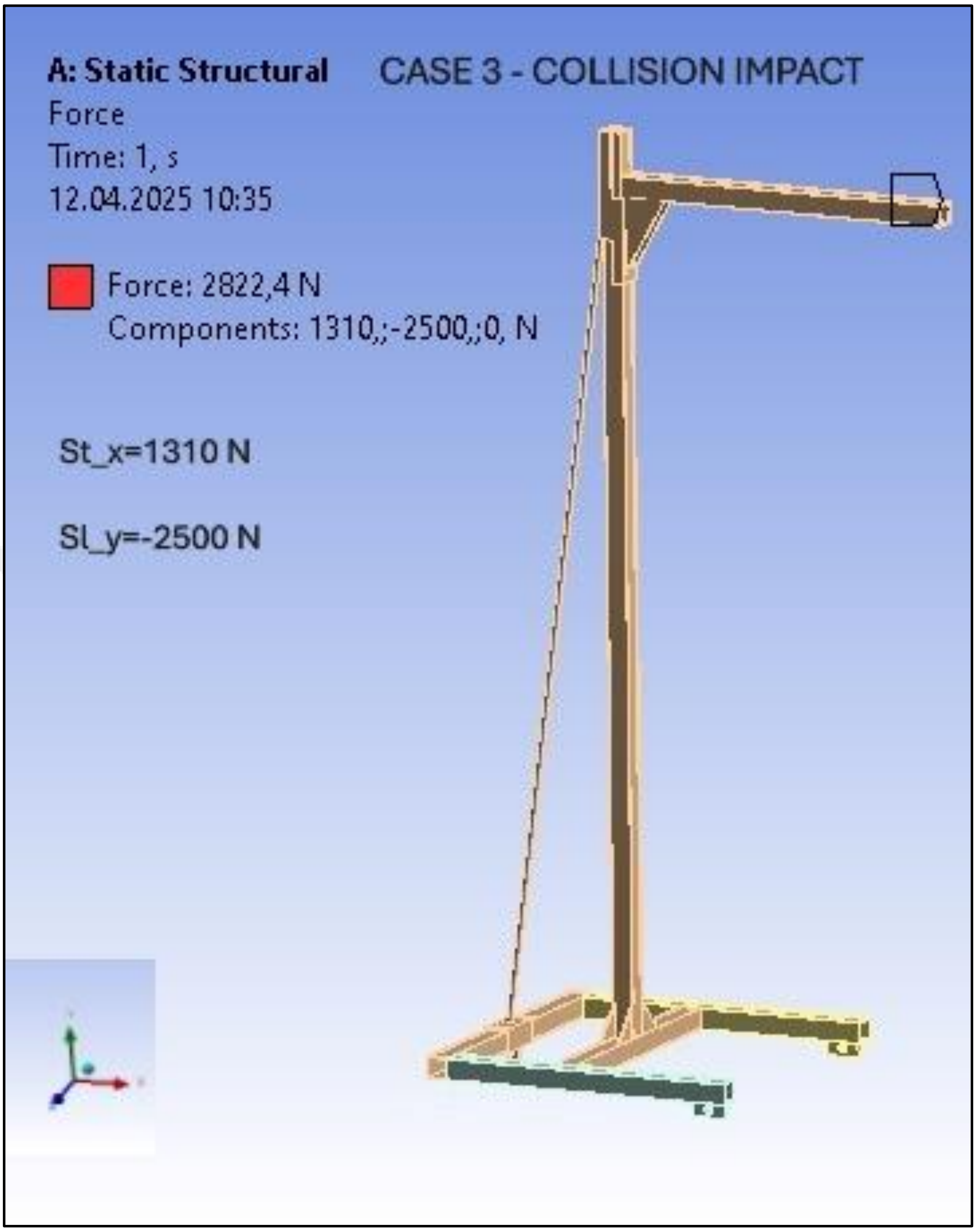

Figure 4.11: Forces. Case 3-Collision Loading.

4.1.6 Case 3-Maximum Wind out of Service Loading Combination Results

For this case, the maximum Equivalent Von Mises' Stress is calculated as 116,86 MPa. The following figures are the ANSYS Structural Analysis results for Case 3-Maximum Wind out of Service Loading;

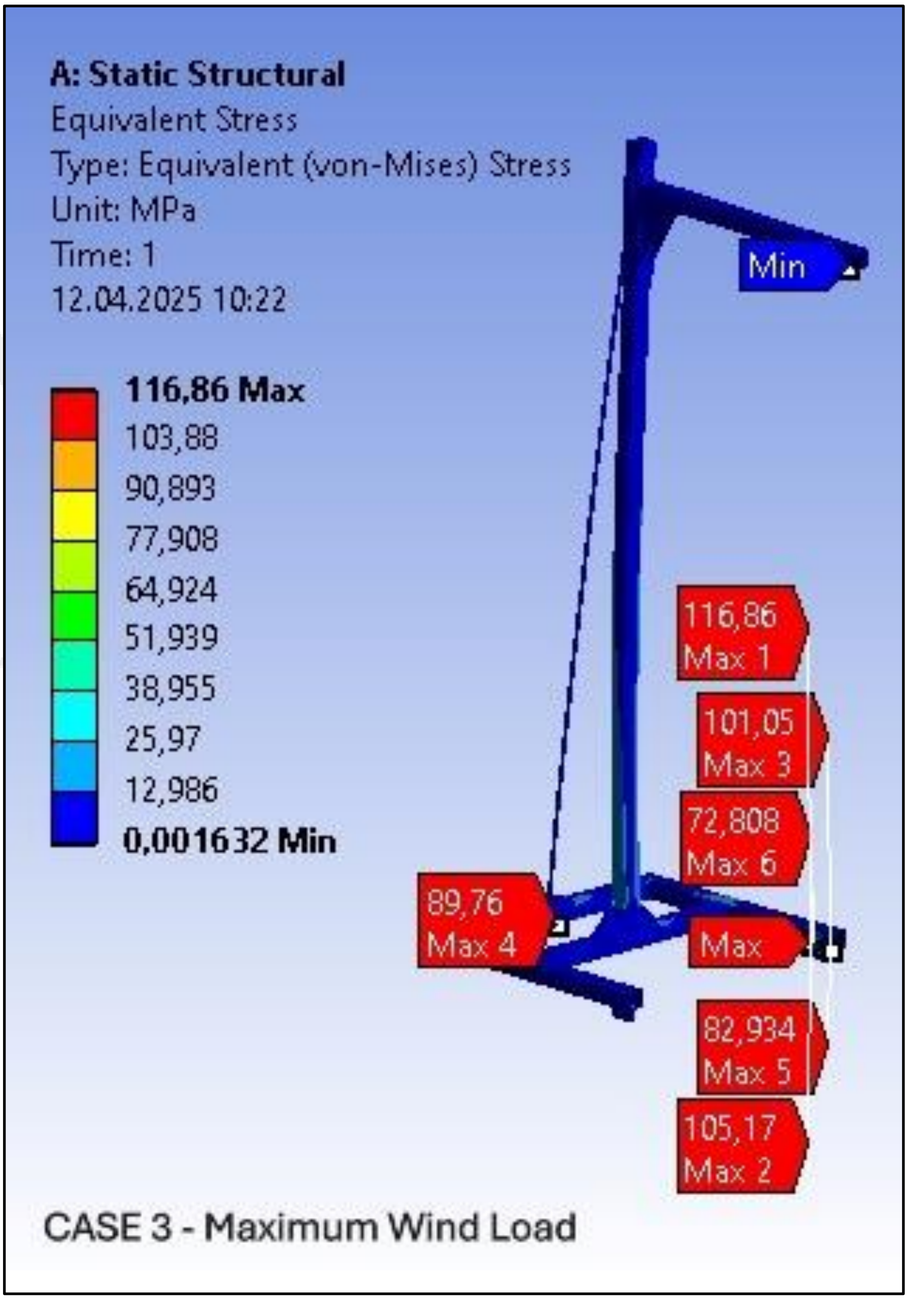

Figure 4.12: Equivalent Von Mises' Stress. Case 3-Maximum Wind Loading.

Figure 4.13: Maximum Wind Pressure on Surfaces. Case 3-Maximum Wind Loading.

4.1.7 Case 3-Maximum Payload Loading Combination Results

For this case, the maximum Equivalent Von Mises' Stress is calculated as 315,59 MPa. The following figures are the ANSYS Structural Analysis results for Case 3-Maximum Payload Loading;

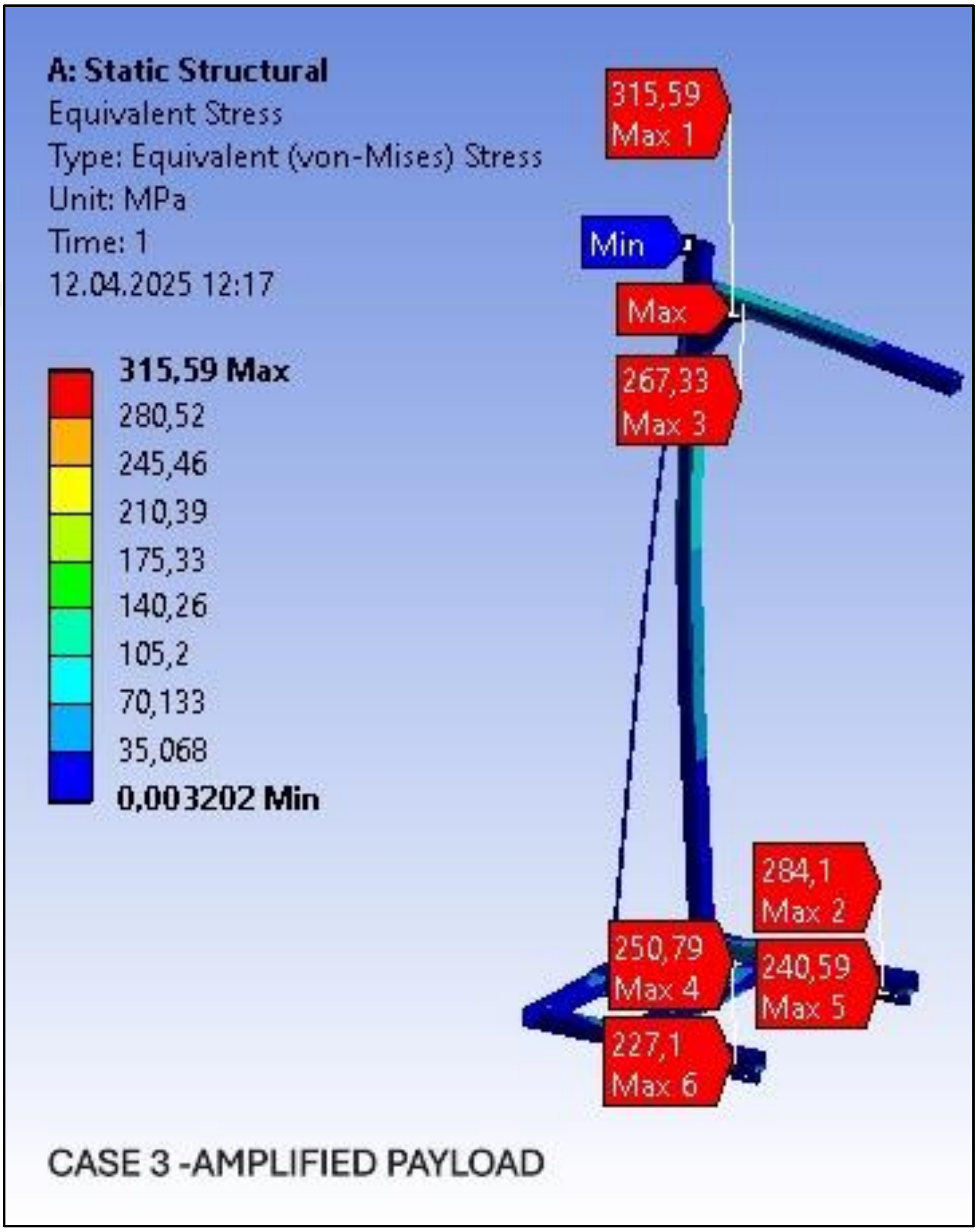

Figure 4.14: Equivalent Von Mises' Stress. Case 3-Maximum Payload Loading.

Figure 4.15: Forces. Case 3-Maximum Payload Loading.

4.1.8 Fatigue Case Loading Combination Results

For this case, the maximum Alternating Equivalent Von Mises' Stress is calculated as 247,43 MPa. Safety Factor FS=1,47 for 250.000 cycles. The minimum safety factors appear near the jib-mast connection where dense welding and HFMI-treatment is going to be applied. The following figures are the ANSYS Structural Analysis results for Fatigue Case Loading;

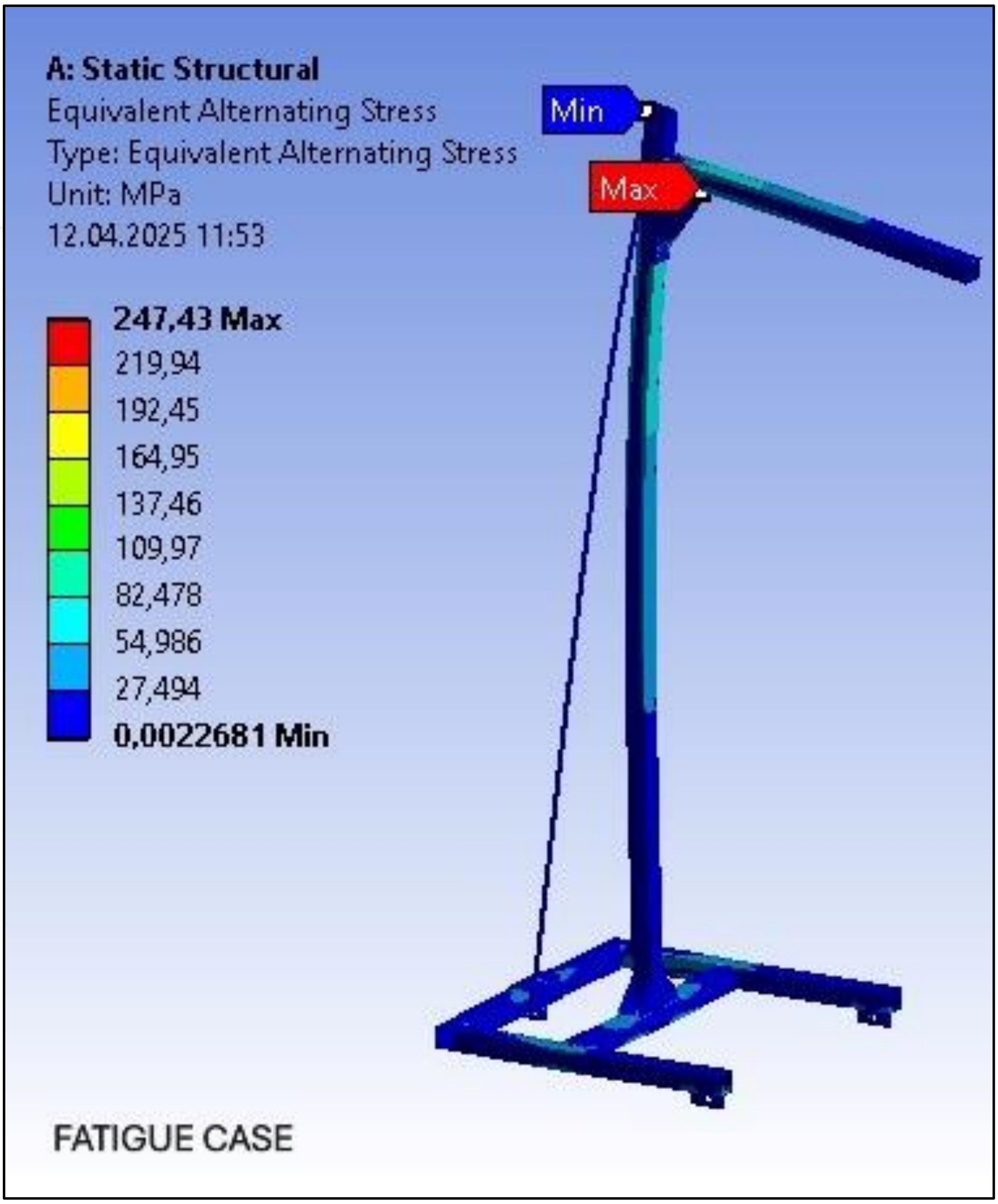

Figure 4.16: Equivalent Alternating Von Mises' Stress. Fatigue Case Loading.

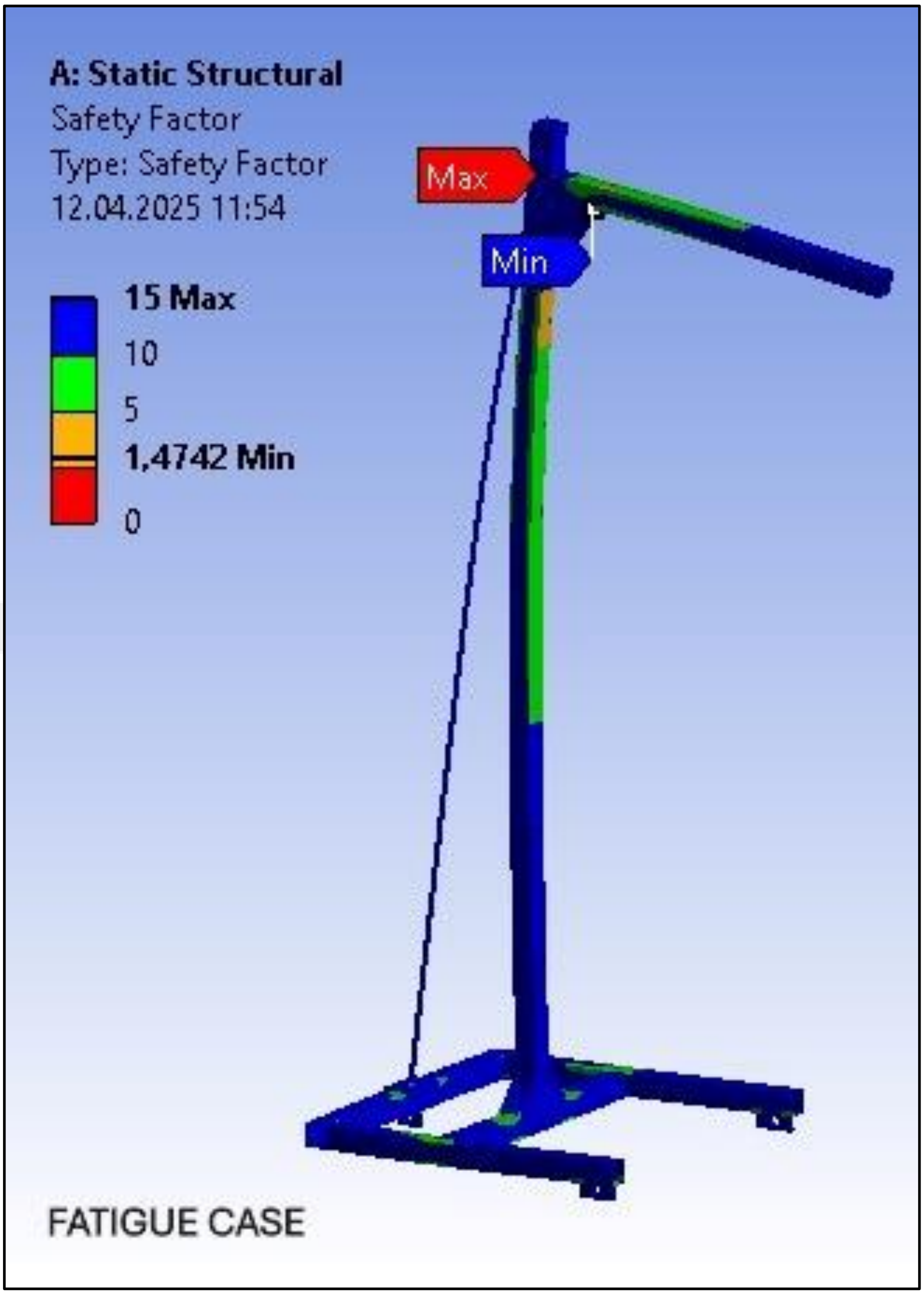

Figure 4.17: Safety Factor for 250.000 Cycles. Fatigue Case Loading.

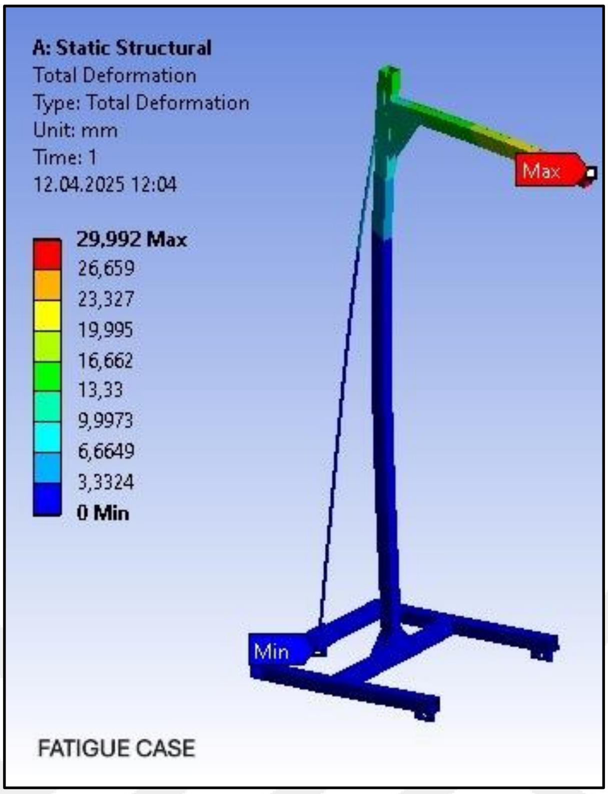

Figure 4.18: Jib Deformation. Fatigue Case Loading.

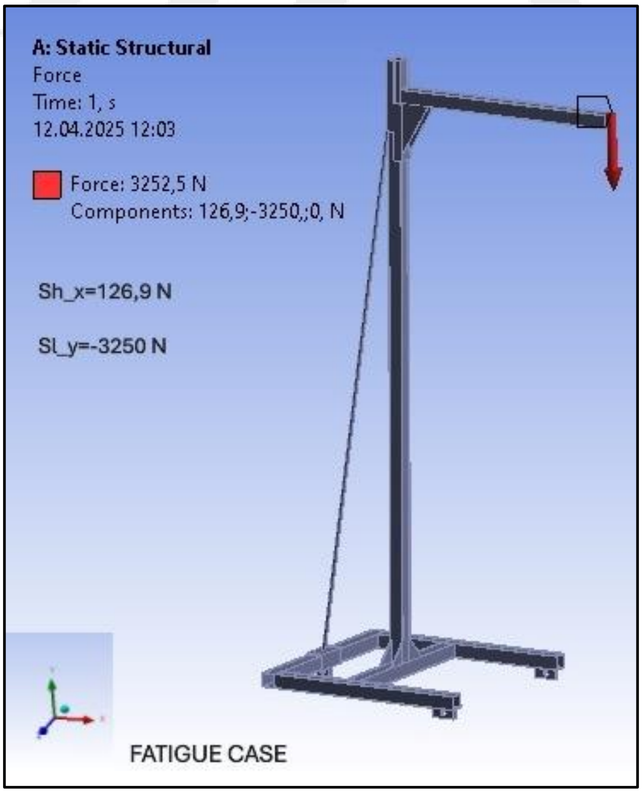

Figure 4.19: Forces. Fatigue Case Loading.

4.1.9 Summarization of Loading Combination Results

So far, all the loading combinations are executed in the computation. Table 4.2 below gives a brief result and comparison of finite element analysis for all cases;

Table 4.2: Safety Factor, Stress and Deformation Values for all Loading Cases.

Case	Deformation (mm)	Stress (MPa)	F.S.
Case 1	32,015	283,93	3,87
Case 2 -Wind X	36,961	356,64	3,08
Case 2-Wind Z	79,647	366,83	3,00
Case 2-Cross Wind	63,373	385,86	2,85
Case 3-Collision	30,311	320,37	3,43
Case 3-Max. Wind	15,412	116,86	9,41
Case 3-Max. Payload	34,620	315,59	3,49
Fatigue Case	29,992	247,43	1,47

The selected design material Strenx-1100 has a yield strength 1100 MPa. None of the stress values in Table 4.2 reaches this value. The design is considered safe in the static loading.

S-N Curve by Jonsson et al. for STRENX-1100 [35] displays an endurance limit as 250 MPa. In Table 4.2, it is clear that Fatigue Case Maximum Stress is under Endurance Limit of the selected design material.

4.2 DYNAMIC ANALYSIS RESULTS

The dynamic analysis of the shop crane is carried out by computer software MATLAB Simulink environment. The Simulink environment has different libraries for many engineering disciplines and among them, SimScape Multibody has a convenient library for mechanical configurations. The built-in ready blocks help the user to easily configure a mechanical system without a necessity of using computer algorithms, especially C++ codes or MATLAB codes. The maximum acceleration to be used in the Static-Structural design is derived from MATLAB results and the related inertial force S_H is later computed with implementing this acceleration. The acceleration and deceleration values are such that the operating velocity of the crane 1 m/s is reached in 3 seconds in acceleration or the crane stops from operating velocity 1 m/s to 0 m/s in 3 seconds.

The analyses are repeated for a system with a double-pendulum model and a system with a single-pendulum model. The single pendulum system has a 1 mass with m_1 and a weightless rope with length l_1. The double-pendulum system has 2 point-masses m_1 and m_2 with different rope length l_1 and l_2. In Figure 4.20, the main physical model differences of the two models are compared.

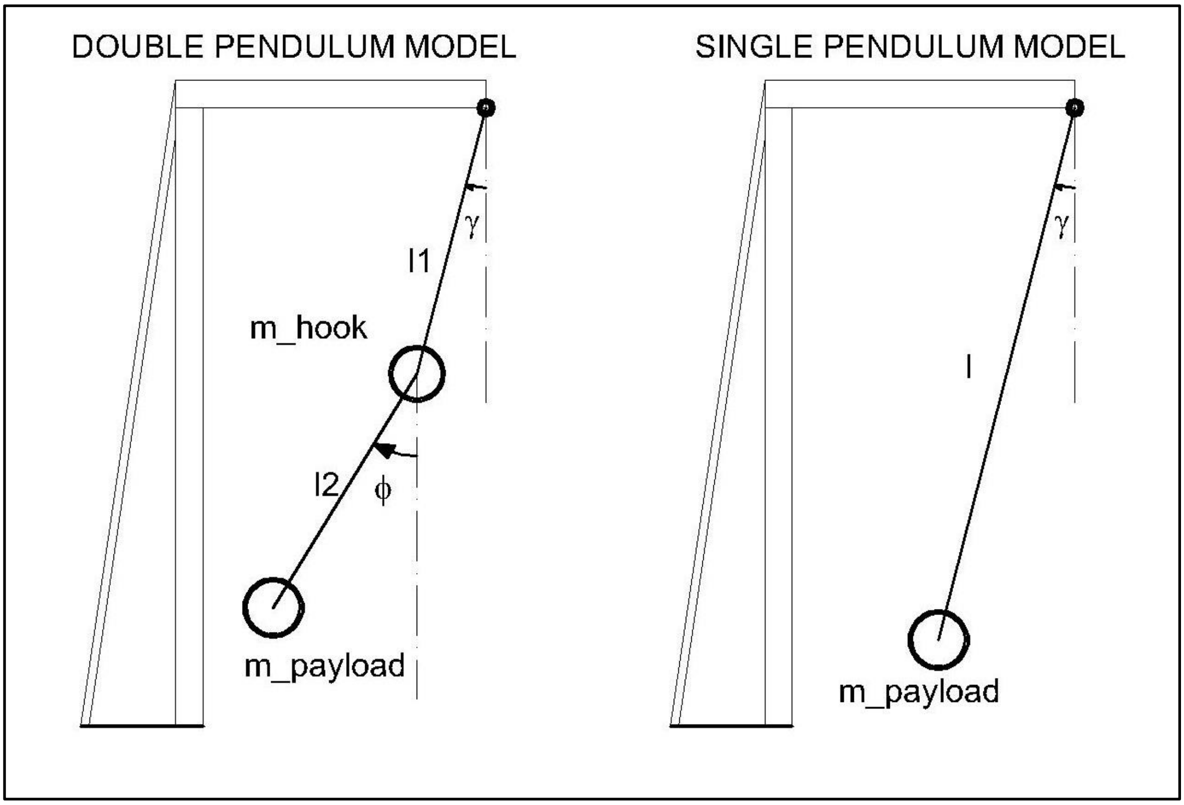

Figure 4.20: Physical Models. Single and Double Pendulum.

The MATLAB analysis diagram for double pendulum model is shown in Figure 4.21 with two strings and two revolute joints. The single pendulum model's only difference is also illustrated in the black-boxed section, consisting of one revolute joint and a single string.

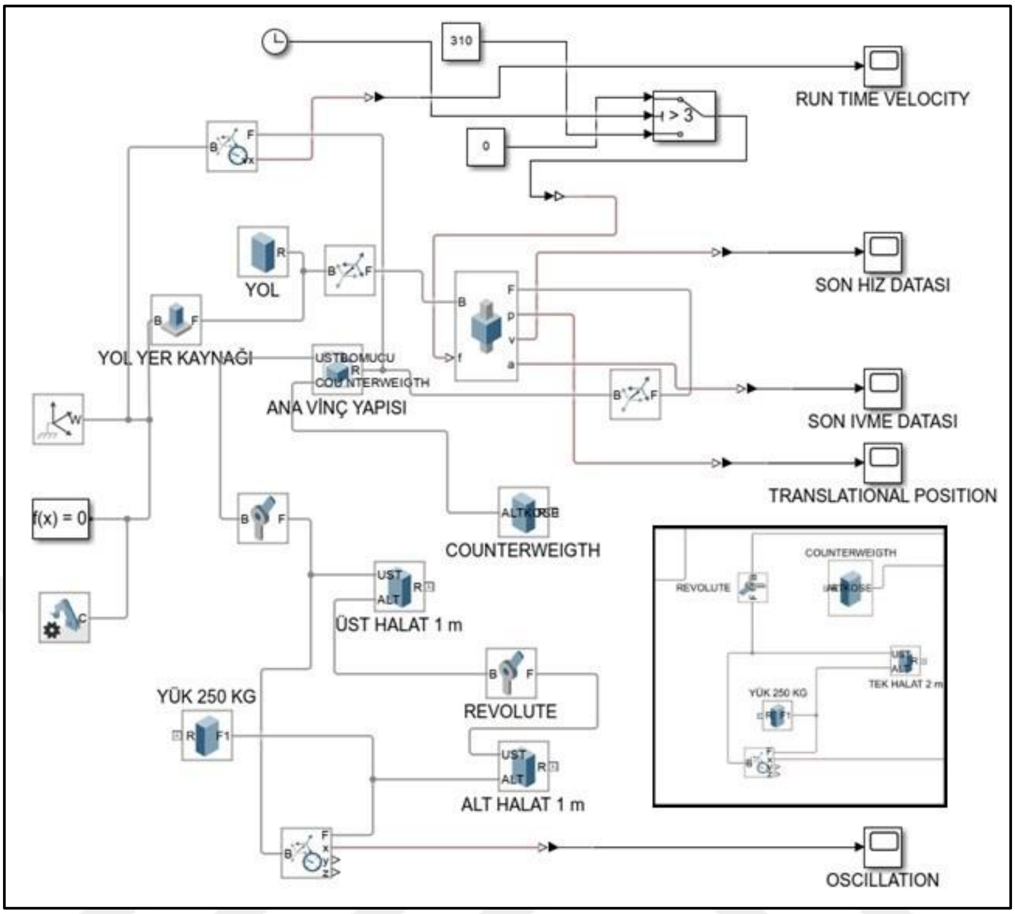

Figure 4.21: MATLAB Simulink Simscape Multibody Diagram of the System.

The diagram consists of several Simulink blocks. These are world frame as main reference frame, solver configuration for Simulink operations, mechanism configuration for Simulink mechanical operations, weld block that connects the reference frame and motion line, a solid block for motion line, a prismatic joint block for connecting the motion line and the crane main body, crane main frame as an exported block from .step file, a revolute joint block that is connecting the rope solid block and the crane frame, a revolute joint connecting the rope solid block and the payload solid block, a switch block to cut the applied torque after the desired motion values are obtained, a counter block for time data, constant blocks for providing input force values to the system as constant values, translational motion sensors to measure motion values between the desired connection lines and scope blocks for measuring and observing the computed results. The switch blocks stop or ignite the force and switch the force to 0 value by activating or deactivating the 0 constant block. The sum block adds up the connected data and outputs the calculated sum.

Later in the PID Control analysis, additional blocks are attached to the diagram. Manual-PID Control system is composed of 3 multipliers; K_P, K_I, and K_D factors. The error of the system is calculated by subtracting target velocity from measured velocity by SIMULINK sensors and later, multiplied by all of these to feed the system back. K_P represents the proportional gain and is used to reach the target rapidly. K_D is the derivative gain and calculates the derivative of the error by derivative block in order to eliminate overshooting and oscillation by detecting the rapid changes of the error. K_I is for the the integral gain and eliminates the steady-state error by tracking the past changes by integral block. Finally, an Auto-PID Simulink block is added and the two control systems are compared.

4.2.1 Dynamic Analysis with Double Pendulum

The data below is taken from the figures below as MATLAB Simulink output of a crane with a double pendulum load attached.

Maximum Acceleration at speed-up case, a=0,465≈0,47 m/s^2 *at time t=0 s.*

Reaching operation velocity at speed-up case, V=1 m/s at time t=3 s.

Maximum pendulum oscillation at speed-up case, 12,99 cm

Maximum Deceleration at break down case, a=-0,465≈-0,47 m/s^2 *at time t=0 s.*

Reaching stop at break down case, V=0 m/s at time t=3 s.

Maximum pendulum oscillation at break down case, 12,99 cm

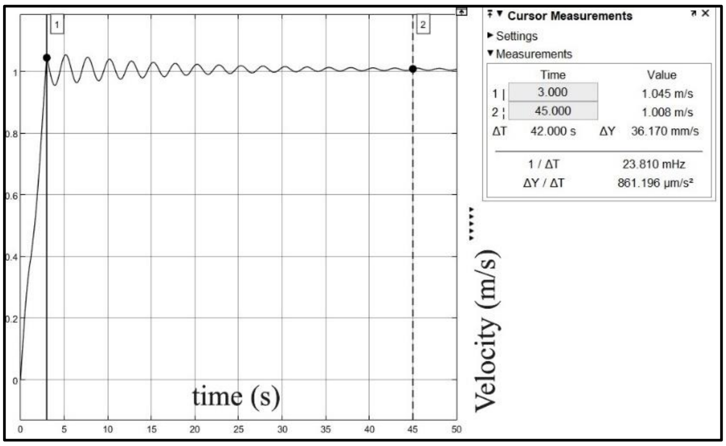

Figure 4.22: Double Pendulum Velocity vs. Time Graph for Speed-Up Case.

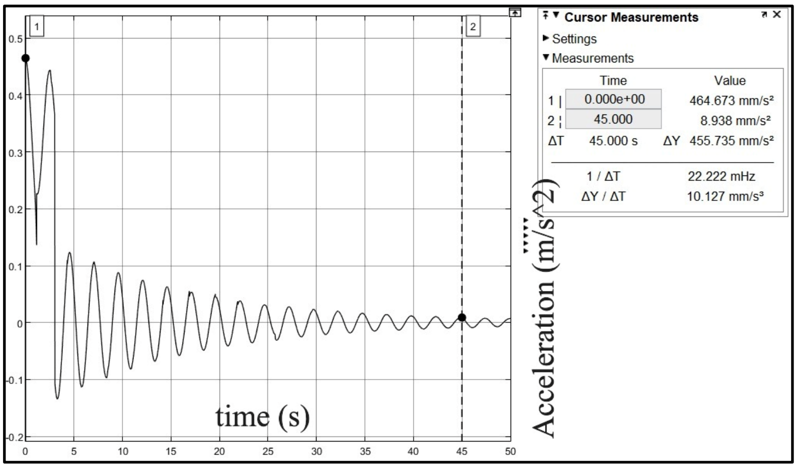

Figure 4.23: Double Pendulum Acceleration vs. Time Graph for Speed-Up Case.

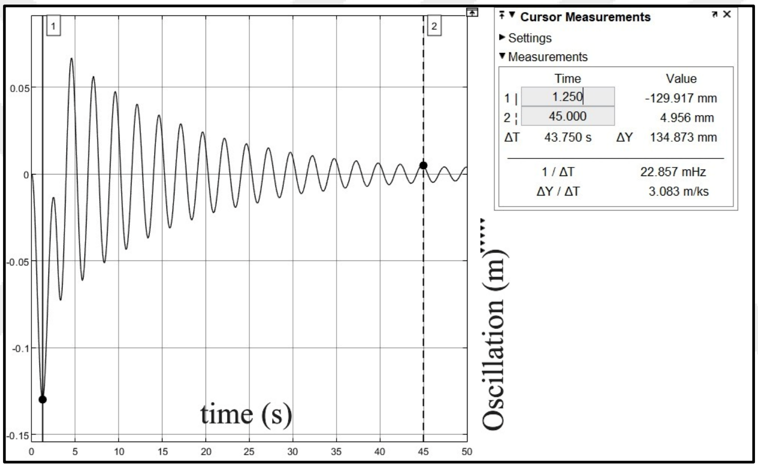

Figure 4.24: Double Pendulum Oscillation vs. Time Graph for Speed-Up Case.

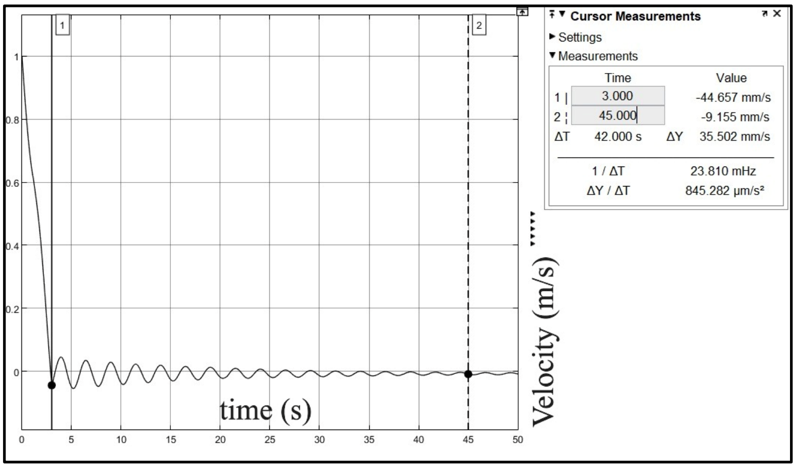

Figure 4.25: Double Pendulum Velocity vs. Time Graph for Break Down Case.

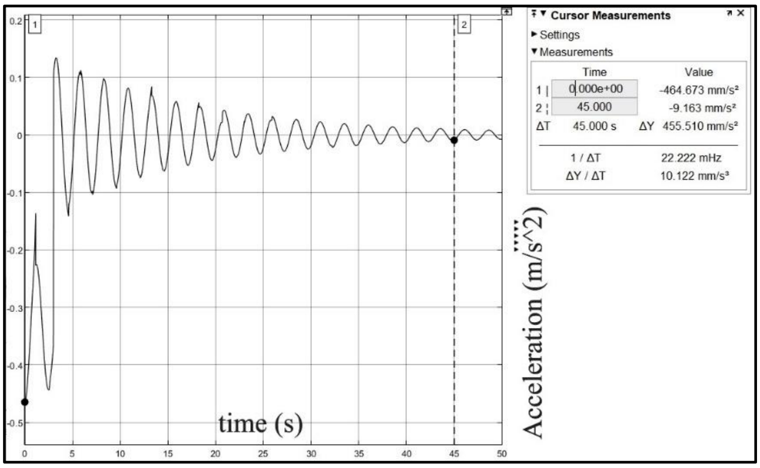

Figure 4.26: Double Pendulum Deceleration vs. Time Graph for Break Down Case.

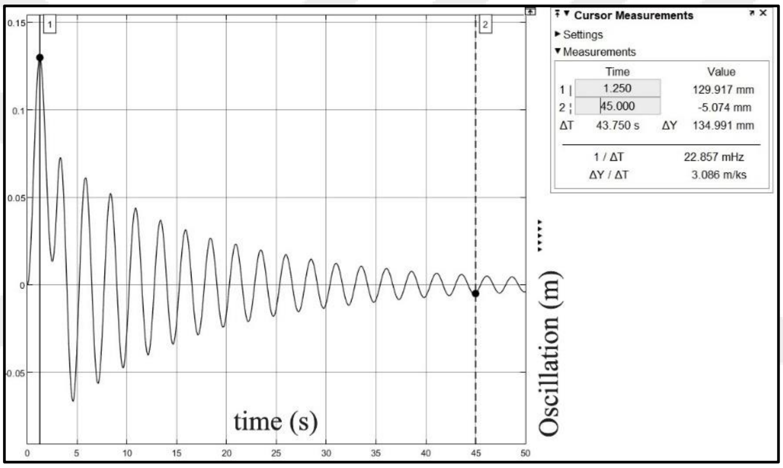

Figure 4.27: Double Pendulum Oscillation vs. Time Graph for Break Down Case.

4.2.2 Dynamic Analysis with Single Pendulum

The data below is taken from the figures below as MATLAB Simulink output of a crane with a single pendulum load attached.

Maximum Acceleration at speed-up case, a=0,465≈0,47 m/s^2 at time t=0 s.

Reaching operation velocity at speed-up case, V=1 m/s at time t=3 s.

Maximum pendulum oscillation at speed-up case, 12,69 cm.

Maximum Deceleration at break down case, a=-0,465≈-0,47 m/s^2 at time t=0 s.

Reaching stop at break down case, V=0 m/s at time t=3 s.

Maximum pendulum oscillation at break down case, 12,80 cm.

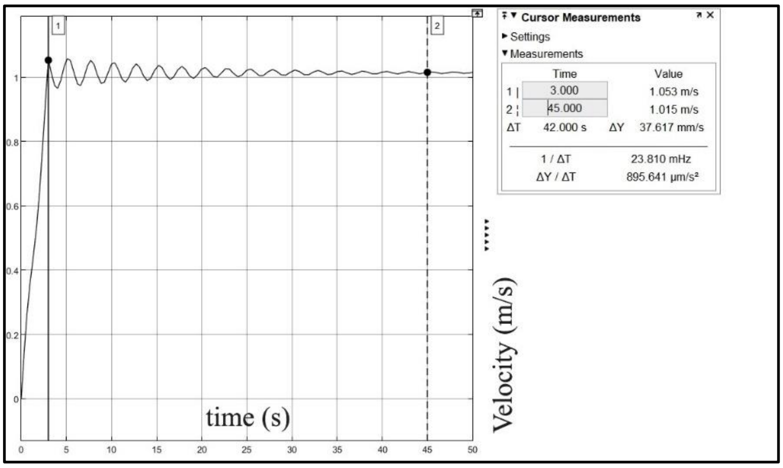

Figure 4.28: Single Pendulum Velocity vs. Time Graph for Speed-Up Case.

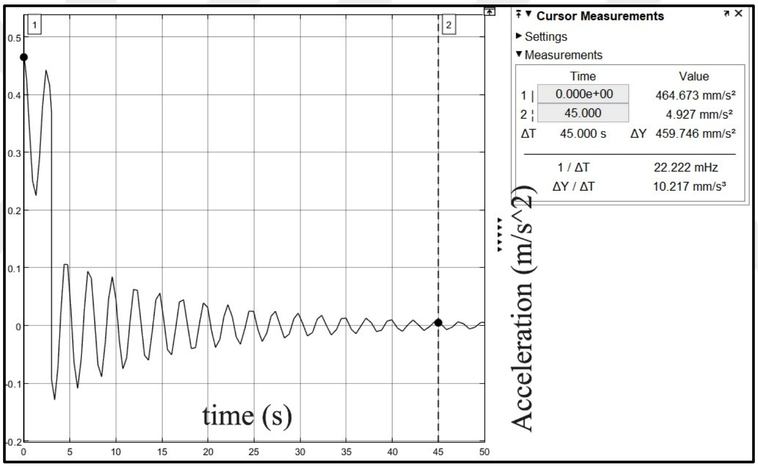

Figure 4.29: Single Pendulum Acceleration vs. Time Graph for Speed-Up Case.

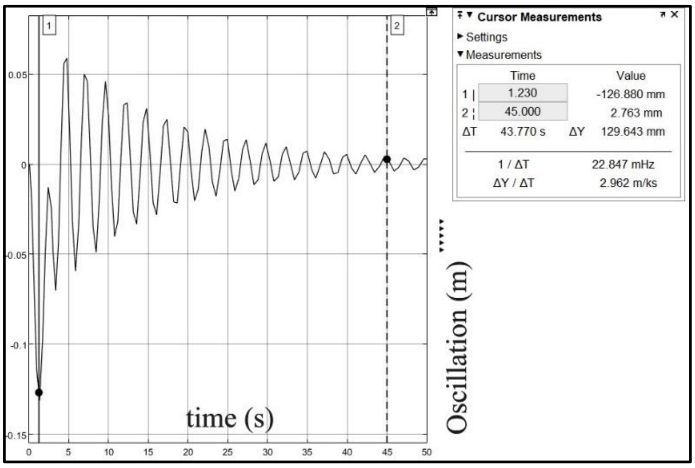

Figure 4.30: Single Pendulum Oscillation vs. Time Graph for Speed-Up Case.

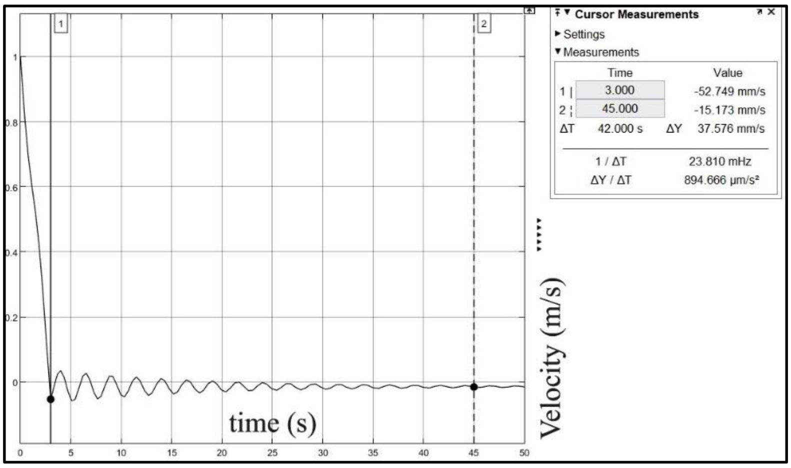

Figure 4.31: Single Pendulum Velocity vs. Time Graph for Break Down Case.

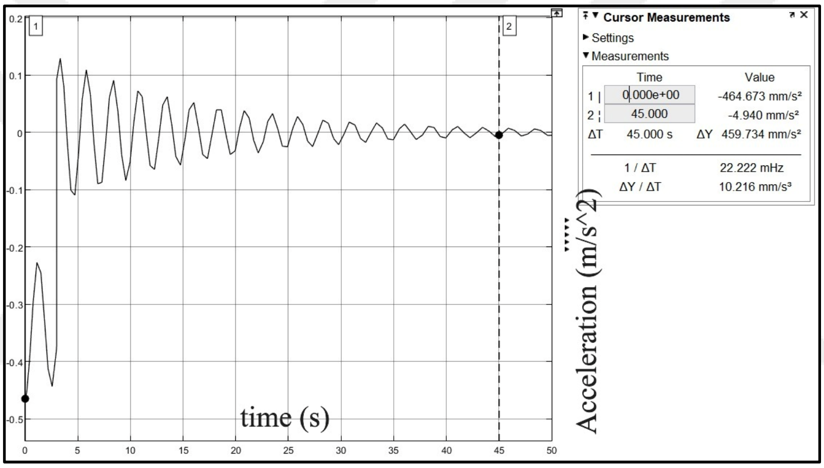

Figure 4.32: Single Pendulum Deceleration vs. Time Graph for Break Down Case.

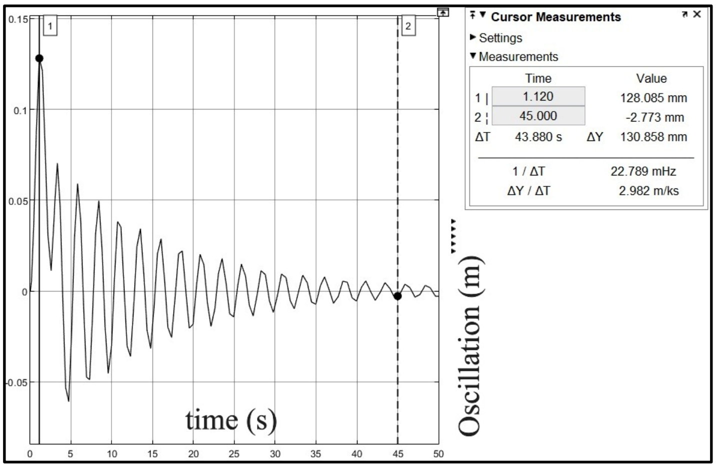

Figure 4.33: Single Pendulum Oscillation vs. Time Graph for Break Down Case.

4.2.3 Dynamic Analysis for S_T Collision Impact (Buffer) Load of FEM 1.001

The S_T collision impact load is derived previously from. As might be remembered, it is the minimum horizontal inertia load exerted by the carried payload to overturn the crane during a sudden collision with surrounding obstacles. In this section, a reverse engineering approach is adopted to verify or assess the collision scenario of FEM 1.001 standard [30].

S_T=131,00 kg, $m_{PAYLOAD}$=250 kg

Using Newton's Second Law of Motion, the following relationship, first introduced in Eq. (3.12), is used once again: *F=m.a*

$$S_T = m_{PAYLOAD} \cdot a_{COLLISIONIMPACT} \tag{4.1}$$

Maximum Deceleration at Collision Case, a=-5,2 m/s^2 at time t=0 s. (putting m=250 and S_T=131 kg at the right above formula)

In the next step of reverse engineering, the deceleration of collision which is *a=-5,2 m/s^2* is searched in the overall Multibody Simscape model. The force necessary to break the crane at exactly a deceleration of this *a=-5,2 m/s^2* rate from 1 m/s operating velocity to 0 m/s is implemented on the model and the following results are obtained.

Reaching stop at collision case, V=0 m/s at time t≤0,2 s.

Maximum pendulum oscillation at speed-up case, 44,10 cm

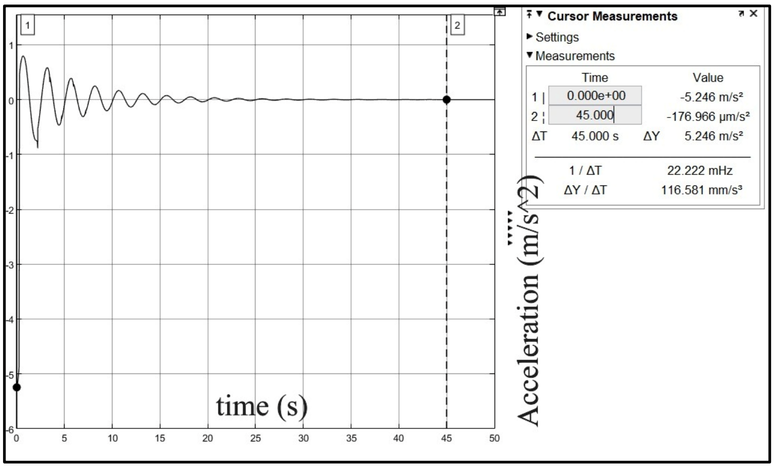

Figure 4.34: Buffer Load Deceleration vs. Time Graph for Collision Case.

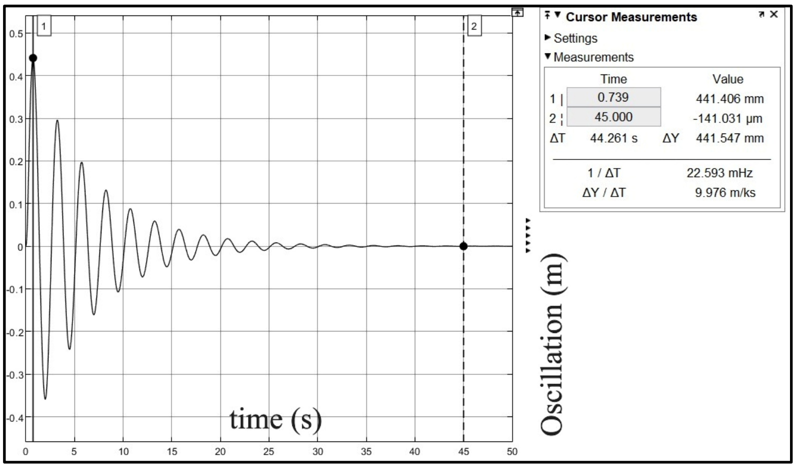

Figure 4.35: Buffer Load Oscillation vs. Time Graph for Collision Case.

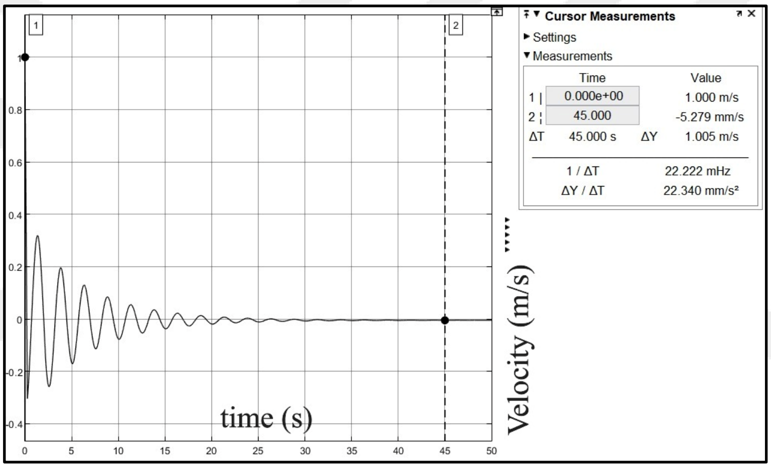

Figure 4.36: Buffer Load Velocity vs. Time Graph for Collision Case.

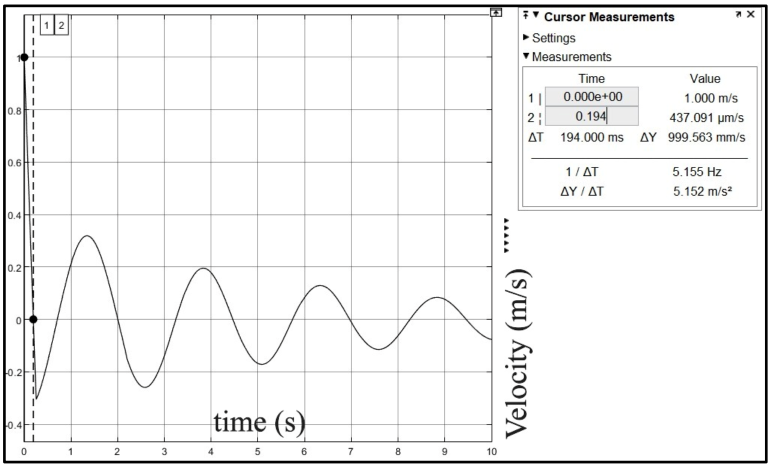

Figure 4.37: Buffer Load Velocity vs. Time Graph for Collision Case.

The figures above prove that S_T load urges the crane to stop less than 0,20 second.

4.2.4 Dynamic Analysis for Heavier Counterweight 800 kg

The counterweight is modified in the system as 800 kg and dynamic analysis results are observed for the single-pendulum speed-up case. It is inspected that the acceleration a_{max}=0,41 m/s^2 is decreased with the shift of center of overall mass to the crane side more and the pendulum effect on the system becomes smaller.

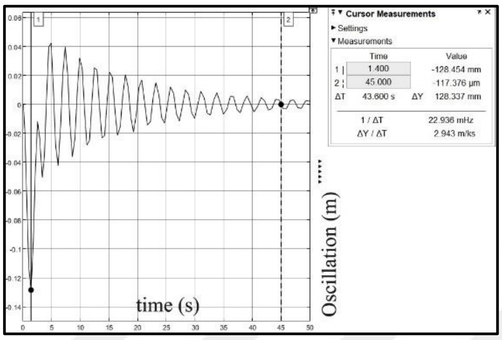

Figure 4.38: Single Pendulum Oscillation vs. Time Graph for Counterweight 800 kg.

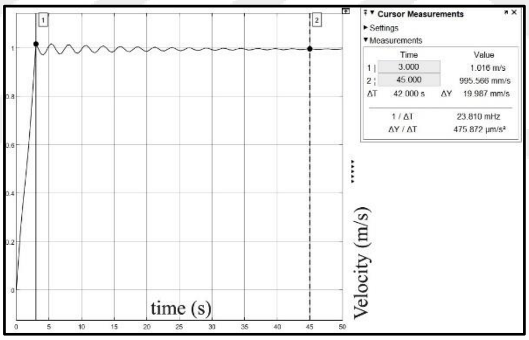

Figure 4.39: Single Pendulum Velocity vs. Time Graph for Counterweight 800 kg.

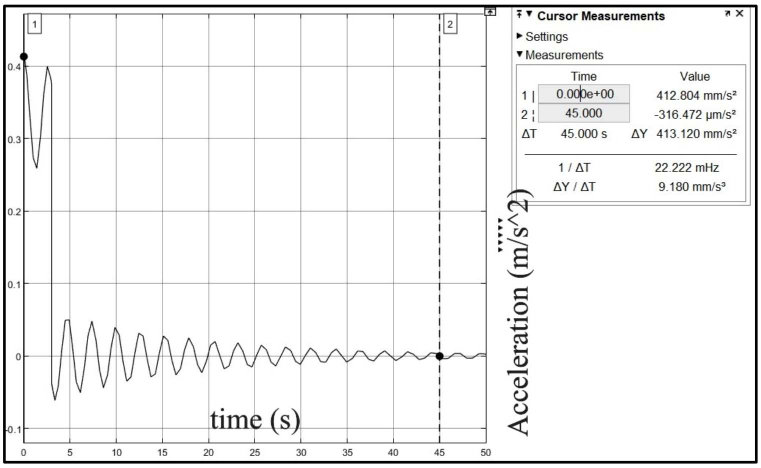

Figure 4.40: Single Pendulum Acceleration vs. Time Graph for Counterweight 800 kg.

4.3 DYNAMIC ANALYSIS IMPROVEMENT AFTER RESULTS OBTAINED

The MATLAB results display that the algorithm of the systems may be enhanced in the way of adding some control to the system for velocity targets. The breaking and acceleration torques in the analysis are applied for a specific time duration to attain the target values but not controlled after the target is reached. Therefore, the additional pendulum in the overall system had a significant oscillation effect on the velocity values. To eliminate these oscillations and to obtain a smooth target value, a proportional control is attached to the system to attain target velocity. The diagram below shows the controlled system.

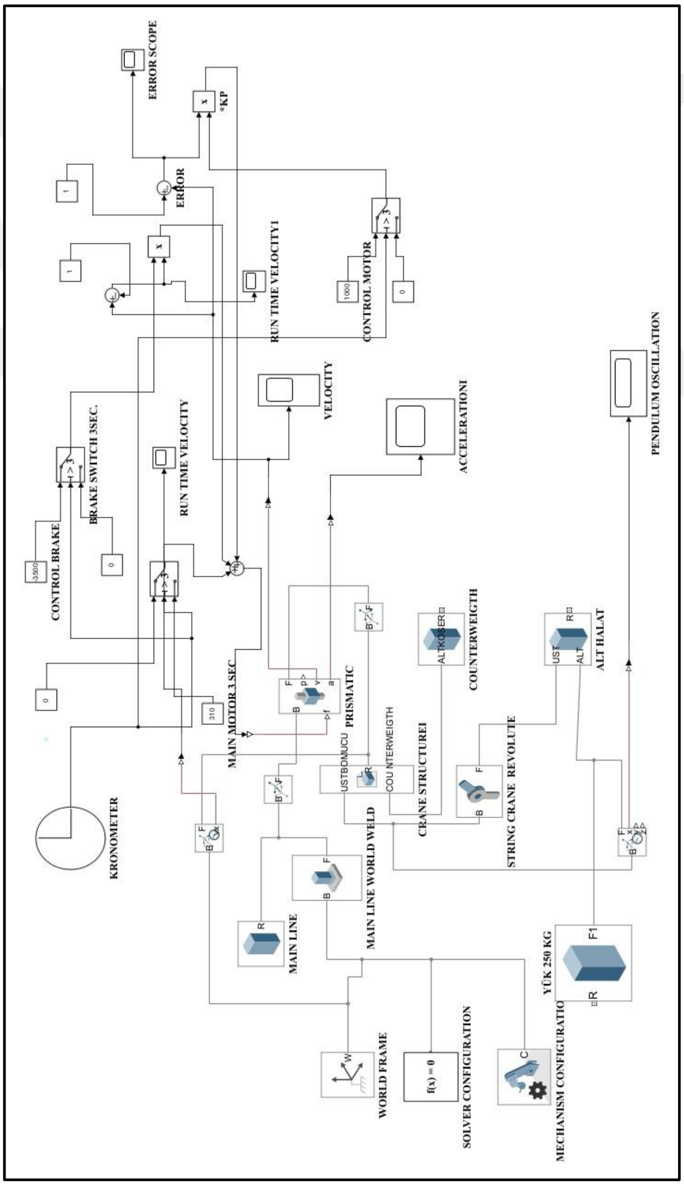

Figure 4.41: MATLAB Simulink Simscape Multibody Diagram of the P Control System.

The improvement in the system is achieved by adding proportional control to the system. The additional switch block asses the signal values that are directed from velocity output of the prismatic joint and when the signal begins overshooting over 0 m/s velocity for break-down or 1m/s velocity for speed-up, the block activates the resistant force to prevent overshooting the target value. The added switch block number is 2, former one to wait for the velocity to reach target with time control value and the latter one to activate the resistant force after overshooting starts.

The improved system is implemented for both the single pendulum case and the collision load or in other words Buffer Load.

4.3.1 Dynamic Analysis Proportional Velocity Control System Results for S_T Load

In the improved condition, velocity oscillations and overshooting are reduced significantly. The impact load is breaking down the crane to 0 m/s velocity within a quarter of a second. The oscillation results differ from the previous analysis that is without velocity control.

Reaching stop at collision case, V=0 m/s at time t≤0,2 s.

Maximum pendulum oscillation at speed-up case, 39,19 cm

Maximum Acceleration a_{max}*≈-5,2 m/s*^{2}

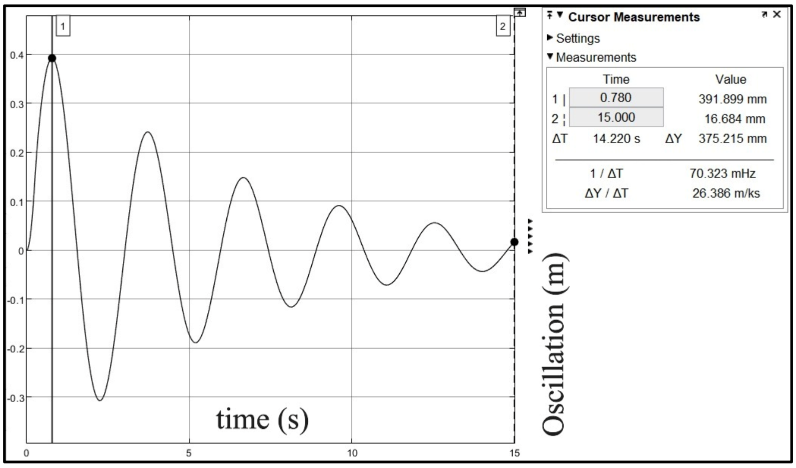

Figure 4.42: Buffer Load Oscillation vs. Time Graph for Collision Case.

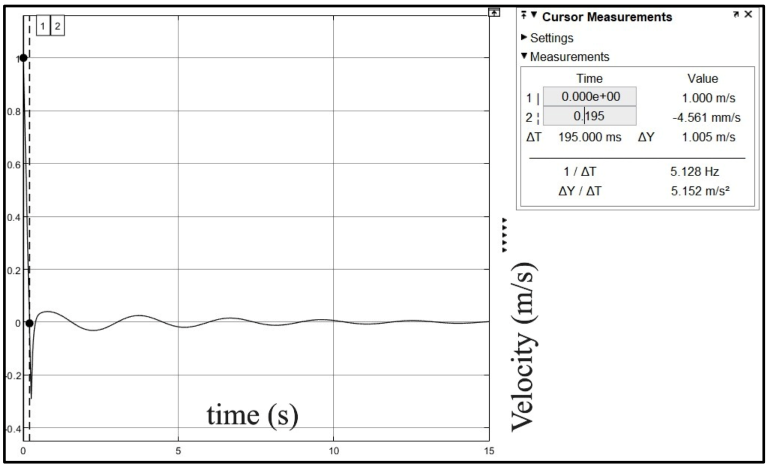

Figure 4.43: Buffer Load Velocity vs. Time Graph for Collision Case.

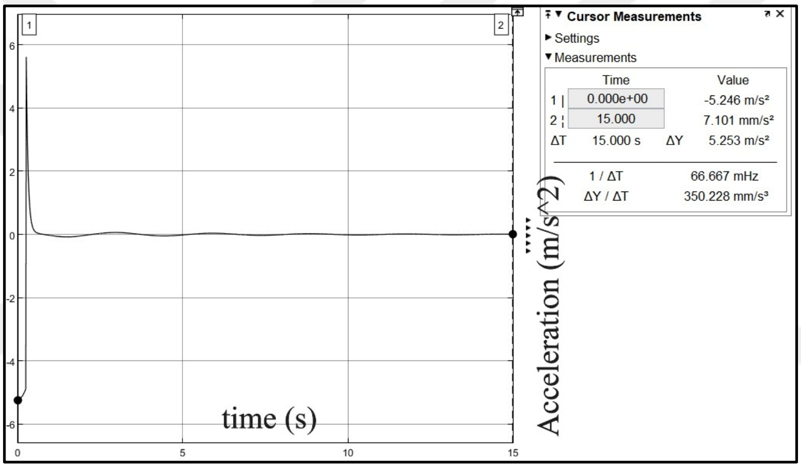

Figure 4.44: Buffer Load Acceleration vs. Time Graph for Collision Case.

4.3.2 Dynamic Analysis Proportional Velocity Control System Results for Single Pendulum

In the improved condition, velocity oscillations and overshooting are reduced significantly. Velocity precisely settles to 1 m/s value. The oscillation result doesn't differ much from the previous analysis without velocity control.

Maximum Acceleration at speed-up case, a=0,464≈0,47 m/s^2 *at time t=0 s.*

Reaching operation velocity at speed-up case, V=1 m/s at time t=3 s.

Maximum pendulum oscillation at speed-up case, 13,10 cm

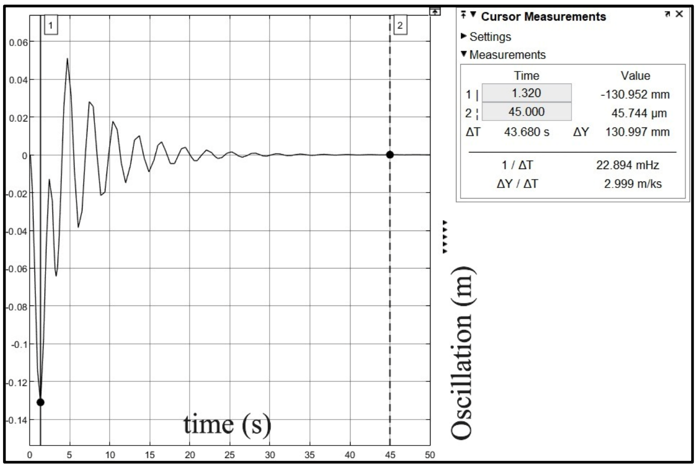

Figure 4.45: Single Pendulum Oscillation vs. Time Graph for Speed-up Case.

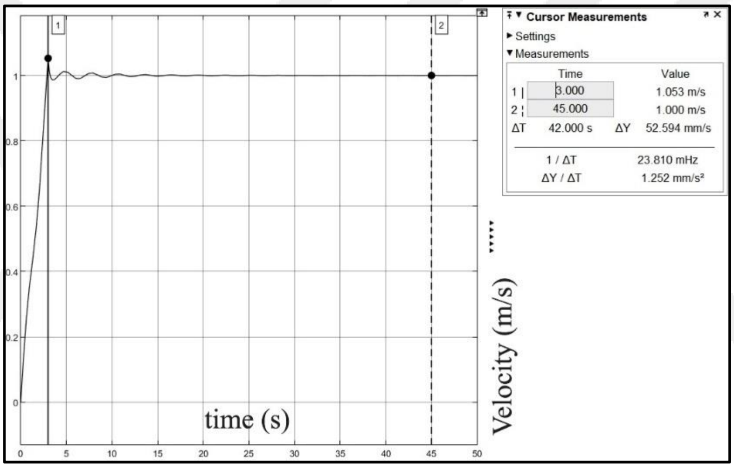

Figure 4.46: Single Pendulum Velocity vs. Time Graph for Speed-up Case.

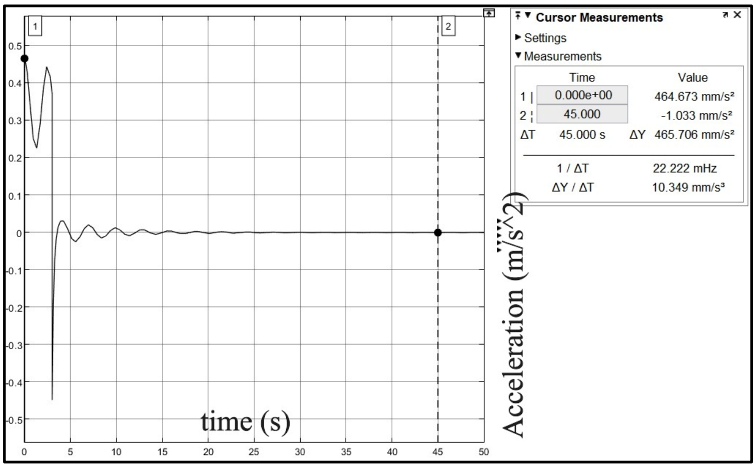

Figure 4.47: Single Pendulum Acceleration vs. Time Graph for Speed-up Case.

4.3.3 Dynamic Analysis PID Velocity Control System Results for Single Pendulum

For further inspection, a manual and an Auto PID control is attached separately to the system to control velocity. Auto-PID is added to check and compare the behavior of Manual-PID system.

Maximum Acceleration at speed-up case – Manual PID, a=0,619 m/s^2 at time t=0 s.

Maximum Acceleration at speed-up case – Auto PID, a=0,619 m/s^2 at time t=0 s.

Reaching operation velocity at speed-up case, - Manual PID, V=0,9914 m/s at time t=3 s.

Reaching operation velocity at speed-up case – Auto PID, V=0,9963 m/s at time t=3 s.

Maximum pendulum oscillation at speed-up case – Manual PID, 18,74 cm

Maximum pendulum oscillation at speed-up case – Auto PID, 19,39 cm

In the figures below, altered system diagrams and system results are available;

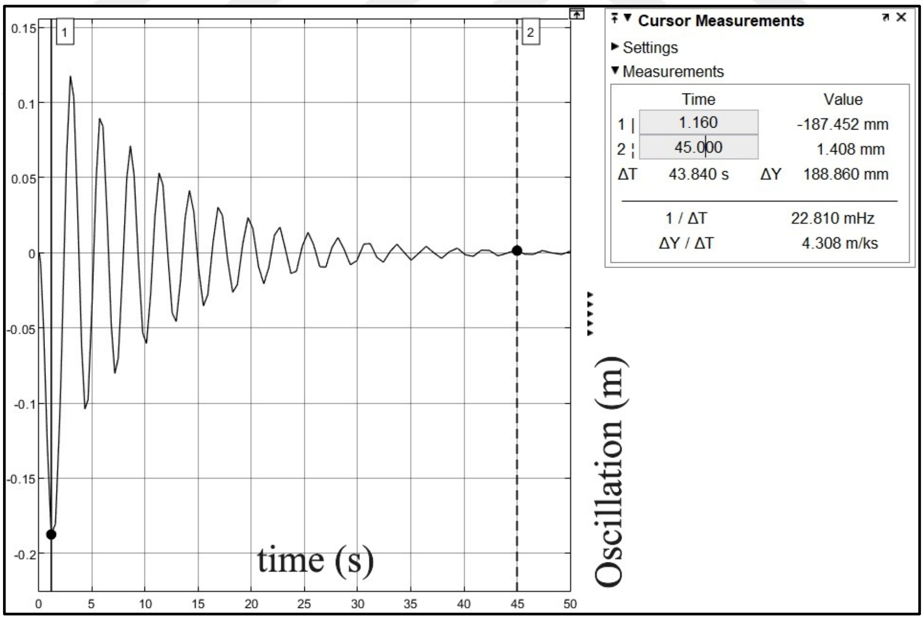

Figure 4.48: Single Pendulum Oscillation vs. Time Graph for Speed-up Case. Manual PID.

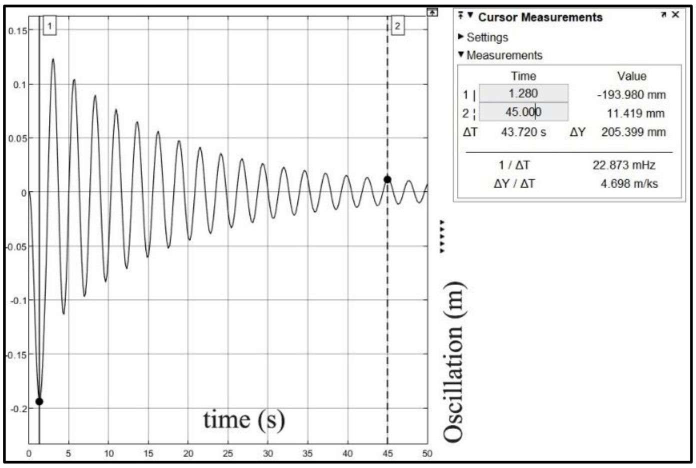

Figure 4.49: Single Pendulum Oscillation vs. Time Graph for Speed-up Case. Auto- PID.

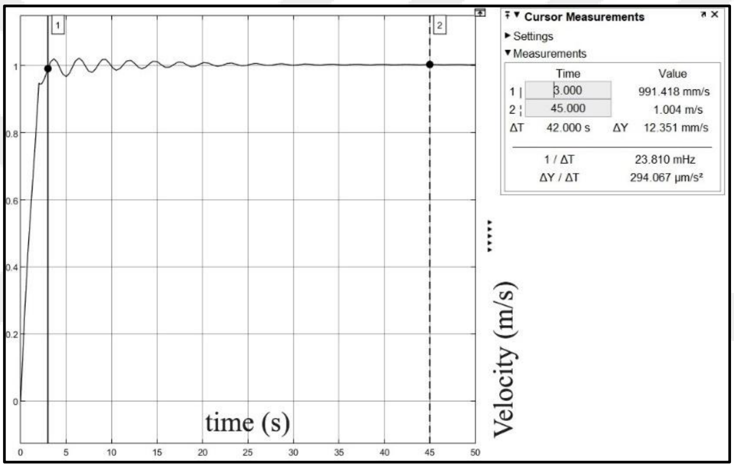

Figure 4.50: Single Pendulum Velocity vs. Time Graph for Speed-up Case. Manual PID.

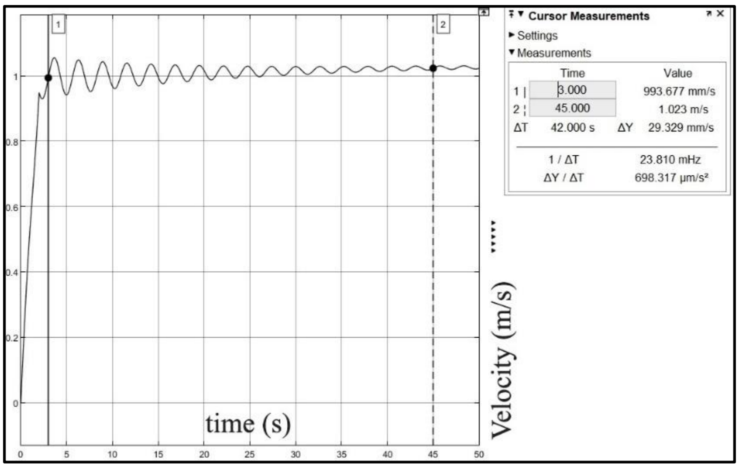

Figure 4.51: Single Pendulum Velocity vs. Time Graph for Speed-up Case. Auto- PID.

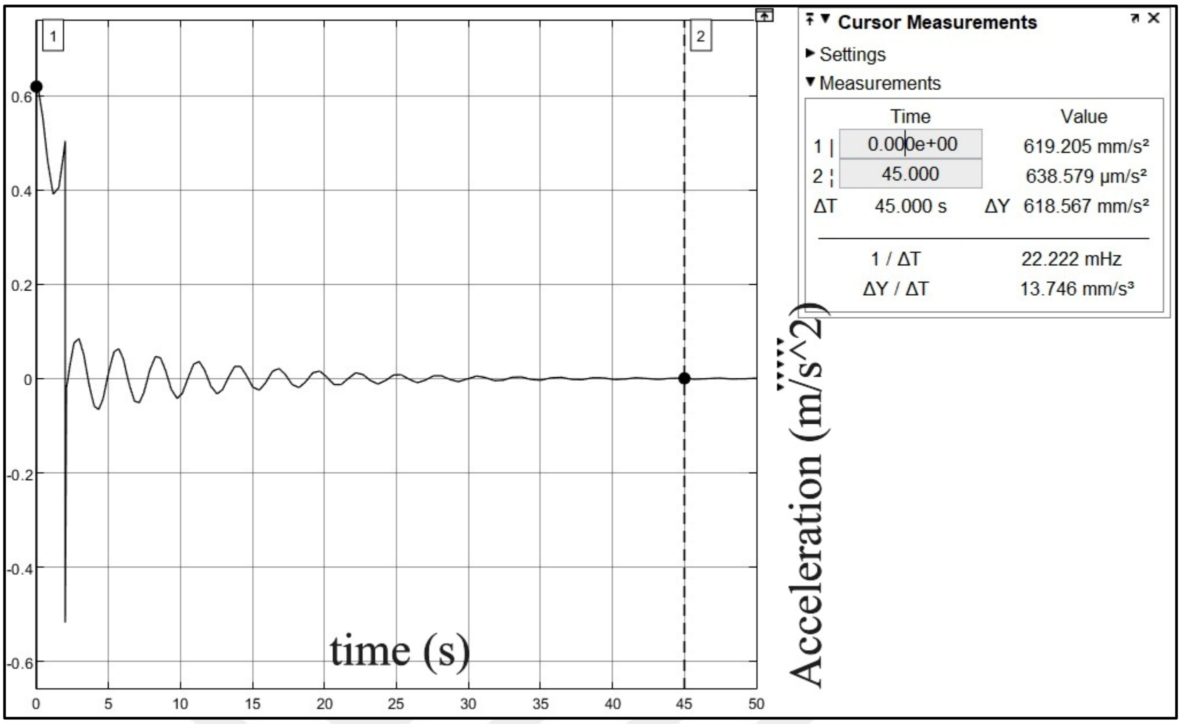

Figure 4.52: Single Pendulum Acceleration vs. Time Graph for Speed-up Case. Manual PID.

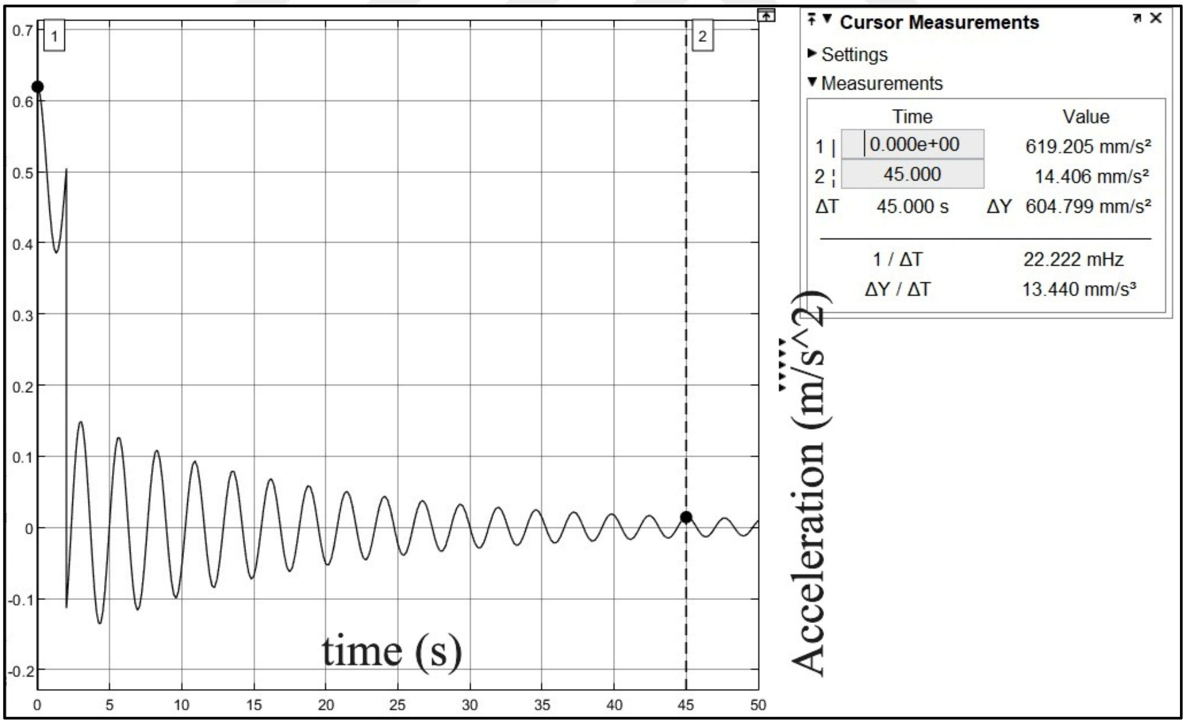

Figure 4.53: Single Pendulum Acceleration vs. Time Graph for Speed-up Case. Auto- PID.

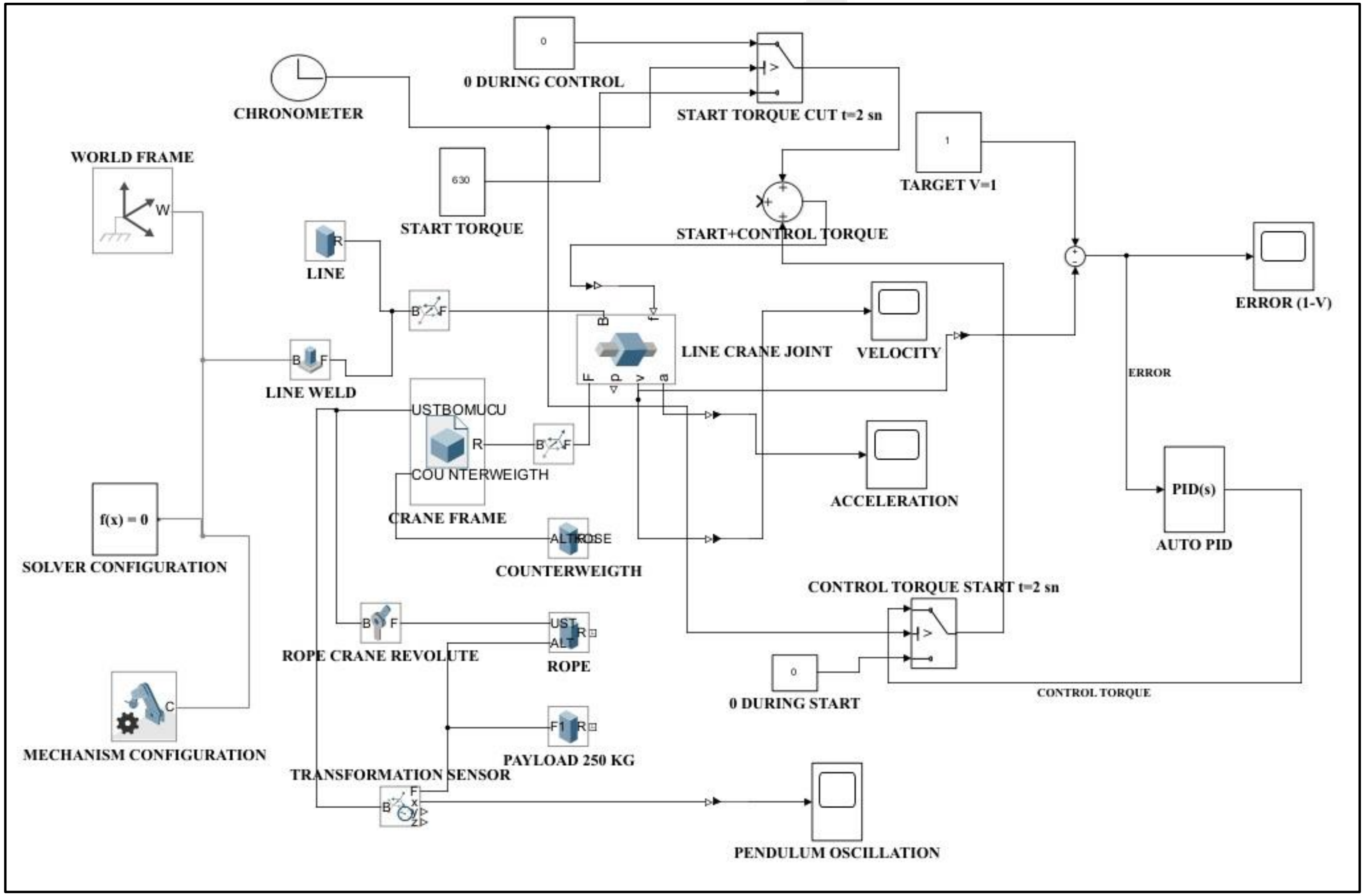

Figure 4.54: Single Pendulum Speed-up Simulink Diagram. Auto- PID.

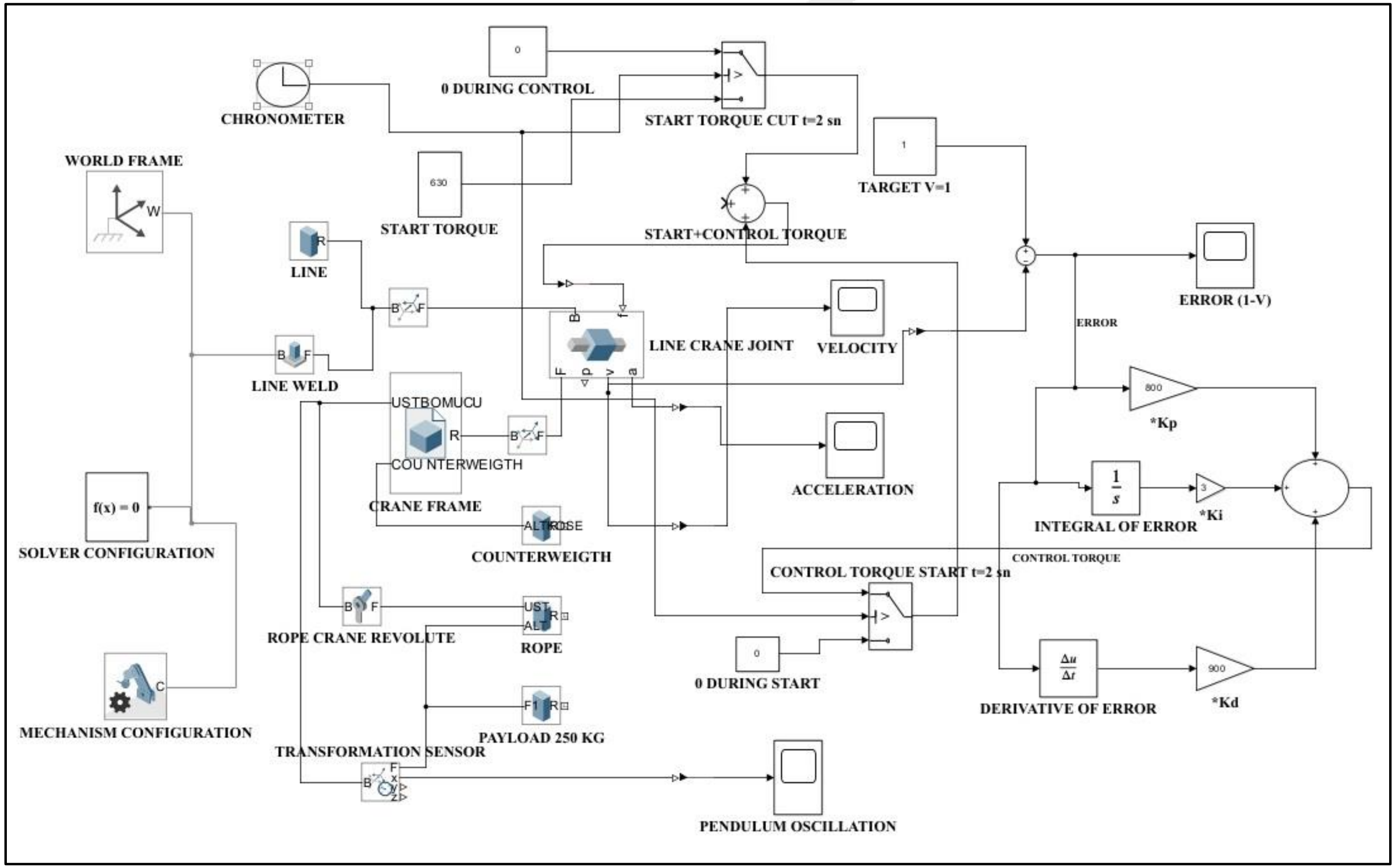

Figure 4.55: Single Pendulum Speed-up Simulink Diagram. Manual- PID.

4.3.4 Video Links of MATLAB Results

The videos of the MATLAB simulations can be found in the links below;

Crane acceleration to 1 m/s and deceleration to 0 m/s. Video available at: https://youtu.be/GfJwEZcbZOE

Crane acceleration to 1 m/s - 3D View. Video available at: https://youtu.be/-I35hzbeKLM

Crane acceleration to 1 m/s. Video available at: https://youtu.be/mfNMGQtZ5oo

5. DISCUSSIONS & CONCLUSIONS

5.1 STRUCTURAL DESIGN

The load combination Case 2 of Section 3.2 for Static-Structural analysis gives results much below the selected steel HSLA-1100 yield strength. The obtained stress results are in the range of 300-400 MPa. Regarding static loading, with a minimum factor of safety 2,85 the selected steel box sections comply with the design factored load combinations in the static loading cases.

The importance of selecting a high strength steel shows up during the fatigue design case. The fatigue analysis load combination of section 3.2 and the S-N curve properties of HFMI treated 1100 MPa high strength steel are combined together. Later, in the ANSYS fatigue analysis, a general fatigue strength factor K_f=0,6 is attached to stay on the safe side. In the fatigue analysis results, a minimum factor of safety value 1,47 is obtained by reaching a life time $2{,}5 \times 10^5$ cycles. Besides, fatigue strength factor K_f is estimated generously as 0,6 for an HFMI-Treated weld section which has been treated to eliminate the notches. Consequently, the fatigue analysis might be considered successful.

The fatigue analysis' minimum factor of safety value is calculated around welded sections in the real manufacturing case. As a result, taking the S-N Curve for HFMI-treated welded section of a 1100 MPa steel seems to be an appropriate selection.

The fatigue analysis safety factor 1,47 can be assessed as an acceptable fatigue design safety factor.

HSLA1100 MPa proves to be a convenient option as this type of steel is mainly used in heavy-lifting industry.

It is also observed that making traffic load with this equipment on a fresh concrete surface without taking the necessary precautions of additional curing is not possible.

To finalize, a light-weight crane is obtained with a main chassis of 217 kg. Keeping the counterweight unit separate and modular with ballasts, motors and batteries together, it is possible to hoist this chassis with a 250 kg capacity construction hoist.

The modification of an engine crane or a shop crane or in other words floor crane to a mobile construction crane might be deemed as completed successfully.

5.2 DYNAMIC ANALYSIS

The maximum oscillation displacement of the payload appears on the implementation of buffer load S_T (131 kg). This is the minimum load to overturn the crane while carrying the maximum payload when a collision creates an impact. The oscillation due to this impact is 39,20 cm after the improvement of control. This size of oscillation is a risky condition as there might be people around the crane. In operating speed-up and operating break-down cases, the oscillations are almost equal, in the range of 12-13 cm.

The impact model is derived based on a dynamic behaviour in which a horizontal load that will generate a -5,20 m/s^2 deceleration on the suspended payload is applied to the system which is previously operating at a 1 m/s velocity and causes the system to stop to 0 m/s velocity abruptly. The sudden stopping time is calculated below 0,20 second. This calculation also verifies that the standard has a good approach in estimating a possible collision impact load effect even in the time criteria as well as the force criteria.

The double-pendulum and single-pendulum inertia loads do not differ too much in the cases of acceleration or deceleration. For both cases, the maximum acceleration or deceleration is almost 0,464 m/s^2. The reason for this is the short length of the rope. Both cases have similar pendulum oscillations for 2 m. rope length.

The computed acceleration is 0,619 m/s^2 for PID control added accurate system. The value of maximum acceleration and deceleration increased after system control.

The counterweight is exactly positioned in the model similar to its original real place. As the multi-particle dynamics of the crane will generate more rotational energy when the applied force gets far from the centre of mass of the crane body, the suspending load will have a larger oscillation. It has been witnessed that the ratio of suspended load mass to the ratio of crane body mass has a large role in the generation of the inertia load that stems from the suspended load. Thus, the counterweight is positioned delicately in the MATLAB Simscape Multibody model. The more the system shifts energy to particles with less constraint, the more will be their unconstrained effects on the system. The more the system shifts energy to constrained lump masses, the more the system will behave like a point mass.

The horizontal inertial force of suspended load which is calculated from the FEM [30] standard and that of the MATLAB Simulink are close to each other. The former is 1/15th and the latter 1/20th of the suspended payload.

The PID S_H force can be calculated as 154,75 N. This value is almost the same with the S_H recommendation of FEM Standard 165 N. Difference between S_H of ANSYS design and last enhancement is only 40 N or 4 kg. This is a negligible amount to alter the design as the design loads increased up to 100 kg by load factors.

It might be concluded that an operating velocity of 1 m/s is an appropriate selection for the available crane size optimization as moving further from this speed endangers the crane stability in case of a collision impact load. Furthermore, it will necessitate installing huge counterweights.

The proportional control enhancement in velocity in order to resemble more like a real-time case doesn't significantly change the inertial acceleration values in speed-up or break-down case.

The additional PID control enhancement in velocity in order to resemble a real-time case makes a slight change in the final horizontal force S_H which will not endanger the design.

Increasing the counterweight stabilizes the system dynamic behaviour. While the stable kinetic energy ratio increases in the constant masses, the ratio of kinetic energy that shifts to pendulum decreases. The Lagrangian of the system intensifies around the mass with more constraints. As a result, the system resembles more like a lump mass compared to the previous case.

5.3 FURTHER INVESTIGATION

Utilizing a floor crane in construction sites is a common application. However, the construction managements generally avoid this option since the risk of overturning, the collision with surrounding and workers is higher compared to utilizing this type of crane in a workshop or manufacturing hall environment. The wind, the surrounding gaps, the elevation of the storeys, the lack of barriers around the storey, a number of people working in the vicinity with rushing mood etc. generates a high risk and probability of an accident. However, by the reveal of new technologies, these risks might be reduced to acceptable limits. A further investigation in installing any of these technologies to a shop crane on open area erection duty will help the managers tend to utilization of this type of crane in installation works. With the AI technologies more coming into our lives, AI systems might be inspected which will use all the available technologies and combine all the information to guide the operator of the crane for any risk.

While the computed results clarifies that it is possible to manufacture a main crane assembly with less than 250 kg weight, an investigation might be conducted to lighten all the appliances that are attached to the main crane assembly. A lighter drive motor, a lighter hoist motor and even using a lighter crane frame with higher strength steel will contribute the users to have more practicality while carrying the crane up and down or here and there around the construction working area.

In the design perspective, modular assemblies and extendable-retractable assemblies might be examined to increase the ease of utilizing the crane in a construction environment.

In this study, the auxiliary standard for determining the crane design loads and drive design loads is used as FEM 1.001 [30]. A comparison with other international standards for design of a shop crane might be held out.

The crane is modified for construction purposes. Therefore, it might be necessary to use it in the edge of the storeys to hoist loads from the ground level. In this position, there is a necessity of additional interlocking safety for the crane. A rail-bogie-guide rim system might be presented to improve the safe working condition of the crane on high level storeys.

A dynamic analysis of the floor crane is presented to the literature with mast modification.

REFERENCES

[1] *Occupational Safety and Health Administration [OSHA]*, USA, 1970.

[2] Derricks. [Online]. Available: https://maritimesafetyinnovationlab.org/derricks/

[3] 11 Types of Cranes Commonly Used in Construction. [Online]. Available: https://www.bigrentz.com/blog/types-of-cranes

[4] Uline. Hydraulic Floor Crane. [Online]. Available: https://www.uline.com/BL_2853/Hydraulic-Floor-Crane

[5] Vestil. Electric Powered Floor Cranes. [Online]. Available: https://www.vestil.com/product.php?FID=586

[6] Bailey. brandon-6-mini-crane-glass-lifter. Available: https://baileycranes.com/glass-lifters/brandon-6-mini-crane-glass-lifter/

[7] Y. D. Kale, K. Pandey, "Design of Hydraulic Floor Crane," *International Journal of Advanced Research in Science, Communication and Technology*, e-ISSN: 2581-9429, vol. 2, Issue 7, June. 2022. doi: 10.48175/IJARSCT-5109. [Online].

[8] R. Duragkar, S. N. Sakhale, M. S. Lande, " A Review: Floor Cranes for Industrial Use," *IJRET: International Journal of Research in Engineering and Technology*, e-ISSN: 2319-1163, vol. 05, Issue 7, Jul. 2016. Available: http://ijret.esatjournals.org.

[9] O. P. Chukwulozie, O. E. Nnaemeka, A. O. Andrew, S. J. Ebieladoh, " Steel Work Design and Analysis of a Mobile Floor Crane," *British Journal of Applied Science & Technology*, ISSN: 2231-0843, vol. 13, Issue 5, pp. 1-9, 2022. doi: 10.9734/BJAST/2016/23079. [Online].

[10] Jadhav, M. Kachroo, M. Hegde, R. Mantri, & H. Ratnaparkhi, " Optimization in design of rotating hydraulic crane," *International Journal of Engineering and Advanced Technology (IJEAT)*, ISSN 2249-8958.

[11] D. Safarzadeh, S. Sulaiman, F. A. Aziz, D. B. Ahmad, G. H. Majzoobi, " The design process of a self-propelled floor crane," *Journal of Terramechanics*, ISSN 0022-4898, vol. 48, Issue. 2, pp. 157-168, 2011. doi: https://doi.org/10.1016/j.jterra.2010.12.002.

[12] L. Peng, D. K.H. Chua, " Decision Support for Mobile Crane Lifting Plan with Building Information Modeling (BIM)," *Procedia Engineering*, ISSN 1877-7058, vol. 182, pp. 563-570, 2017. doi: https://doi.org/10.1016/j.proeng.2017.03.154.

[13] S. Park, M. F. Antwi-Afari, S. Han, S. Moon, "Classification and Improvement Directions for Mobile Crane Path Planning Algorithms: A Comprehensive Review," *in 10th International conference on construction engineering and project management*, Sapporo, 2024. doi: https://dx.doi.org/10.6106/ICCEPM.2024.0018.

[14] Urbaś, K. Augustynek, J. Stadnicki, " Dynamics analysis of a crane with consideration of a load geometry and a rope sling system," *Journal of Sound and Vibration*, ISSN 0022-460X, vol. 572, no. 118133, Jul. 2024. doi: https://doi.org/10.1016/j.jsv.2023.118133.

[15] D. Cekus, P. Kwiatoń, " Effect of the rope system deformation on the working cycle of the mobile crane during interaction of wind pressure," *Mechanism and Machine Theory*, ISSN 0094-114X, vol. 153, 2020. https://doi.org/10.1016/j.mechmachtheory.2020.104011. [Online].

[16] D. Fujioka, "Tip-over stability analysis for mobile boom cranes with single-and double-pendulum payloads," Doctoral dissertation, Mech. Eng. Dept., G.I.T. , Georgia, 2010.

[17] Zhu, Z. Zhiqian & W. Pan, " Technologies, levels and directions of crane-lift automation in construction," *Automation in Construction*, vol. 153, no. 104960, 2023. doi:10.1016/j.autcon.2023.104960.

[18] Z. Towarek, " The Dynamic Stability of a Crane Standing on Soil During the Rotation of the Boom," *International Journal of Mechanical Science*, vol. 40, no. 6, pp. 557-574, 1997.

[19] G. Romanello, "Stability Analysis of Mobile Cranes and Determination of Outriggers Loading," *Journal of Engineering, Design and Technology*, vol. 16, no. 6, pp. 938-958, 2018. Accessed: Sept. 19, 2018.

[20] B. Posiadala, "Influence of Crane Support System on Motion of the Lifted Load," *Mech. Mach. Theory*, PII: S0094-114X(96)00044-4, vol. 32, no. 1, pp. 9-20, 1997.

[21] U. Yılmaz, M. Kalyoncu, " Mobil Hidrolik Teleskobik Vinçlerde Yük Salınım Kontrolü," *Selcuk Univ. J. Eng. Sci. Tech.*, e-ISSN: 2147-9364, vol. 2, no. 2, 2014.

[22] Ö. F. Görçün, G. Doğan, " Mobile crane selection in project logistics operations using Best and Worst Method (BWM) and fuzzy Measurement of Alternatives and Ranking according to Compromise Solution (MARCOS)," *Automation in Construction*, ISSN 0926-5805, vol. 147, no. 104729, 2023. https://doi.org/10.1016/j.autcon.2022.104729.

[23] MidTech, Middle East Technology for Engineering. Compressive Strength of Concrete. [Online]. Available: https://midtech.com.jo/1867-2/

[24] R. Chapman, S. Shah, " Early age bond strength in reinforced concrete," *ACI Mater J*, vol. 84, no. 6, pp. 501-510, 1987.

[25] W. Cooper, "Determination of early strength of singly and doubly reinforced beams," Department of Civil Engineering, North Carolina State, 1975.

[26] X. Song, Y. Wu, C. Chen, " Bond behaviour of reinforcing steel bars in early age concrete," *Construction and Building Materials*, vol. 94, pp. 209-217, 2015. Accessed: Jun. 29, 2015. doi: http://dx.doi.org/10.1016/j.conbuildmat.2015.06.060

[27] L. W. Cole & P. A. Okamoto, " Flexural Strength Criteria for Opening Concrete Roadways to Traffic," *Transportation Research Record*, vol. 1478.

[28] T. L. Cavalline, B. Q. Tempest, R. B. Biggers, A. J. Lukavsky, M. S. McEntyre & R. A. Newsome, "Durable and Sustainable Concrete Through Performance Engineered Concrete Mixtures," State of California Department of Transportation, 2020.

[29] O. Tezel, İ. Bektaş, İ. Gökalp & M. Tarhan, "Properties of High Early Strength Concretes Manufactured with New Generation Hardening Accelerators," pp.359-366.

[30] *FEM 1.001-Rules for the Design of Hoisting Appliances*, 3rd ed., Federation Europeenne de la Manutention Section 1, 1998.

[31] Ssab. Strenx. [Online]. Available: https://www.ssab.com/tr-tr/markalar-ve-urunler/strenx

[32] S. Dhua & S. Sen, " Effect of direct quenching on the microstructure and mechanical properties of the lean-chemistry HSLA-100 steel plates," *Materials Science and Engineering*, vol. 528, pp. 6356-6365, 2011. doi:10.1016/j.msea.2011.04.084

[33] Y. Gür, "MİG/MAG Kaynağı ile Birleştirilen S700 MC Yüksek Dayanımlı Yapı Çeliğinin Mikroyapı ve Mekanik Özelliklerinin İncelenmesi," M.S. thesis, G.Ü.F.B.E., G.Ü., Ankara, 2022.

[34] M. Leitner, S. Gerstbrein, M. Ottersböck, M. Stoschka, "Fatigue Strength of HFMI-treated and Stress-Releif Annealed High-Strength Steel Weld Joints," *in 6th Fatigue Design Conference*, Leoben, 2015, pp. 477–484. doi: 10.1016/j.proeng.2015.12.618.

[35] T. Jonsson, T. Narström, Z. Barsoum, "Fatigue and Ultimate Strength Assessment of Post-Weld Treated Strenx 1100 Plus Butt Welds," *in 9th Edition of the International Conference on Fatigue Design*, Stockholm, 2021, pp. 411–417.

[36] Iso 12482:2014(en). Cranes- Monitoring for Crane Design Working Period. [Online]. Available: https://www.iso.org/obp/ui/en/#iso:std:iso:12482:ed-1:v1:en

[37] Groschopp. Technical Resources. [Online]. Available: http://www.groschopp.com

[38] N. Isaac, "Philosophiæ Naturalis Principia Mathematica," in *Jussu Societatis Regiæ ac Typis Josephi Streater*. Londini: Prostat apud plures Bibliopolas, 1687.

[39] Decadura. ShangHai, China. Forklifts: The Struggle Against Resistances. [Online]. Available: https://www.decadura.com/news/forklifts-the-struggle-against-resistances/

[40] Karadeniz Makina. Sessiz İnşaat Vinci. [Online]. Available: https://www.karadenizmakina.com/urun/sessiz-insaat-vinci